



Holtec Center, 555 Lincoln Drive West, Marlton, NJ 08053

Telephone (856) 797-0900

Fax (856) 797-0909

June 13, 2003

U.S. Nuclear Regulatory Commission
ATTN: Document Control Desk
Washington, DC 20555-0001

Subject: USNRC Docket No. 71-9261, TAC L23474
HI-STAR 100 Certificate of Compliance 9261
HI-STAR License Amendment Request 9261-2, Revision 1, Supplement 1
Clarification of Thermal Analyses

References: 1. Holtec Project 5014
2. Holtec Letter, B. Gutherman, "Response to Request for Additional Information – Holtec HI-STAR 100 Amendment – Certificate of Compliance No. 9261", to USNRC Document Control Desk, dated May 23, 2003.

Dear Sir:

During our telephone conference of June 9, 2003, the NRC staff requested clarification of the treatment of the optional MPC aluminum heat conduction elements (AHCEs) in the HI-STAR 100 transportation thermal analysis. We state the question below in order to provide an unambiguous response:

Question

Clarify the treatment of the optional AHCEs in the HI-STAR 100 transportation normal condition and fire accident condition thermal analyses, in particular as they relate to the baseline thermal model (BTM) and the refined thermal model (RTM). Clearly describe the differences between the BTM and the RTM.

Response

The AHCEs were included in the original storage certifications of the HI-STORM 100 (Docket 72-1014) and HI-STAR 100 (Docket No. 72-1008) because, at the time, the benchmarking of the FLUENT model incorporating the thermosiphon action in the vertically oriented MPC was not yet approved by the SFPO. The AHCEs, located in the peripheral spaces between the basket and the MPC shell, provided a conduction path for heat rejection to the external surface of the MPC and thus allowed the systems to be certified despite the absence of recognition of the thermosiphon effect. From a purely performance standpoint, the AHCEs impeded the thermosiphon action by reducing the net downcomer flow area for helium circulation. The AHCEs, in other words, detracted modestly

NMSS01



Holtec Center, 555 Lincoln Drive West, Marlton, NJ 08053

Telephone (856) 797-0900

Fax (856) 797-0909

U. S. Nuclear Regulatory Commission
 ATTN: Document Control Desk
 Document ID 5014486
 Page 2 of 5

from the thermal performance of the system, but served the key objective of enabling the system to meet the fuel cladding temperature limits (in the absence of the recognition of the thermosiphon effect) by providing a heat transmission bridge between the basket and the MPC shell.

Subsequently, when the thermosiphon effect was recognized in the HI-STORM thermal model that underlies Amendment 1 to the HI-STORM CoC, the need to retain the AHCEs disappeared. Accordingly, the MPCs being manufactured today do not contain AHCEs. However, the MPCs whose deployment pre-dates Revision 1 of the HI-STORM CoC are equipped with AHCEs. Therefore, from the thermal/hydraulic standpoint, for the HI-STAR 100 transport package, MPCs equipped with and without AHCEs must be considered.

Normal Conditions of Transport

In the thermal analysis submitted in support of HI-STAR's original transport certification (now referred to as the Baseline Thermal Model (BTM)), the AHCEs provided a convenient means to satisfy the regulatory temperature limits with the MPC and overpack in the horizontal orientation, and permitting the basket thermal model to be made in an exceedingly conservative manner. In particular, the axial conductance of the fuel basket assemblage was assumed to be equal to the in-plane conductance (in reality, the in-plane conductance is much smaller than the axial conductance due to the presence of physical gaps between the fuel and the cell wall, and within the fuel assemblies). In the "no-AHCE" scenario, this significant conservatism was removed while certain other, less sweeping, conservatisms were maintained. The revised model, which we refer to as the Refined Thermal Model (RTM), forms the basis of this amendment request submittal. The conservatisms germane to the RTM are summarized in Appendix 3.A of the SAR, Proposed Revision 10A.

In summary, the principal differences between the BTM and RTM are as follows:

Item	Description	BTM Assumption	RTM Assumption
1	AHCE heat dissipation	Included	Excluded
2	Rayleigh effect	Included	Excluded
3	Basket Axial Conductivity	Grossly Understated	Realistic modeling (See discussion in SAR Subsection 3.4.1.1.4)



Holtec Center, 555 Lincoln Drive West, Marlton, NJ 08053

Telephone (856) 797-0900

Fax (856) 797-0909

U. S. Nuclear Regulatory Commission
ATTN: Document Control Desk
Document ID 5014486
Page 3 of 5

Of the three chief distinguishing features between the BTM and RTM listed in the above table, one (neglect of the Rayleigh effect) is more conservative in the RTM than the BTM. However, in the aggregate, the BTM is a more conservative model. In essence, the RTM is more accurate, yet still conservative. Conservatisms such as assuming that the fuel basket is levitated in the MPC enclosure vessel coaxially with it (i.e., no physical contact between the basket and the MPC shell) is retained. The RTM-based solution, as noted in this submittal, meets the regulatory temperature limits without any problem.

Fire Accident Conditions

In the fire event analysis, summarized in Section 3.5 of the SAR, the aim of the analysis is to bound both the “with-AHCE” and “without-AHCE” scenarios. To achieve this objective, the analysis to characterize the response of the HI-STAR package in enveloping a Part 71 fire event assumes that the AHCE heat transfer bridge is present during the fire period so that the computed heat flow to the fuel is maximized. Further, the emissivity (and absorptivity) of the overpack surface, normally set at 0.85 (SAR Table 3.5.2) is increased to 0.9 during this event.

In the existing post-fire cooldown period model, the AHCEs are included, which would overstate the heat transfer away from the fuel for those MPCs not equipped with AHCEs. To account for the “no-AHCE” scenario in the thermal model, the emissivity of the overpack was reduced to 0.66 as soon as the fire event ends, thus retarding the rejection of heat to the environment and compensating for the presence of the AHCEs in the thermal model during this period. The fuel cladding temperature limits presented in SAR Section 3.5 use the above approach (hereafter called Model #1).

An alternate modeling approach for the fire event was also considered to validate the conservatism of the existing fire analysis. In the alternate modeling, the following assumptions are made:

- i. The AHCEs are assumed to be installed during the fire event.
- ii. The AHCEs are assumed to be absent as soon as the fire subsides (post-fire cooldown).

The emissivity (and absorptivity) of the overpack surface was assumed to be at the normal value of 0.85 before and after the fire event and at the increased value of 0.9 during the fire event.



HOLTEC
INTERNATIONAL

Holtec Center, 555 Lincoln Drive West, Marlton, NJ 08053

Telephone (856) 797-0900

Fax (856) 797-0909

U. S. Nuclear Regulatory Commission
ATTN: Document Control Desk
Document ID 5014486
Page 4 of 5

The results of the analysis using the above model, hereafter called Model #2, are tabulated below, along with the Model #1 results.

Fuel Cladding Temperature Results [°F]		
	Model #1	Model #2
Initial temperature (at start of fire)	708.2	708.2
Temperature at the end of fire	708.2	708.2
Max. temperature during post fire cooldown	750.9	727.7

Comparing the Model #1 and Model #2 fuel cladding temperature values, it is concluded that Model #1 is more conservative and is therefore maintained as the licensing basis calculation method in the SAR.

In closing, we should observe that both of the above models are premised on other conservatisms that maximize fuel cladding temperature. For example, no credit is taken for the added resistance to the inward transmission of heat from the separation of the gamma shell layers due to differential thermal expansion during the fire event. Likewise, the Holcite neutron shielding material surrounding the overpack body is conservatively assumed to have zero conductivity in the pre-fire and post-fire cooldown period and a conductivity of 1.0 BTU/ft-hr-°F during the fire event (SAR Table 3.2.2). We also note, as a reminder, that no MPC can both have, and not have AHCEs installed. These conservatisms, among others listed in Section 3.5, serve to ensure that both Models #1 and #2 provide upper bounds on the temperature rise of the stored fuel for the fire event.

We have enclosed the following revised documents for your information and use:

- Replacement SAR Sections 3.4 and 3.5, Proposed Revision 10B, which have been revised to clarify this matter.
- A replacement List of Effective Pages.
- Revision 1 to the Holtec Thermal Analysis Report, which includes the Model #2 sensitivity study



HOLTEC
INTERNATIONAL

Holtec Center, 555 Lincoln Drive West, Marlton, NJ 08053

Telephone (856) 797-0900

Fax (856) 797-0909

U. S. Nuclear Regulatory Commission
ATTN: Document Control Desk
Document ID 5014486
Page 5 of 5

Please contact the undersigned if you require additional information.

Sincerely,

Brian Gutherman, P.E.
Manager, Licensing and Technical Services

- Enclosures:
1. Holtec Report HI-2033009, "HI-STAR License Amendment 9261-2 Thermal Analyses," Revision 1 (Holtec Proprietary)
 2. Replacement SAR Sections 3.4 and 3.5, Proposed Revision 10B
 3. List of Effective Pages, Revision 10B

Attachment: Affidavit Pursuant to 10 CFR 2.790

Document ID: 5014486

Distribution: Mr. Meraj Rahimi, USNRC (Cover letter w/attachment, one copy of Enclosure 1 and 7 copies of Enclosures 2 and 3.)
NRC Document Control Desk (Cover letter w/attach. and encl.)

emcc: HUG Licensing Committee (cover letter only)
Holtec NRC Correspondence Distribution (cover letter only)
Holtec Groups 1, 2, and 4 (cover letter only)

AFFIDAVIT PURSUANT TO 10CFR2.790

I, Brian Gutherman, being duly sworn, depose and state as follows:

- (1) I am Manager, Licensing and Technical Services of Holtec International and have reviewed the information described in paragraph (2) which is sought to be withheld, and am authorized to apply for its withholding.
- (2) The information sought to be withheld is Holtec Report No. HI-2033009, "HI-STAR License Amendment 9261-2 Thermal Analysis," Revision 1, enclosed with Holtec Letter No. 5014486, appropriately identified as containing confidential information. This information is considered proprietary to Holtec International.
- (3) In making this application for withholding of proprietary information of which it is the owner, Holtec International relies upon the exemption from disclosure set forth in the Freedom of Information Act ("FOIA"), 5 USC Sec. 552(b)(4) and the Trade Secrets Act, 18 USC Sec. 1905, and NRC regulations 10CFR Part 9.17(a)(4), 2.790(a)(4), and 2.790(b)(1) for "trade secrets and commercial or financial information obtained from a person and privileged or confidential" (Exemption 4). The material for which exemption from disclosure is here sought is all "confidential commercial information", and some portions also qualify under the narrower definition of "trade secret", within the meanings assigned to those terms for purposes of FOIA Exemption 4 in, respectively, Critical Mass Energy Project v. Nuclear Regulatory Commission, 975F2d871 (DC Cir. 1992), and Public Citizen Health Research Group v. FDA, 704F2d1280 (DC Cir. 1983).
- (4) Some examples of categories of information which fit into the definition of proprietary information are:
 - a. Information that discloses a process, method, or apparatus, including supporting data and analyses, where prevention of its use by Holtec's competitors without license from Holtec International constitutes a competitive economic advantage over other companies;

AFFIDAVIT PURSUANT TO 10CFR2.790

- b. Information which, if used by a competitor, would reduce his expenditure of resources or improve his competitive position in the design, manufacture, shipment, installation, assurance of quality, or licensing of a similar product.
- c. Information which reveals cost or price information, production, capacities, budget levels, or commercial strategies of Holtec International, its customers, or its suppliers;
- d. Information which reveals aspects of past, present, or future Holtec International customer-funded development plans and programs of potential commercial value to Holtec International;
- e. Information which discloses patentable subject matter for which it may be desirable to obtain patent protection.

The information sought to be withheld is considered to be proprietary for the reasons set forth in paragraphs 4.a, 4.b, 4.d, and 4.e, above.

- (5) The information sought to be withheld is being submitted to the NRC in confidence. The information (including that compiled from many sources) is of a sort customarily held in confidence by Holtec International, and is in fact so held. The information sought to be withheld has, to the best of my knowledge and belief, consistently been held in confidence by Holtec International. No public disclosure has been made, and it is not available in public sources. All disclosures to third parties, including any required transmittals to the NRC, have been made, or must be made, pursuant to regulatory provisions or proprietary agreements which provide for maintenance of the information in confidence. Its initial designation as proprietary information, and the subsequent steps taken to prevent its unauthorized disclosure, are as set forth in paragraphs (6) and (7) following.

AFFIDAVIT PURSUANT TO 10CFR2.790

- (6) Initial approval of proprietary treatment of a document is made by the manager of the originating component, the person most likely to be acquainted with the value and sensitivity of the information in relation to industry knowledge. Access to such documents within Holtec International is limited on a "need to know" basis.
- (7) The procedure for approval of external release of such a document typically requires review by the staff manager, project manager, principal scientist or other equivalent authority, by the manager of the cognizant marketing function (or his designee), and by the Legal Operation, for technical content, competitive effect, and determination of the accuracy of the proprietary designation. Disclosures outside Holtec International are limited to regulatory bodies, customers, and potential customers, and their agents, suppliers, and licensees, and others with a legitimate need for the information, and then only in accordance with appropriate regulatory provisions or proprietary agreements.
- (8) The information classified as proprietary was developed and compiled by Holtec International at a significant cost to Holtec International. This information is classified as proprietary because it contains detailed descriptions of analytical approaches and methodologies not available elsewhere. This information would provide other parties, including competitors, with information from Holtec International's technical database and the results of evaluations performed by Holtec International. A substantial effort has been expended by Holtec International to develop this information. Release of this information would improve a competitor's position because it would enable Holtec's competitor to copy our technology and offer it for sale in competition with our company, causing us financial injury.
- (9) Public disclosure of the information sought to be withheld is likely to cause substantial harm to Holtec International's competitive position and foreclose or reduce the availability of profit-making opportunities. The information is part of Holtec International's comprehensive spent fuel storage technology base, and its commercial value extends beyond the original development cost. The value

AFFIDAVIT PURSUANT TO 10CFR2.790

of the technology base goes beyond the extensive physical database and analytical methodology, and includes development of the expertise to determine and apply the appropriate evaluation process.

The research, development, engineering, and analytical costs comprise a substantial investment of time and money by Holtec International.

The precise value of the expertise to devise an evaluation process and apply the correct analytical methodology is difficult to quantify, but it clearly is substantial.

Holtec International's competitive advantage will be lost if its competitors are able to use the results of the Holtec International experience to normalize or verify their own process or if they are able to claim an equivalent understanding by demonstrating that they can arrive at the same or similar conclusions.

The value of this information to Holtec International would be lost if the information were disclosed to the public. Making such information available to competitors without their having been required to undertake a similar expenditure of resources would unfairly provide competitors with a windfall, and deprive Holtec International of the opportunity to exercise its competitive advantage to seek an adequate return on its large investment in developing these very valuable analytical tools.

U.S. Nuclear Regulatory Commission
ATTN: Document Control Desk
Document ID 5014486
Attachment

AFFIDAVIT PURSUANT TO 10CFR2.790

STATE OF NEW JERSEY)
)
) ss:
COUNTY OF BURLINGTON)

Mr. Brian Gutherman, being duly sworn, deposes and says:

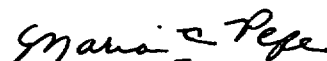
That he has read the foregoing affidavit and the matters stated therein are true and correct to the best of his knowledge, information, and belief.

Executed at Marlton, New Jersey, this 13th day of June, 2003.



Brian Gutherman
Holtec International

Subscribed and sworn before me this 13th day of June, 2003.



MARIA C. PEPE
NOTARY PUBLIC OF NEW JERSEY
My Commission Expires April 25, 2005

INSTRUCTIONS FOR LAR 9261.2, REVISION 1, SUPPLEMENT 1

1. Remove the SAR List of Effective Pages, Revision 10A in Attachment 6, and replace with Revision 10B of the List of Effective Pages.
2. Remove SAR Section 3.4 and 3.5 text and tables, Proposed Revision 10A and replace with Proposed Revision 10B text and tables. Do not remove the figures from Sections 3.4 or 3.5.

LIST OF EFFECTIVE PAGES FOR PROPOSED REVISION 10B

<u>Page</u>	<u>Revision</u>	<u>Page</u>	<u>Revision</u>
i	10A	xxx	10A
ii	10A	xxxi	10A
iii	10A	xxxii	10A
iv	10A	xxxiii	10A
v	10A	xxxiv	10A
vi	10A		
vii	10A		
viii	10A		
ix	10A		
x	10A		
xi	10A		
xii	10A		
xiii	10A		
xiv	10A		
xv	10A		
xvi	10A		
xvii	10A		
xviii	10A		
xix	10A		
xx	10A		
xxi	10A		
xxii	10A		
xxiii	10A		
xxiv	10A		
xxv	10A		
xxvi	10A		
xxvii	10A		
xxviii	10A		
xxix	10A		
xxx	10A		
xxvi	10A		
xxvii	10A		
xxvi	10A		
xxvii	10A		
xxviii	10A		
xxix	10A		
xxvii	10A		
xxvi	10A		
xxvii	10A		
xxviii	10A		
xxix	10A		
xxvii	10A		
xxvi	10A		
xxvii	10A		
xxviii	10A		
xxix	10A		
xxvii	10A		
xxvi	10A		
xxvii	10A		
xxviii	10A		
xxix	10A		
xxvii	10A		
xxvi	10A		
xxvii	10A		
xxviii	10A		
xxix	10A		

LIST OF EFFECTIVE PAGES FOR PROPOSED REVISION 10B

<u>Page</u>	<u>Revision</u>	<u>Page</u>	<u>Revision</u>
1.0-1	10A	1.2-34	10A
1.0-2	10A	1.2-35	10A
1.0-3	10A	1.2-36	10A
1.0-4	10A	1.2-37	10A
1.0-5	10A	1.2-38	10A
1.0-6	10A	1.2-39	10A
1.0-7	10A	1.2-40	10A
1.0-8	10A	1.2-41	10A
1.0-9	10A	1.2-42	10A
1.0-10	10A	1.2-43	10A
1.0-11	10A	1.2-44	10A
1.1-1	10A	1.2-45	10A
Fig. 1.1.1	7	1.2-46	10A
Fig. 1.1.2	10	1.2-47	10A
Fig. 1.1.3	10	1.2-48	10A
Fig. 1.1.4	10	1.2-49	10A
1.2-1	10A	1.2-50	10A
1.2-2	10A	1.2-51	10A
1.2-3	10A	1.2-52	10A
1.2-4	10A	1.2-53	10A
1.2-5	10A	1.2-54	10A
1.2-6	10A	1.2-55	10A
1.2-7	10A	1.2-56	10A
1.2-8	10A	1.2-57	10A
1.2-9	10A	1.2-58	10A
1.2-10	10A	1.2-59	10A
1.2-11	10A	1.2-60	10A
1.2-12	10A	1.2-61	10A
1.2-13	10A	1.2-62	10A
1.2-14	10A	1.2-63	10A
1.2-15	10A	1.2-64	10A
1.2-16	10A	1.2-65	10A
1.2-17	10A	1.2-66	10A
1.2-18	10A	1.2-67	10A
1.2-19	10A	1.2-68	10A
1.2-20	10A	1.2-69	10A
1.2-21	10A	1.2-70	10A
1.2-22	10A	1.2-71	10A
1.2-23	10A	1.2-72	10A
1.2-24	10A	1.2-73	10A
1.2-25	10A	1.2-74	10A
1.2-26	10A	1.2-75	10A
1.2-27	10A	1.2-76	10A
1.2-28	10A	1.2-77	10A
1.2-29	10A	1.2-78	10A
1.2-30	10A	Fig. 1.2.1	7
1.2-31	10A	Fig. 1.2.2	7
1.2-32	10A	Fig. 1.2.3	10
1.2-33	10A	Fig. 1.2.4	10

LIST OF EFFECTIVE PAGES FOR PROPOSED REVISION 10B

<u>Page</u>	<u>Revision</u>	<u>Page</u>	<u>Revision</u>
Fig. 1.2.5	10	1.A-3	10A
Fig. 1.2.6	7	1.A-4	10A
Fig. 1.2.7	7	1.A-5	10A
Fig. 1.2.8	10	1.A-6	10A
Fig. 1.2.9	10	1.A-7	10A
Fig. 1.2.10	10	Fig. 1.A.1	4
Fig. 1.2.10A	10	Fig. 1.A.2	4
Fig. 1.2.10B	10	Fig. 1.A.3	4
Fig. 1.2.10C	10	Fig. 1.A.4	4
Fig. 1.2.10D	10	Fig. 1.A.5	4
Fig. 1.2.11	9	1.B-1	10A
Fig. 1.2.11A	9	1.B-2	10A
Fig. 1.2.12	Deleted in Rev. 10	1.B-3	10A
Fig. 1.2.13	4	1.B-4	Deleted in Rev. 10
Fig. 1.2.13A	10A	1.B-5	Deleted in Rev. 10
Fig. 1.2.14	4	1.B-6	Deleted in Rev. 10
Fig. 1.2.15	10	1.B-7	Deleted in Rev. 10
Fig. 1.2.16	10	1.B-8	Deleted in Rev. 10
Fig. 1.2.17	10	1.B-9	Deleted in Rev. 10
1.3-1	10A	1.B-10	Deleted in Rev. 10
1.3-2	10A	1.B-11	Deleted in Rev. 10
1.3-3	10A	1.B-12	Deleted in Rev. 10
1.3-4	10A	1.B-13	Deleted in Rev. 10
1.3-5	10A	1.B-14	Deleted in Rev. 10
1.3-6	10A	1.B-15	Deleted in Rev. 10
1.3-7	10A	1.B-16	Deleted in Rev. 10
1.3-8	10A	1.B-17	Deleted in Rev. 10
1.3-9	10A	1.B-18	Deleted in Rev. 10
1.3-10	10A	1.B-19	Deleted in Rev. 10
1.3-11	10A	1.B-20	Deleted in Rev. 10
1.3-12	10A	1.C-1	9
1.3-13	10A	1.C-2	7
1.3-14	10A	1.C-3	7
1.3-15	10A	1.C-4	7
1.3-16	10A	1.C-5	7
1.3-17	10A	1.C-6	7
1.3-18	10A	1.C-7	7
1.3-19	10A	1.C-8	7
1.3-20	10A	App. 1.D (Total of 83 Pages)	8
1.4-1	10A		
1.4-2	10A		
1.4-3	Deleted in Rev. 10		
Drawings	See Section 1.4		
3 Bills-of-Material w/ 6 sheets	Deleted in Rev. 10		
1.5-1	10A		
1.5-2	10A		
1.6-1	10A		
1.6-2	10A		
1.A-1	10A		
1.A-2	10A		

LIST OF EFFECTIVE PAGES FOR PROPOSED REVISION 10B

<u>Page</u>	<u>Revision</u>	<u>Page</u>	<u>Revision</u>
2.0-1	10	Fig. 2.1.1	7
2.0-2	10	Fig. 2.1.2	6
2.0-3	10	Fig. 2.1.3	10
2.0-4	10	Fig. 2.1.4	10
2.0-5	10	Fig. 2.1.5	4
2.0-6	10	Fig. 2.1.6	4
2.1-1	10A	Fig. 2.1.7	4
2.1-2	10A	Fig. 2.1.8	4
2.1-3	10A	Fig. 2.1.9	4
2.1-4	10A	Fig. 2.1.10	6
2.1-5	10A	Fig. 2.1.11	4
2.1-6	10A	Fig. 2.1.12	4
2.1-7	10A	Fig. 2.1.13	4
2.1-8	10A	Fig. 2.1.14	6
2.1-9	10A	2.2-1	10A
2.1-10	10A	2.2-2	10A
2.1-11	10A	2.2-3	10A
2.1-12	10A	2.2-4	10A
2.1-13	10A	2.2-5	10A
2.1-14	10A	Fig. 2.2.1	4
2.1-15	10A	2.3-1	10A
2.1-16	10A	2.3-2	10A
2.1-17	10A	2.3-3	10A
2.1-18	10A	2.3-4	10A
2.1-19	10A	2.3-5	10A
2.1-20	10A	2.3-6	10A
2.1-21	10A	2.3-7	10A
2.1-22	10A	2.3-8	10A
2.1-23	10A	2.3-9	10A
2.1-24	10A	2.3-10	10A
2.1-25	10A	2.3-11	10A
2.1-26	10A	2.3-12	Deleted in Rev. 10
2.1-27	10A	Fig. 2.3.1	4
2.1-28	10A	Fig. 2.3.2	7
2.1-29	10A	2.4-1	10A
2.1-30	10A	2.4-2	10A
2.1-31	10A	2.4-3	10A
2.1-32	10A	2.4-4	10A
2.1-33	10A	2.4-5	10A
2.1-34	10A	2.4-6	10A
2.1-35	10A	2.4-7	10A
2.1-36	10A	2.5-1	10A
2.1-37	10A	2.5-2	10A
2.1-38	10A	2.5-3	10A
2.1-39	10A	2.5-4	10A
2.1-40	10A	2.5-5	10A
2.1-41	10A	2.5-6	10A
2.1-42	10A	2.5-7	10A
2.1-43	10A	2.5-8	10A
2.1-44	Deleted in Rev. 10	2.5-9	10A

LIST OF EFFECTIVE PAGES FOR PROPOSED REVISION 10B

<u>Page</u>	<u>Revision</u>	<u>Page</u>	<u>Revision</u>
2.5-10	10A	2.6-18	10A
2.5-11	10A	2.6-19	10A
2.5-12	10A	2.6-20	10A
2.5-13	10A	2.6-21	10A
2.5-14	10A	2.6-22	10A
2.5-15	10A	2.6-23	10A
2.5-16	10A	2.6-24	10A
2.5-17	10A	2.6-25	10A
2.5-18	10A	2.6-26	10A
2.5-19	10A	2.6-27	10A
2.5-20	Deleted in Rev. 10	2.6-28	10A
2.5-21	Deleted in Rev. 10	2.6-29	10A
2.5-22	Deleted in Rev. 10	2.6-30	10A
2.5-23	Deleted in Rev. 10	2.6-31	10A
2.5-24	Deleted in Rev. 10	2.6-32	10A
2.5-25	Deleted in Rev. 10	2.6-33	10A
2.5-26	Deleted in Rev. 10	2.6-34	10A
2.5-27	Deleted in Rev. 10	2.6-35	10A
2.5-28	Deleted in Rev. 10	2.6-36	10A
2.5-29	Deleted in Rev. 10	2.6-37	10A
Fig. 2.5.1	10	2.6-38	10A
Fig. 2.5.2	10	2.6-39	10A
Fig. 2.5.3	Deleted in Rev. 10	2.6-40	10A
Fig. 2.5.4	Deleted in Rev. 10	2.6-41	10A
Fig. 2.5.5	Deleted in Rev. 10	2.6-42	10A
Fig. 2.5.6	Deleted in Rev. 10	2.6-43	10A
Fig. 2.5.7	Deleted in Rev. 10	2.6-44	10A
Fig. 2.5.8	Deleted in Rev. 10	2.6-45	10A
Fig. 2.5.9	Deleted in Rev. 10	2.6-46	10A
Fig. 2.5.10	Deleted in Rev. 10	2.6-47	10A
Fig. 2.5.11	Deleted in Rev. 10	2.6-48	10A
Fig. 2.5.12	10	2.6-49	10A
Fig. 2.5.13	10	2.6-50	10A
2.6-1	10A	2.6-51	10A
2.6-2	10A	2.6-52	10A
2.6-3	10A	2.6-53	10A
2.6-4	10A	2.6-54	10A
2.6-5	10A	2.6-55	10A
2.6-6	10A	2.6-56	10A
2.6-7	10A	2.6-57	10A
2.6-8	10A	2.6-58	10A
2.6-9	10A	2.6-59	10A
2.6-10	10A	2.6-60	10A
2.6-11	10A	2.6-61	10A
2.6-12	10A	2.6-62	10A
2.6-13	10A	2.6-63	10A
2.6-14	10A	2.6-64	10A
2.6-15	10A	2.6-65	10A
2.6-16	10A	2.6-66	10A
2.6-17	10A	2.6-67	10A

LIST OF EFFECTIVE PAGES FOR PROPOSED REVISION 10B

<u>Page</u>	<u>Revision</u>	<u>Page</u>	<u>Revision</u>
2.6-68	10A	2.7-17	10A
2.6-69	10A	2.7-18	10A
2.6-70	10A	2.7-19	10A
2.6-71	10A	2.7-20	10A
2.6-72	10A	2.7-21	10A
2.6-73	10A	2.7-22	10A
Fig. 2.6.1	4	2.7-23	10A
Fig. 2.6.2	4	2.7-24	10A
Fig. 2.6.3	10A	2.7-25	10A
Fig. 2.6.4	10	2.7-26	10A
Fig. 2.6.5	6	2.7-27	10A
Fig. 2.6.6	10A	2.7-28	10A
Fig. 2.6.7	10	2.7-29	10A
Fig. 2.6.8	6	2.7-30	10A
Fig. 2.6.9	10A	2.7-31	10A
Fig. 2.6.10	10	2.7-32	10A
Fig. 2.6.11	6	2.7-33	10A
Fig. 2.6.12	7	2.7-34	10A
Fig. 2.6.13	7	2.7-35	10A
Fig. 2.6.14	7	2.7-36	10A
Fig. 2.6.15	4	2.7-37	10A
Fig. 2.6.16	8	2.7-38	10A
Fig. 2.6.17	8	2.7-39	10A
Fig. 2.6.18	8	2.7-40	10A
Fig. 2.6.19	8	2.7-41	10A
Fig. 2.6.19A	8	2.7-42	10A
Fig. 2.6.19B	8	2.7-43	10A
Fig. 2.6.19C	8	2.7-44	10A
Fig. 2.6.20	10A	2.7-45	10A
Fig. 2.6.21	7	2.7-46	10A
Fig. 2.6.22	6	2.7-47	10A
Fig. 2.6.23	8	2.7-48	10A
Fig. 2.6.24	10	2.7-49	10A
Fig. 2.6.25	10A	2.7-50	10A
2.7-1	10A	2.7-51	10A
2.7-2	10A	2.7-52	10A
2.7-3	10A	2.7-53	10A
2.7-4	10A	2.7-54	10A
2.7-5	10A	2.7-55	10A
2.7-6	10A	Fig. 2.7.1	10
2.7-7	10A	Fig. 2.7.2	10
2.7-8	10A	Fig. 2.7.3	10
2.7-9	10A	Fig. 2.7.4	10
2.7-10	10A	Fig. 2.7.5	6
2.7-11	10A	Fig. 2.7.6	6
2.7-12	10A	Fig. 2.7.7	8
2.7-13	10A	Fig. 2.7.8	8
2.7-14	10A	Fig. 2.7.9	8
2.7-15	10A	Fig. 2.7.10	8
2.7-16	10A	Fig. 2.7.11	8

LIST OF EFFECTIVE PAGES FOR PROPOSED REVISION 10B

<u>Page</u>	<u>Revision</u>	<u>Page</u>	<u>Revision</u>
Fig. 2.7.12	8	2.A-6	10A
Fig. 2.7.13	8	2.A-7	10A
Fig. 2.7.14	8	2.A-8	10A
Fig. 2.7.15	8	2.A-9	10A
Fig. 2.7.16	8	2.A-10	10A
Fig. 2.7.17	8	2.A-11	10A
Fig. 2.7.18	8	2.A-12	10A
Fig. 2.7.19 through -22	8	2.A-13	10A
2.8-1	7	2.A-14	10A
2.9-1	10A	2.A-15	10A
2.9-2	10A	2.A-16	10A
2.9-3	10A	2.A-17	10A
2.9-4	10A	2.A-18	10A
2.9-5	10A	2.A-19	10A
2.9-6	10A	2.A-20	10A
2.9-7	10A	2.A-21	10A
2.9-8	10A	2.A-22	10A
2.9-9	10A	2.A-23	10A
2.9-10	10A	2.A-24	10A
2.9-11	10A	2.A-25	10A
2.9-12	10A	2.A-26	10A
2.9-13	10A	2.A-27	10A
2.9-14	10A	2.A-28	10A
2.9-15	10A	Fig. 2.A.1.1	10
2.9-16	10A	Fig. 2.A.1.2	10
2.9-17	10A	Fig. 2.A.1.3	10
2.9-18	10A	Fig. 2.A.2.1	10
2.9-19	10A	Fig. 2.A.3.1	10
Fig. 2.9.1	8	Fig. 2.A.4.1	10
Fig. 2.9.2	8	Fig. 2.A.4.2	10
Fig. 2.9.3	8	Fig. 2.A.4.3	10
Fig. 2.9.4	8	Fig. 2.A.4.4	10
Fig. 2.9.5	8	Fig. 2.A.5.1	10
Fig. 2.9.6	8	Fig. 2.A.5.2	10
Fig. 2.9.7	8	Fig. 2.A.5.3	10
Fig. 2.9.8	8	Fig. 2.A.5.4	10
Fig. 2.9.9	8	Fig. 2.A.5.5	10
2.10-1	10	Fig. 2.A.5.6	10
2.10-2	10	Fig. 2.A.5.7	10
2.10-3	10	Fig. 2.A.5.8	10
2.10-4	10	Fig. 2.A.5.9	10
2.10-5	10	Fig. 2.A.5.10	10
2.11-1	10	Fig. 2.A.5.11	10
2.11-2	10	Fig. 2.A.5.12	10
2.11-3	10	Fig. 2.A.5.13	10
2.A-1	10A	Fig. 2.A.5.14	10
2.A-2	10A	Fig. 2.A.5.15	10
2.A-3	10A	Fig. 2.A.5.15A	10
2.A-4	10A	Fig. 2.A.5.15B	10
2.A-5	10A	Fig. 2.A.5.15C	10

LIST OF EFFECTIVE PAGES FOR PROPOSED REVISION 10B

<u>Page</u>	<u>Revision</u>	<u>Page</u>	<u>Revision</u>
Fig. 2.A.5.6		2.D-2	Deleted in Rev. 10
Fig. 2.A.5.17		2.D-3	Deleted in Rev. 10
Fig. 2.A.5.17A		2.D-4	Deleted in Rev. 10
Fig. 2.A.5.18		2.D-5	Deleted in Rev. 10
Fig. 2.A.5.19		2.D-6	Deleted in Rev. 10
Fig. 2.a.5.19A		2.D-7	Deleted in Rev. 10
2.A.5.20		2.D-8	Deleted in Rev. 10
Fig. 2.A.5.21		2.D-9	Deleted in Rev. 10
Fig. 2.A.5.21A		2.D-10	Deleted in Rev. 10
Fig. 2.A.6.1		Fig. 2.D.1	Deleted in Rev. 10
Fig. 2.A.6.2		2.F-1	Deleted in Rev. 10
Fig. 2.A.6.3		2.F-2	Deleted in Rev. 10
Fig. 2.A.6.4		2.F-3	Deleted in Rev. 10
Fig. 2.A.6.5		2.F-4	Deleted in Rev. 10
Fig. 2.A.6.6		2.F-5	Deleted in Rev. 10
Fig. 2.A.7.1		2.F-6	Deleted in Rev. 10
Fig. 2.A.7.2		2.F-7	Deleted in Rev. 10
Fig. 2.A.7.3		2.F-8	Deleted in Rev. 10
Fig. 2.A.10.1		2.F-9	Deleted in Rev. 10
Fig. 2.A.10.2		2.F-10	Deleted in Rev. 10
Fig. 2.A.10.3		Fig. 2.F.1	Deleted in Rev. 10
2.B-1	10A	2.G-1	Deleted in Rev. 10
2.B-2	10A	2.G-2	Deleted in Rev. 10
2.B-3	10A	2.G-3	Deleted in Rev. 10
2.B-4	Deleted in Rev. 10	2.G-4	Deleted in Rev. 10
2.B-5	Deleted in Rev. 10	2.G-5	Deleted in Rev. 10
2.B-6	Deleted in Rev. 10	2.G-6	Deleted in Rev. 10
2.B-7	Deleted in Rev. 10	2.G-7	Deleted in Rev. 10
2.B-8	Deleted in Rev. 10	2.G-8	Deleted in Rev. 10
2.B-9	Deleted in Rev. 10	2.G-9	Deleted in Rev. 10
2.B-10	Deleted in Rev. 10	2.G-10	Deleted in Rev. 10
2.B-11	Deleted in Rev. 10	2.H-1	Deleted in Rev. 10
2.B-12	Deleted in Rev. 10	2.H-2	Deleted in Rev. 10
2.B-13	Deleted in Rev. 10	2.H-3	Deleted in Rev. 10
2.C-1	Deleted in Rev. 10	2.H-4	Deleted in Rev. 10
2.C-2	Deleted in Rev. 10	2.H-5	Deleted in Rev. 10
2.C-3	Deleted in Rev. 10	2.H-6	Deleted in Rev. 10
2.C-4	Deleted in Rev. 10	2.H-7	Deleted in Rev. 10
2.C-5	Deleted in Rev. 10	2.H-8	Deleted in Rev. 10
2.C-6	Deleted in Rev. 10	2.H-9	Deleted in Rev. 10
2.C-7	Deleted in Rev. 10	2.H-10	Deleted in Rev. 10
2.C-8	Deleted in Rev. 10	2.H-11	Deleted in Rev. 10
2.C-9	Deleted in Rev. 10	2.H-12	Deleted in Rev. 10
2.C-10	Deleted in Rev. 10	2.H-13	Deleted in Rev. 10
2.C-11	Deleted in Rev. 10	2.H-14	Deleted in Rev. 10
2.C-12	Deleted in Rev. 10	2.H-15	Deleted in Rev. 10
2.C-13	Deleted in Rev. 10	2.H-16	Deleted in Rev. 10
2.C-14	Deleted in Rev. 10	2.H-17	Deleted in Rev. 10
Fig. 2.C.1	Deleted in Rev. 10	2.H-18	Deleted in Rev. 10
2.D-1	Deleted in Rev. 10	2.H-19	Deleted in Rev. 10

LIST OF EFFECTIVE PAGES FOR PROPOSED REVISION 10B

<u>Page</u>	<u>Revision</u>	<u>Page</u>	<u>Revision</u>
2.H-20	Deleted in Rev. 10	Fig. 2.H.6.6	Deleted in Rev. 10
2.H-21	Deleted in Rev. 10	Fig. 2.H.7.1	Deleted in Rev. 10
2.H-22	Deleted in Rev. 10	Fig. 2.H.7.2	Deleted in Rev. 10
2.H-23	Deleted in Rev. 10	Fig. 2.H.7.3	Deleted in Rev. 10
2.H-24	Deleted in Rev. 10	Fig. 2.H.10.1	Deleted in Rev. 10
2.H-25	Deleted in Rev. 10	Fig. 2.H.10.2	Deleted in Rev. 10
2.H-26	Deleted in Rev. 10	Fig. 2.H.10.3	Deleted in Rev. 10
2.H-27	Deleted in Rev. 10	2.I-1	Deleted in Rev. 10
2.H-28	Deleted in Rev. 10	2.I-2	Deleted in Rev. 10
Fig. 2.H.1	Deleted in Rev. 10	2.I-3	Deleted in Rev. 10
Fig. 2.H.2	Deleted in Rev. 10	2.I-4	Deleted in Rev. 10
Fig. 2.H.3	Deleted in Rev. 10	2.I-5	Deleted in Rev. 10
Fig. 2.H.2.1	Deleted in Rev. 10	2.I-6	Deleted in Rev. 10
Fig. 2.H.3.1	Deleted in Rev. 10	2.I-7	Deleted in Rev. 10
Fig. 2.H.4.1	Deleted in Rev. 10	2.I-8	Deleted in Rev. 10
Fig. 2.H.4.2	Deleted in Rev. 10	2.I-9	Deleted in Rev. 10
Fig. 2.H.4.3	Deleted in Rev. 10	2.I-10	Deleted in Rev. 10
Fig. 2.H.4.4	Deleted in Rev. 10	2.I-11	Deleted in Rev. 10
Fig. 2.H.5.1	Deleted in Rev. 10	Fig. 2.I.1	Deleted in Rev. 10
Fig. 2.H.5.2	Deleted in Rev. 10	Fig. 2.I.2	Deleted in Rev. 10
Fig. 2.H.5.3	Deleted in Rev. 10	Fig. 2.I.3	Deleted in Rev. 10
Fig. 2.H.5.4	Deleted in Rev. 10	Fig. 2.I.4	Deleted in Rev. 10
Fig. 2.H.5.5	Deleted in Rev. 10	Fig. 2.I.5	Deleted in Rev. 10
Fig. 2.H.5.6	Deleted in Rev. 10	Fig. 2.I.6	Deleted in Rev. 10
Fig. 2.H.5.7	Deleted in Rev. 10	Fig. 2.I.7	Deleted in Rev. 10
Fig. 2.H.5.8	Deleted in Rev. 10	2.J-1	Deleted in Rev. 10
Fig. 2.H.5.9	Deleted in Rev. 10	2.J-2	Deleted in Rev. 10
Fig. 2.H.5.10	Deleted in Rev. 10	2.J-3	Deleted in Rev. 10
Fig. 2.H.5.11	Deleted in Rev. 10	2.J-4	Deleted in Rev. 10
Fig. 2.H.5.12	Deleted in Rev. 10	2.J-5	Deleted in Rev. 10
Fig. 2.H.5.13	Deleted in Rev. 10	2.J-6	Deleted in Rev. 10
Fig. 2.H.5.14	Deleted in Rev. 10	2.J-7	Deleted in Rev. 10
Fig. 2.H.5.15	Deleted in Rev. 10	2.J-8	Deleted in Rev. 10
Fig. 2.H.5.15A	Deleted in Rev. 10	2.J-9	Deleted in Rev. 10
Fig. 2.H.5.15B	Deleted in Rev. 10	2.J-10	Deleted in Rev. 10
Fig. 2.H.5.15C	Deleted in Rev. 10	2.J-11	Deleted in Rev. 10
Fig. 2.H.5.16	Deleted in Rev. 10	2.J-12	Deleted in Rev. 10
Fig. 2.H.5.17	Deleted in Rev. 10	2.J-13	Deleted in Rev. 10
Fig. 2.H.5.17A	Deleted in Rev. 10	2.J-14	Deleted in Rev. 10
Fig. 2.H.5.18	Deleted in Rev. 10	2.J-15	Deleted in Rev. 10
Fig. 2.H.5.19	Deleted in Rev. 10	2.J-16	Deleted in Rev. 10
Fig. 2.H.5.19A	Deleted in Rev. 10	2.J-17	Deleted in Rev. 10
Fig. 2.H.5.20	Deleted in Rev. 10	2.J-18	Deleted in Rev. 10
Fig. 2.H.5.21	Deleted in Rev. 10	2.J-19	Deleted in Rev. 10
Fig. 2.H.5.21A	Deleted in Rev. 10	2.J-20	Deleted in Rev. 10
Fig. 2.H.6.1	Deleted in Rev. 10	2.J-21	Deleted in Rev. 10
Fig. 2.H.6.2	Deleted in Rev. 10	2.J-22	Deleted in Rev. 10
Fig. 2.H.6.3	Deleted in Rev. 10	2.J-23	Deleted in Rev. 10
Fig. 2.H.6.4	Deleted in Rev. 10	2.J-24	Deleted in Rev. 10
Fig. 2.H.6.5	Deleted in Rev. 10	2.J-25	Deleted in Rev. 10

LIST OF EFFECTIVE PAGES FOR PROPOSED REVISION 10B

<u>Page</u>	<u>Revision</u>		<u>Page</u>	<u>Revision</u>
2.J-26	Deleted in Rev. 10		Fig. 2.N.1	Deleted in Rev. 10
2.J-27	Deleted in Rev. 10		2.O-1	Deleted in Rev. 10
2.J-28	Deleted in Rev. 10		2.O-2	Deleted in Rev. 10
2.J-29	Deleted in Rev. 10		2.O-3	Deleted in Rev. 10
2.J-30	Deleted in Rev. 10		2.O-4	Deleted in Rev. 10
2.J-31	Deleted in Rev. 10		2.O-5	Deleted in Rev. 10
2.J-32	Deleted in Rev. 10		2.O-6	Deleted in Rev. 10
2.J-33	Deleted in Rev. 10		2.O-7	Deleted in Rev. 10
2.J-34	Deleted in Rev. 10		2.O-8	Deleted in Rev. 10
2.J-35	Deleted in Rev. 10		2.O-9	Deleted in Rev. 10
2.K-1	Deleted in Rev. 10		2.O-10	Deleted in Rev. 10
2.K-2	Deleted in Rev. 10		2.O-11	Deleted in Rev. 10
2.K-3	Deleted in Rev. 10		2.O-12	Deleted in Rev. 10
2.K-4	Deleted in Rev. 10		2.O-13	Deleted in Rev. 10
2.K-5	Deleted in Rev. 10		2.O-14	Deleted in Rev. 10
2.K-6	Deleted in Rev. 10		2.O-15	Deleted in Rev. 10
2.K-7	Deleted in Rev. 10		2.O-16	Deleted in Rev. 10
2.K-8	Deleted in Rev. 10		2.O-17	Deleted in Rev. 10
2.K-9	Deleted in Rev. 10		2.O-18	Deleted in Rev. 10
2.K-10	Deleted in Rev. 10		2.O-19	Deleted in Rev. 10
Fig. 2.K.1	Deleted in Rev. 10		2.O-20	Deleted in Rev. 10
Fig. 2.K.2	Deleted in Rev. 10		2.O-21	Deleted in Rev. 10
Fig. 2.K.3	Deleted in Rev. 10		2.O-22	Deleted in Rev. 10
Fig. 2.K.4	Deleted in Rev. 10		2.O-23	Deleted in Rev. 10
Fig. 2.K.5	Deleted in Rev. 10		2.O-24	Deleted in Rev. 10
Fig. 2.K.6	Deleted in Rev. 10		2.P-1	Deleted in Rev. 10
2.L-1	Deleted in Rev. 10		2.P-2	Deleted in Rev. 10
2.L-2	Deleted in Rev. 10		2.P-3	Deleted in Rev. 10
2.L-3	Deleted in Rev. 10		2.P-4	Deleted in Rev. 10
2.L-4	Deleted in Rev. 10		2.P-5	Deleted in Rev. 10
2.L-5	Deleted in Rev. 10		2.P-6	Deleted in Rev. 10
2.L-6	Deleted in Rev. 10		2.P-7	Deleted in Rev. 10
2.L-7	Deleted in Rev. 10		2.P-8	Deleted in Rev. 10
2.L-8	Deleted in Rev. 10		2.P-9	Deleted in Rev. 10
2.L-9	Deleted in Rev. 10		2.P-10	Deleted in Rev. 10
2.M-1	Deleted in Rev. 10		2.P-11	Deleted in Rev. 10
2.M-2	Deleted in Rev. 10		Fig. 2.P.1	Deleted in Rev. 10
2.M-3	Deleted in Rev. 10		Fig. 2.P.2	Deleted in Rev. 10
2.M-4	Deleted in Rev. 10		2.Q-1	Deleted in Rev. 10
2.M-5	Deleted in Rev. 10		2.Q-2	Deleted in Rev. 10
2.M-6	Deleted in Rev. 10			
2.M-7	Deleted in Rev. 10			
2.M-8	Deleted in Rev. 10			
2.N-1	Deleted in Rev. 10			
2.N-2	Deleted in Rev. 10			
2.N-3	Deleted in Rev. 10			
2.N-4	Deleted in Rev. 10			
2.N-5	Deleted in Rev. 10			
2.N-6	Deleted in Rev. 10			
2.N-7	Deleted in Rev. 10			

LIST OF EFFECTIVE PAGES FOR PROPOSED REVISION 10B

<u>Page</u>	<u>Revision</u>	<u>Page</u>	<u>Revision</u>
2.Q-3	Deleted in Rev. 10	2.V-2	Deleted in Rev. 10
Fig. 2.Q.1	Deleted in Rev. 10	2.V-3	Deleted in Rev. 10
Fig. 2.Q.2	Deleted in Rev. 10	2.V-4	Deleted in Rev. 10
2.R-1	Deleted in Rev. 10	2.V-5	Deleted in Rev. 10
2.R-2	Deleted in Rev. 10	2.V-6	Deleted in Rev. 10
2.R-3	Deleted in Rev. 10	2.V-7	Deleted in Rev. 10
2.R-4	Deleted in Rev. 10	2.V-8	Deleted in Rev. 10
2.R-5	Deleted in Rev. 10	2.V-9	Deleted in Rev. 10
2.R-6	Deleted in Rev. 10	2.V-10	Deleted in Rev. 10
2.R-7	Deleted in Rev. 10	2.V-11	Deleted in Rev. 10
2.R-8	Deleted in Rev. 10	2.V-12	Deleted in Rev. 10
2.R-9	Deleted in Rev. 10	2.W-1	Deleted in Rev. 10
Fig. 2.R.1	Deleted in Rev. 10	2.W-2	Deleted in Rev. 10
Fig. 2.R.2	Deleted in Rev. 10	2.W-3	Deleted in Rev. 10
2.T-1	Deleted in Rev. 10	2.W-4	Deleted in Rev. 10
2.T-2	Deleted in Rev. 10	2.W-5	Deleted in Rev. 10
2.T-3	Deleted in Rev. 10	2.W-6	Deleted in Rev. 10
2.T-4	Deleted in Rev. 10	2.W-7	Deleted in Rev. 10
2.T-5	Deleted in Rev. 10	2.W-8	Deleted in Rev. 10
2.S-1	Deleted in Rev. 10	2.W-9	Deleted in Rev. 10
2.S-2	Deleted in Rev. 10	2.W-10	Deleted in Rev. 10
2.S-3	Deleted in Rev. 10	2.W-11	Deleted in Rev. 10
2.S-4	Deleted in Rev. 10	2.W-12	Deleted in Rev. 10
2.S-5	Deleted in Rev. 10	2.W-13	Deleted in Rev. 10
2.S-6	Deleted in Rev. 10	2.W-14	Deleted in Rev. 10
2.U-1	Deleted in Rev. 10	2.W-15	Deleted in Rev. 10
2.U-2	Deleted in Rev. 10	2.W-16	Deleted in Rev. 10
2.U-3	Deleted in Rev. 10	2.W-17	Deleted in Rev. 10
2.U-4	Deleted in Rev. 10	2.W-18	Deleted in Rev. 10
2.U-5	Deleted in Rev. 10	2.W-19	Deleted in Rev. 10
2.U-6	Deleted in Rev. 10	2.W-20	Deleted in Rev. 10
2.U-7	Deleted in Rev. 10	2.W-21	Deleted in Rev. 10
2.U-8	Deleted in Rev. 10	2.W-22	Deleted in Rev. 10
2.U-9	Deleted in Rev. 10	2.W-23	Deleted in Rev. 10
2.U-10	Deleted in Rev. 10	2.W-24	Deleted in Rev. 10
2.U-11	Deleted in Rev. 10	2.W-25	Deleted in Rev. 10
2.U-12	Deleted in Rev. 10	2.W-26	Deleted in Rev. 10
2.U-13	Deleted in Rev. 10	2.X-1	Deleted in Rev. 10
2.U-14	Deleted in Rev. 10	2.X-2	Deleted in Rev. 10
2.U-15	Deleted in Rev. 10	2.X-3	Deleted in Rev. 10
2.U-16	Deleted in Rev. 10	2.X-4	Deleted in Rev. 10
2.U-17	Deleted in Rev. 10	2.X-5	Deleted in Rev. 10
2.U-18	Deleted in Rev. 10	2.X-6	Deleted in Rev. 10
2.U-19	Deleted in Rev. 10	2.X-7	Deleted in Rev. 10
2.U-20	Deleted in Rev. 10	2.X-8	Deleted in Rev. 10
2.U-21	Deleted in Rev. 10	2.X-9	Deleted in Rev. 10
2.U-22	Deleted in Rev. 10	2.X-10	Deleted in Rev. 10
2.U-23	Deleted in Rev. 10	2.X-11	Deleted in Rev. 10
2.U-24	Deleted in Rev. 10	2.X-12	Deleted in Rev. 10
2.U-25	Deleted in Rev. 10	2.X-13	Deleted in Rev. 10
2.V-1	Deleted in Rev. 10	2.X-14	Deleted in Rev. 10

LIST OF EFFECTIVE PAGES FOR PROPOSED REVISION 10B

<u>Page</u>	<u>Revision</u>	<u>Page</u>	<u>Revision</u>
2.Y-1	Deleted in Rev. 10	2.AA-49	Deleted in Rev. 10
2.Z-1	Deleted in Rev. 10	2.AA-50	Deleted in Rev. 10
2.AA-1	Deleted in Rev. 10	2.AA-51	Deleted in Rev. 10
2.AA-2	Deleted in Rev. 10	2.AA-52	Deleted in Rev. 10
2.AA-3	Deleted in Rev. 10	2.AA-53	Deleted in Rev. 10
2.AA-4	Deleted in Rev. 10	2.AA-54	Deleted in Rev. 10
2.AA-5	Deleted in Rev. 10	2.AA-55	Deleted in Rev. 10
2.AA-6	Deleted in Rev. 10	2.AA-56	Deleted in Rev. 10
2.AA-7	Deleted in Rev. 10	2.AA-57	Deleted in Rev. 10
2.AA-8	Deleted in Rev. 10	2.AA-58	Deleted in Rev. 10
2.AA-9	Deleted in Rev. 10	2.AA-59	Deleted in Rev. 10
2.AA-10	Deleted in Rev. 10	2.AA-60	Deleted in Rev. 10
2.AA-11	Deleted in Rev. 10	2.AA-61	Deleted in Rev. 10
2.AA-12	Deleted in Rev. 10	2.AA-62	Deleted in Rev. 10
2.AA-13	Deleted in Rev. 10	2.AA-63	Deleted in Rev. 10
2.AA-14	Deleted in Rev. 10	2.AA-64	Deleted in Rev. 10
2.AA-14	Deleted in Rev. 10	2.AA-65	Deleted in Rev. 10
2.AA-15	Deleted in Rev. 10	2.AA-66	Deleted in Rev. 10
2.AA-16	Deleted in Rev. 10	2.AA-67	Deleted in Rev. 10
2.AA-17	Deleted in Rev. 10	2.AA-68	Deleted in Rev. 10
2.AA-18	Deleted in Rev. 10	2.AA-69	Deleted in Rev. 10
2.AA-19	Deleted in Rev. 10	2.AA-70	Deleted in Rev. 10
2.AA-20	Deleted in Rev. 10	2.AB-1	Deleted in Rev. 10
2.AA-21	Deleted in Rev. 10	2.AB-2	Deleted in Rev. 10
2.AA-22	Deleted in Rev. 10	2.AB-3	Deleted in Rev. 10
2.AA-23	Deleted in Rev. 10	2.AB-4	Deleted in Rev. 10
2.AA-24	Deleted in Rev. 10	2.AB-5	Deleted in Rev. 10
2.AA-25	Deleted in Rev. 10	2.AB-6	Deleted in Rev. 10
2.AA-26	Deleted in Rev. 10	2.AB-7	Deleted in Rev. 10
2.AA-27	Deleted in Rev. 10	2.AB-8	Deleted in Rev. 10
2.AA-28	Deleted in Rev. 10	2.AB-9	Deleted in Rev. 10
2.AA-29	Deleted in Rev. 10	2.AB-10	Deleted in Rev. 10
2.AA-30	Deleted in Rev. 10	2.AC-1	Deleted in Rev. 10
2.AA-31	Deleted in Rev. 10	2.AC-2	Deleted in Rev. 10
2.AA-32	Deleted in Rev. 10	2.AC-3	Deleted in Rev. 10
2.AA-33	Deleted in Rev. 10	2.AC-4	Deleted in Rev. 10
2.AA-34	Deleted in Rev. 10	2.AC-5	Deleted in Rev. 10
2.AA-35	Deleted in Rev. 10	2.AC-6	Deleted in Rev. 10
2.AA-36	Deleted in Rev. 10	2.AC-7	Deleted in Rev. 10
2.AA-37	Deleted in Rev. 10	2.AC-8	Deleted in Rev. 10
2.AA-38	Deleted in Rev. 10	2.AC-9	Deleted in Rev. 10
2.AA-39	Deleted in Rev. 10	2.AC-10	Deleted in Rev. 10
2.AA-40	Deleted in Rev. 10	2.AC-11	Deleted in Rev. 10
2.AA-41	Deleted in Rev. 10	2.AC-12	Deleted in Rev. 10
2.AA-42	Deleted in Rev. 10	2.AC-13	Deleted in Rev. 10
2.AA-43	Deleted in Rev. 10	2.AC-14	Deleted in Rev. 10
2.AA-44	Deleted in Rev. 10	2.AC-15	Deleted in Rev. 10
2.AA-45	Deleted in Rev. 10	2.AC-16	Deleted in Rev. 10
2.AA-46	Deleted in Rev. 10	2.AC-17	Deleted in Rev. 10
2.AA-47	Deleted in Rev. 10	2.AC-18	Deleted in Rev. 10
2.AA-48	Deleted in Rev. 10	2.AC-19	Deleted in Rev. 10

LIST OF EFFECTIVE PAGES FOR PROPOSED REVISION 10B

<u>Page</u>	<u>Revision</u>	<u>Page</u>	<u>Revision</u>
2.AC-20	Deleted in Rev. 10	2.AC-71	Deleted in Rev. 10
2.AC-21	Deleted in Rev. 10	2.AC-72	Deleted in Rev. 10
2.AC-22	Deleted in Rev. 10	2.AC-73	Deleted in Rev. 10
2.AC-23	Deleted in Rev. 10	2.AC-74	Deleted in Rev. 10
2.AC-24	Deleted in Rev. 10	2.AC-75	Deleted in Rev. 10
2.AC-25	Deleted in Rev. 10	2.AC-76	Deleted in Rev. 10
2.AC-26	Deleted in Rev. 10	2.AC-77	Deleted in Rev. 10
2.AC-27	Deleted in Rev. 10	2.AC-78	Deleted in Rev. 10
2.AC-28	Deleted in Rev. 10	2.AC-79	Deleted in Rev. 10
2.AC-29	Deleted in Rev. 10	2.AC-80	Deleted in Rev. 10
2.AC-30	Deleted in Rev. 10	2.AC-81	Deleted in Rev. 10
2.AC-31	Deleted in Rev. 10	2.AC-82	Deleted in Rev. 10
2.AC-32	Deleted in Rev. 10	2.AC-83	Deleted in Rev. 10
2.AC-33	Deleted in Rev. 10	2.AC-84	Deleted in Rev. 10
2.AC-34	Deleted in Rev. 10	2.AC-85	Deleted in Rev. 10
2.AC-35	Deleted in Rev. 10	2.AC-86	Deleted in Rev. 10
2.AC-36	Deleted in Rev. 10	2.AC-87	Deleted in Rev. 10
2.AC-37	Deleted in Rev. 10	2.AC-88	Deleted in Rev. 10
2.AC-38	Deleted in Rev. 10	2.AC-89	Deleted in Rev. 10
2.AC-39	Deleted in Rev. 10	2.AC-90	Deleted in Rev. 10
2.AC-40	Deleted in Rev. 10	2.AC-91	Deleted in Rev. 10
2.AC-41	Deleted in Rev. 10	2.AC-92	Deleted in Rev. 10
2.AC-42	Deleted in Rev. 10	2.AC-93	Deleted in Rev. 10
2.AC-43	Deleted in Rev. 10	2.AC-94	Deleted in Rev. 10
2.AC-44	Deleted in Rev. 10	2.AC-95	Deleted in Rev. 10
2.AC-45	Deleted in Rev. 10	2.AC-96	Deleted in Rev. 10
2.AC-46	Deleted in Rev. 10	2.AC-97	Deleted in Rev. 10
2.AC-47	Deleted in Rev. 10	2.AC-98	Deleted in Rev. 10
2.AC-48	Deleted in Rev. 10	2.AC-99	Deleted in Rev. 10
2.AC-49	Deleted in Rev. 10	2.AC-100	Deleted in Rev. 10
2.AC-50	Deleted in Rev. 10	2.AC-101	Deleted in Rev. 10
2.AC-51	Deleted in Rev. 10	2.AC-102	Deleted in Rev. 10
2.AC-52	Deleted in Rev. 10	2.AC-103	Deleted in Rev. 10
2.AC-53	Deleted in Rev. 10	2.AC-104	Deleted in Rev. 10
2.AC-54	Deleted in Rev. 10	2.AC-105	Deleted in Rev. 10
2.AC-55	Deleted in Rev. 10	2.AC-106	Deleted in Rev. 10
2.AC-56	Deleted in Rev. 10	2.AC-107	Deleted in Rev. 10
2.AC-57	Deleted in Rev. 10	2.AC-108	Deleted in Rev. 10
2.AC-58	Deleted in Rev. 10	2.AC-109	Deleted in Rev. 10
2.AC-59	Deleted in Rev. 10	2.AC-110	Deleted in Rev. 10
2.AC-60	Deleted in Rev. 10	2.AC-111	Deleted in Rev. 10
2.AC-61	Deleted in Rev. 10	2.AC-112	Deleted in Rev. 10
2.AC-62	Deleted in Rev. 10	2.AC-113	Deleted in Rev. 10
2.AC-63	Deleted in Rev. 10	2.AC-114	Deleted in Rev. 10
2.AC-64	Deleted in Rev. 10	2.AC-115	Deleted in Rev. 10
2.AC-65	Deleted in Rev. 10	2.AC-116	Deleted in Rev. 10
2.AC-66	Deleted in Rev. 10	2.AC-117	Deleted in Rev. 10
2.AC-67	Deleted in Rev. 10	2.AC-118	Deleted in Rev. 10
2.AC-68	Deleted in Rev. 10	2.AC-170	Deleted in Rev. 10
2.AC-69	Deleted in Rev. 10	2.AC-171	Deleted in Rev. 10
2.AC-70	Deleted in Rev. 10	2.AC-172	Deleted in Rev. 10

LIST OF EFFECTIVE PAGES FOR PROPOSED REVISION 10B

<u>Page</u>	<u>Revision</u>		<u>Page</u>	<u>Revision</u>
2.AC-173	Deleted in Rev. 10		2.AC-224	Deleted in Rev. 10
2.AC-174	Deleted in Rev. 10		2.AC-225	Deleted in Rev. 10
2.AC-175	Deleted in Rev. 10		2.AC-226	Deleted in Rev. 10
2.AC-176	Deleted in Rev. 10		2.AC-227	Deleted in Rev. 10
2.AC-177	Deleted in Rev. 10		2.AC-228	Deleted in Rev. 10
2.AC-178	Deleted in Rev. 10		2.AC-229	Deleted in Rev. 10
2.AC-179	Deleted in Rev. 10		2.AC-230	Deleted in Rev. 10
2.AC-180	Deleted in Rev. 10		2.AC-231	Deleted in Rev. 10
2.AC-181	Deleted in Rev. 10		2.AC-232	Deleted in Rev. 10
2.AC-182	Deleted in Rev. 10		2.AC-233	Deleted in Rev. 10
2.AC-183	Deleted in Rev. 10		2.AC-234	Deleted in Rev. 10
2.AC-184	Deleted in Rev. 10		2.AC-235	Deleted in Rev. 10
2.AC-185	Deleted in Rev. 10		2.AC-236	Deleted in Rev. 10
2.AC-186	Deleted in Rev. 10		2.AC-237	Deleted in Rev. 10
2.AC-187	Deleted in Rev. 10		2.AC-238	Deleted in Rev. 10
2.AC-188	Deleted in Rev. 10		2.AC-239	Deleted in Rev. 10
2.AC-189	Deleted in Rev. 10		2.AC-240	Deleted in Rev. 10
2.AC-190	Deleted in Rev. 10		2.AC-241	Deleted in Rev. 10
2.AC-191	Deleted in Rev. 10		2.AC-242	Deleted in Rev. 10
2.AC-192	Deleted in Rev. 10		2.AC-243	Deleted in Rev. 10
2.AC-193	Deleted in Rev. 10		2.AC-244	Deleted in Rev. 10
2.AC-194	Deleted in Rev. 10		2.AC-245	Deleted in Rev. 10
2.AC-195	Deleted in Rev. 10		2.AC-246	Deleted in Rev. 10
2.AC-196	Deleted in Rev. 10		2.AC-247	Deleted in Rev. 10
2.AC-197	Deleted in Rev. 10		2.AC-248	Deleted in Rev. 10
2.AC-198	Deleted in Rev. 10		2.AC-249	Deleted in Rev. 10
2.AC-199	Deleted in Rev. 10		2.AC-250	Deleted in Rev. 10
2.AC-200	Deleted in Rev. 10		2.AC-251	Deleted in Rev. 10
2.AC-201	Deleted in Rev. 10		2.AC-252	Deleted in Rev. 10
2.AC-202	Deleted in Rev. 10		2.AC-253	Deleted in Rev. 10
2.AC-203	Deleted in Rev. 10		2.AC-254	Deleted in Rev. 10
2.AC-204	Deleted in Rev. 10		2.AC-255	Deleted in Rev. 10
2.AC-205	Deleted in Rev. 10		2.AC-256	Deleted in Rev. 10
2.AC-206	Deleted in Rev. 10		2.AC-257	Deleted in Rev. 10
2.AC-207	Deleted in Rev. 10		2.AC-258	Deleted in Rev. 10
2.AC-208	Deleted in Rev. 10		2.AC-259	Deleted in Rev. 10
2.AC-209	Deleted in Rev. 10		2.AC-260	Deleted in Rev. 10
2.AC-210	Deleted in Rev. 10		2.AC-261	Deleted in Rev. 10
2.AC-211	Deleted in Rev. 10		2.AC-262	Deleted in Rev. 10
2.AC-212	Deleted in Rev. 10		2.AC-263	Deleted in Rev. 10
2.AC-213	Deleted in Rev. 10		2.AC-264	Deleted in Rev. 10
2.AC-214	Deleted in Rev. 10		2.AC-265	Deleted in Rev. 10
2.AC-215	Deleted in Rev. 10		2.AC-266	Deleted in Rev. 10
2.AC-216	Deleted in Rev. 10		2.AC-267	Deleted in Rev. 10
2.AC-217	Deleted in Rev. 10		2.AC-268	Deleted in Rev. 10
2.AC-218	Deleted in Rev. 10		2.AC-269	Deleted in Rev. 10
2.AC-219	Deleted in Rev. 10		2.AC-270	Deleted in Rev. 10
2.AC-220	Deleted in Rev. 10		2.AC-271	Deleted in Rev. 10
2.AC-221	Deleted in Rev. 10		2.AC-272	Deleted in Rev. 10
2.AC-222	Deleted in Rev. 10		2.AC-273	Deleted in Rev. 10
2.AC-223	Deleted in Rev. 10		2.AC-274	Deleted in Rev. 10

LIST OF EFFECTIVE PAGES FOR PROPOSED REVISION 10B

<u>Page</u>	<u>Revision</u>	<u>Page</u>	<u>Revision</u>
2.AC-275	Deleted in Rev. 10	2.AC-326	Deleted in Rev. 10
2.AC-276	Deleted in Rev. 10	2.AC-327	Deleted in Rev. 10
2.AC-277	Deleted in Rev. 10	2.AC-328	Deleted in Rev. 10
2.AC-278	Deleted in Rev. 10	2.AC-329	Deleted in Rev. 10
2.AC-279	Deleted in Rev. 10	2.AC-330	Deleted in Rev. 10
2.AC-280	Deleted in Rev. 10	2.AC-331	Deleted in Rev. 10
2.AC-281	Deleted in Rev. 10	2.AC-332	Deleted in Rev. 10
2.AC-282	Deleted in Rev. 10	2.AC-333	Deleted in Rev. 10
2.AC-283	Deleted in Rev. 10	2.AC-334	Deleted in Rev. 10
2.AC-284	Deleted in Rev. 10	2.AC-335	Deleted in Rev. 10
2.AC-285	Deleted in Rev. 10	2.AC-336	Deleted in Rev. 10
2.AC-286	Deleted in Rev. 10	2.AC-337	Deleted in Rev. 10
2.AC-287	Deleted in Rev. 10	2.AC-338	Deleted in Rev. 10
2.AC-288	Deleted in Rev. 10	2.AC-339	Deleted in Rev. 10
2.AC-289	Deleted in Rev. 10	2.AC-340	Deleted in Rev. 10
2.AC-290	Deleted in Rev. 10	2.AC-341	Deleted in Rev. 10
2.AC-291	Deleted in Rev. 10	2.AC-342	Deleted in Rev. 10
2.AC-292	Deleted in Rev. 10	2.AC-343	Deleted in Rev. 10
2.AC-293	Deleted in Rev. 10	2.AC-344	Deleted in Rev. 10
2.AC-294	Deleted in Rev. 10	2.AC-345	Deleted in Rev. 10
2.AC-295	Deleted in Rev. 10	2.AC-346	Deleted in Rev. 10
2.AC-296	Deleted in Rev. 10	2.AC-347	Deleted in Rev. 10
2.AC-297	Deleted in Rev. 10	2.AC-348	Deleted in Rev. 10
2.AC-298	Deleted in Rev. 10	2.AC-349	Deleted in Rev. 10
2.AC-299	Deleted in Rev. 10	2.AC-350	Deleted in Rev. 10
2.AC-300	Deleted in Rev. 10	2.AC-351	Deleted in Rev. 10
2.AC-301	Deleted in Rev. 10	2.AC-352	Deleted in Rev. 10
2.AC-302	Deleted in Rev. 10	2.AC-353	Deleted in Rev. 10
2.AC-303	Deleted in Rev. 10	2.AC-354	Deleted in Rev. 10
2.AC-304	Deleted in Rev. 10	2.AC-355	Deleted in Rev. 10
2.AC-305	Deleted in Rev. 10	2.AC-356	Deleted in Rev. 10
2.AC-306	Deleted in Rev. 10	2.AC-357	Deleted in Rev. 10
2.AC-307	Deleted in Rev. 10	2.AC-358	Deleted in Rev. 10
2.AC-308	Deleted in Rev. 10	2.AC-359	Deleted in Rev. 10
2.AC-309	Deleted in Rev. 10	2.AC-360	Deleted in Rev. 10
2.AC-310	Deleted in Rev. 10	2.AC-361	Deleted in Rev. 10
2.AC-311	Deleted in Rev. 10	2.AC-362	Deleted in Rev. 10
2.AC-312	Deleted in Rev. 10	2.AC-363	Deleted in Rev. 10
2.AC-313	Deleted in Rev. 10	2.AC-364	Deleted in Rev. 10
2.AC-314	Deleted in Rev. 10	2.AC-365	Deleted in Rev. 10
2.AC-315	Deleted in Rev. 10	2.AC-366	Deleted in Rev. 10
2.AC-316	Deleted in Rev. 10	2.AC-367	Deleted in Rev. 10
2.AC-317	Deleted in Rev. 10	2.AC-368	Deleted in Rev. 10
2.AC-318	Deleted in Rev. 10	2.AC-369	Deleted in Rev. 10
2.AC-319	Deleted in Rev. 10	2.AC-370	Deleted in Rev. 10
2.AC-320	Deleted in Rev. 10	2.AC-371	Deleted in Rev. 10
2.AC-321	Deleted in Rev. 10	2.AC-372	Deleted in Rev. 10
2.AC-322	Deleted in Rev. 10	2.AC-373	Deleted in Rev. 10
2.AC-323	Deleted in Rev. 10	2.AC-374	Deleted in Rev. 10
2.AC-324	Deleted in Rev. 10	2.AC-375	Deleted in Rev. 10
2.AC-325	Deleted in Rev. 10	2.AC-376	Deleted in Rev. 10

LIST OF EFFECTIVE PAGES FOR PROPOSED REVISION 10B

<u>Page</u>	<u>Revision</u>	<u>Page</u>	<u>Revision</u>
2.AC-377	Deleted in Rev. 10	Fig. 2.AD.2	Deleted in Rev. 10
2.AC-378	Deleted in Rev. 10	2.AE-1	Deleted in Rev. 10
2.AC-379	Deleted in Rev. 10	2.AE-2	Deleted in Rev. 10
2.AC-380	Deleted in Rev. 10	2.AE-3	Deleted in Rev. 10
2.AC-381	Deleted in Rev. 10	2.AE-4	Deleted in Rev. 10
2.AC-382	Deleted in Rev. 10	2.AE-5	Deleted in Rev. 10
2.AC-383	Deleted in Rev. 10	2.AE-6	Deleted in Rev. 10
2.AC-384	Deleted in Rev. 10	2.AE-7	Deleted in Rev. 10
2.AC-385	Deleted in Rev. 10	2.AE-8	Deleted in Rev. 10
2.AC-386	Deleted in Rev. 10	2.AE-9	Deleted in Rev. 10
2.AC-387	Deleted in Rev. 10	2.AE-10	Deleted in Rev. 10
2.AC-388	Deleted in Rev. 10	2.AE-11	Deleted in Rev. 10
2.AC-389	Deleted in Rev. 10	2.AE-12	Deleted in Rev. 10
2.AC-390	Deleted in Rev. 10	2.AE-13	Deleted in Rev. 10
2.AC-391	Deleted in Rev. 10	2.AE-14	Deleted in Rev. 10
2.AC-392	Deleted in Rev. 10	2.AE-15	Deleted in Rev. 10
2.AC-393	Deleted in Rev. 10	2.AE-16	Deleted in Rev. 10
2.AC-394	Deleted in Rev. 10	2.AE-17	Deleted in Rev. 10
2.AC-395	Deleted in Rev. 10	2.AE-18	Deleted in Rev. 10
2.AC-396	Deleted in Rev. 10	2.AE-19	Deleted in Rev. 10
2.AC-397	Deleted in Rev. 10	2.AE-20	Deleted in Rev. 10
2.AC-398	Deleted in Rev. 10	2.AE-21	Deleted in Rev. 10
2.AC-399	Deleted in Rev. 10	2.AE-22	Deleted in Rev. 10
2.AC-400	Deleted in Rev. 10	2.AE-23	Deleted in Rev. 10
2.AD-1	Deleted in Rev. 10	2.AE-24	Deleted in Rev. 10
2.AD-2	Deleted in Rev. 10	2.AE-25	Deleted in Rev. 10
2.AD-3	Deleted in Rev. 10	2.AE-26	Deleted in Rev. 10
2.AD-4	Deleted in Rev. 10	2.AE-27	Deleted in Rev. 10
2.AD-5	Deleted in Rev. 10	2.AE-28	Deleted in Rev. 10
2.AD-6	Deleted in Rev. 10	2.AE-29	Deleted in Rev. 10
2.AD-7	Deleted in Rev. 10	2.AE-30	Deleted in Rev. 10
2.AD-8	Deleted in Rev. 10	2.AE-31	Deleted in Rev. 10
2.AD-9	Deleted in Rev. 10	2.AE-32	Deleted in Rev. 10
2.AD-10	Deleted in Rev. 10	2.AE-33	Deleted in Rev. 10
2.AD-11	Deleted in Rev. 10	2.AE-34	Deleted in Rev. 10
2.AD-12	Deleted in Rev. 10	2.AE-35	Deleted in Rev. 10
2.AD-13	Deleted in Rev. 10	2.AE-36	Deleted in Rev. 10
2.AD-14	Deleted in Rev. 10	2.AE-37	Deleted in Rev. 10
2.AD-15	Deleted in Rev. 10	2.AE-38	Deleted in Rev. 10
2.AD-16	Deleted in Rev. 10	2.AE-39	Deleted in Rev. 10
2.AD-17	Deleted in Rev. 10	2.AE-40	Deleted in Rev. 10
2.AD-18	Deleted in Rev. 10	2.AE-41	Deleted in Rev. 10
2.AD-19	Deleted in Rev. 10	2.AE-42	Deleted in Rev. 10
2.AD-20	Deleted in Rev. 10	2.AE-43	Deleted in Rev. 10
2.AD-21	Deleted in Rev. 10	2.AE-44	Deleted in Rev. 10
2.AD-22	Deleted in Rev. 10	2.AE-45	Deleted in Rev. 10
2.AD-23	Deleted in Rev. 10	2.AE-46	Deleted in Rev. 10
2.AD-24	Deleted in Rev. 10	2.AE-47	Deleted in Rev. 10
2.AD-25	Deleted in Rev. 10	2.AE-48	Deleted in Rev. 10
2.AD-26	Deleted in Rev. 10	2.AE-49	Deleted in Rev. 10
Fig. 2.AD.1	Deleted in Rev. 10	2.AE-50	Deleted in Rev. 10

LIST OF EFFECTIVE PAGES FOR PROPOSED REVISION 10B

<u>Page</u>	<u>Revision</u>	<u>Page</u>	<u>Revision</u>
2.AE-51	Deleted in Rev. 10	2.AE-102	Deleted in Rev. 10
2.AE-52	Deleted in Rev. 10	2.AE-103	Deleted in Rev. 10
2.AE-53	Deleted in Rev. 10	2.AE-104	Deleted in Rev. 10
2.AE-54	Deleted in Rev. 10	2.AE-105	Deleted in Rev. 10
2.AE-55	Deleted in Rev. 10	2.AE-106	Deleted in Rev. 10
2.AE-56	Deleted in Rev. 10	2.AE-107	Deleted in Rev. 10
2.AE-57	Deleted in Rev. 10	2.AE-108	Deleted in Rev. 10
2.AE-58	Deleted in Rev. 10	2.AE-109	Deleted in Rev. 10
2.AE-59	Deleted in Rev. 10	2.AE-110	Deleted in Rev. 10
2.AE-60	Deleted in Rev. 10	2.AE-111	Deleted in Rev. 10
2.AE-61	Deleted in Rev. 10	2.AE-112	Deleted in Rev. 10
2.AE-62	Deleted in Rev. 10	2.AE-113	Deleted in Rev. 10
2.AE-63	Deleted in Rev. 10	2.AE-114	Deleted in Rev. 10
2.AE-64	Deleted in Rev. 10	2.AE-115	Deleted in Rev. 10
2.AE-65	Deleted in Rev. 10	2.AE-116	Deleted in Rev. 10
2.AE-66	Deleted in Rev. 10	2.AE-117	Deleted in Rev. 10
2.AE-67	Deleted in Rev. 10	2.AE-118	Deleted in Rev. 10
2.AE-68	Deleted in Rev. 10	2.AE-119	Deleted in Rev. 10
2.AE-69	Deleted in Rev. 10	2.AE-120	Deleted in Rev. 10
2.AE-70	Deleted in Rev. 10	2.AE-121	Deleted in Rev. 10
2.AE-71	Deleted in Rev. 10	2.AE-122	Deleted in Rev. 10
2.AE-72	Deleted in Rev. 10	2.AE-123	Deleted in Rev. 10
2.AE-73	Deleted in Rev. 10	2.AE-124	Deleted in Rev. 10
2.AE-74	Deleted in Rev. 10	2.AE-125	Deleted in Rev. 10
2.AE-75	Deleted in Rev. 10	2.AE-126	Deleted in Rev. 10
2.AE-76	Deleted in Rev. 10	2.AE-127	Deleted in Rev. 10
2.AE-77	Deleted in Rev. 10	2.AE-128	Deleted in Rev. 10
2.AE-78	Deleted in Rev. 10	2.AE-129	Deleted in Rev. 10
2.AE-79	Deleted in Rev. 10	2.AE-130	Deleted in Rev. 10
2.AE-80	Deleted in Rev. 10	2.AE-131	Deleted in Rev. 10
2.AE-81	Deleted in Rev. 10	2.AE-132	Deleted in Rev. 10
2.AE-82	Deleted in Rev. 10	2.AE-133	Deleted in Rev. 10
2.AE-83	Deleted in Rev. 10	2.AE-134	Deleted in Rev. 10
2.AE-84	Deleted in Rev. 10	2.AE-135	Deleted in Rev. 10
2.AE-85	Deleted in Rev. 10	2.AE-136	Deleted in Rev. 10
2.AE-86	Deleted in Rev. 10	2.AE-137	Deleted in Rev. 10
2.AE-87	Deleted in Rev. 10	2.AE-138	Deleted in Rev. 10
2.AE-88	Deleted in Rev. 10	2.AE-139	Deleted in Rev. 10
2.AE-89	Deleted in Rev. 10	2.AE-140	Deleted in Rev. 10
2.AE-90	Deleted in Rev. 10	2.AE-141	Deleted in Rev. 10
2.AE-91	Deleted in Rev. 10	2.AE-142	Deleted in Rev. 10
2.AE-92	Deleted in Rev. 10	2.AE-143	Deleted in Rev. 10
2.AE-93	Deleted in Rev. 10	2.AE-144	Deleted in Rev. 10
2.AE-94	Deleted in Rev. 10	2.AE-145	Deleted in Rev. 10
2.AE-95	Deleted in Rev. 10	2.AE-146	Deleted in Rev. 10
2.AE-96	Deleted in Rev. 10	2.AE-147	Deleted in Rev. 10
2.AE-97	Deleted in Rev. 10	2.AE-148	Deleted in Rev. 10
2.AE-98	Deleted in Rev. 10	2.AE-149	Deleted in Rev. 10
2.AE-99	Deleted in Rev. 10	2.AE-150	Deleted in Rev. 10
2.AE-100	Deleted in Rev. 10	2.AE-151	Deleted in Rev. 10
2.AE-101	Deleted in Rev. 10	2.AE-152	Deleted in Rev. 10

LIST OF EFFECTIVE PAGES FOR PROPOSED REVISION 10B

Page	Revision	Page	Revision
2.AE-153	Deleted in Rev. 10	Fig. 2.AG.4(b)	Deleted in Rev. 10
2.AE-154	Deleted in Rev. 10	Fig. 2.AG.4(c)	Deleted in Rev. 10
2.AE-155	Deleted in Rev. 10	Fig. 2.AG.4(d)	Deleted in Rev. 10
2.AE-156	Deleted in Rev. 10	Fig. 2.AG.4(e)	Deleted in Rev. 10
2.AE-157	Deleted in Rev. 10	2.AH-1	Deleted in Rev. 10
2.AE-158	Deleted in Rev. 10	2.AH-2	Deleted in Rev. 10
2.AE-159	Deleted in Rev. 10	2.AH-3	Deleted in Rev. 10
2.AE-160	Deleted in Rev. 10	2.AH-4	Deleted in Rev. 10
2.AE-161	Deleted in Rev. 10	2.AH-5	Deleted in Rev. 10
2.AE-162	Deleted in Rev. 10	2.AH-6	Deleted in Rev. 10
2.AE-163	Deleted in Rev. 10	2.AH-7	Deleted in Rev. 10
2.AE-164	Deleted in Rev. 10	2.AH-8	Deleted in Rev. 10
2.AE-165	Deleted in Rev. 10	2.AI-1	Deleted in Rev. 10
2.AE-166	Deleted in Rev. 10	2.AI-2	Deleted in Rev. 10
2.AE-167	Deleted in Rev. 10	2.AI-3	Deleted in Rev. 10
2.AE-168	Deleted in Rev. 10	2.AI-4	Deleted in Rev. 10
2.AE-169	Deleted in Rev. 10	2.AI-5	Deleted in Rev. 10
2.AE-170	Deleted in Rev. 10	2.AI-6	Deleted in Rev. 10
2.AE-171	Deleted in Rev. 10	2.AI-7	Deleted in Rev. 10
2.AE-172	Deleted in Rev. 10	2.AI-8	Deleted in Rev. 10
2.AE-173	Deleted in Rev. 10	2.AI-9	Deleted in Rev. 10
2.AF-1	Deleted in Rev. 10	2.AI-10	Deleted in Rev. 10
2.AF-2	Deleted in Rev. 10	2.AK-1	Deleted in Rev. 10
2.AF-3	Deleted in Rev. 10	2.AK-2	Deleted in Rev. 10
2.AF-4	Deleted in Rev. 10	2.AK-3	Deleted in Rev. 10
2.AF-5	Deleted in Rev. 10	2.AK-4	Deleted in Rev. 10
2.AF-6	Deleted in Rev. 10	2.AK-5	Deleted in Rev. 10
2.AF-7	Deleted in Rev. 10	2.AK-6	Deleted in Rev. 10
2.AF-8	Deleted in Rev. 10	2.AK-7	Deleted in Rev. 10
2.AF-9	Deleted in Rev. 10	2.AK-8	Deleted in Rev. 10
2.AF-10	Deleted in Rev. 10	2.AK-9	Deleted in Rev. 10
2.AF-11	Deleted in Rev. 10	2.AK-10	Deleted in Rev. 10
2.AF-12	Deleted in Rev. 10	2.AL-1	Deleted in Rev. 10
2.AF-13	Deleted in Rev. 10	2.AL-2	Deleted in Rev. 10
2.AF-14	Deleted in Rev. 10	2.AL-3	Deleted in Rev. 10
2.AF-15	Deleted in Rev. 10	2.AL-4	Deleted in Rev. 10
2.AF-16	Deleted in Rev. 10	2.AL-5	Deleted in Rev. 10
Fig. 2.AF.1	Deleted in Rev. 10	2.AL-6	Deleted in Rev. 10
2.AG-1	Deleted in Rev. 10	2.AL-7	Deleted in Rev. 10
2.AG-2	Deleted in Rev. 10	2.AL-8	Deleted in Rev. 10
2.AG-3	Deleted in Rev. 10	2.AL-9	Deleted in Rev. 10
2.AG-4	Deleted in Rev. 10	2.AL-10	Deleted in Rev. 10
2.AG-5	Deleted in Rev. 10	2.AL-11	Deleted in Rev. 10
2.AG-6	Deleted in Rev. 10	2.AL-12	Deleted in Rev. 10
2.AG-7	Deleted in Rev. 10	2.AM-1	Deleted in Rev. 10
2.AG-8	Deleted in Rev. 10	2.AM-2	Deleted in Rev. 10
2.AG-9	Deleted in Rev. 10	2.AM-3	Deleted in Rev. 10
Fig. 2.AG.1	Deleted in Rev. 10	2.AM-4	Deleted in Rev. 10
Fig. 2.AG.2	Deleted in Rev. 10	2.AM-5	Deleted in Rev. 10
Fig. 2.AG.3	Deleted in Rev. 10	2.AM-6	Deleted in Rev. 10
Fig. 2.AG.4(a)	Deleted in Rev. 10		

LIST OF EFFECTIVE PAGES FOR PROPOSED REVISION 10B

<u>Page</u>	<u>Revision</u>		<u>Page</u>	<u>Revision</u>
2.AN-1	Deleted in Rev. 10		2.AO-1	Deleted in Rev. 10
2.AN-2	Deleted in Rev. 10		2.AO-2	Deleted in Rev. 10
2.AN-3	Deleted in Rev. 10		2.AO-3	Deleted in Rev. 10
2.AN-4	Deleted in Rev. 10		2.AO-4	Deleted in Rev. 10
2.AN-5	Deleted in Rev. 10		2.AO-5	Deleted in Rev. 10
2.AN-6	Deleted in Rev. 10		2.AO-6	Deleted in Rev. 10
2.AN-7	Deleted in Rev. 10		2.AO-7	Deleted in Rev. 10
2.AN-8	Deleted in Rev. 10		2.AO-8	Deleted in Rev. 10
2.AN-9	Deleted in Rev. 10		2.AO-9	Deleted in Rev. 10
2.AN-10	Deleted in Rev. 10		2.AO-10	Deleted in Rev. 10
2.AN-11	Deleted in Rev. 10		2.AO-11	Deleted in Rev. 10
2.AN-12	Deleted in Rev. 10			
2.AN-13	Deleted in Rev. 10			
Fig. 2.AN.1	Deleted in Rev. 10			
Fig. 2.AN.2	Deleted in Rev. 10			

LIST OF EFFECTIVE PAGES FOR PROPOSED REVISION 10B

<u>Page</u>	<u>Revision</u>	<u>Page</u>	<u>Revision</u>
3.0-1	10A	3.4-21	10B
3.0-2	10A	3.4-22	10B
3.0-3	10A	3.4-23	10B
3.1-1	10A	3.4-24	10B
3.1-2	10A	3.4-25	10B
3.1-3	10A	3.4-26	10B
3.2-1	10A	3.4-27	10B
3.2-2	10A	3.4-28	10B
3.2-3	10A	3.4-29	10B
3.2-4	10A	3.4-30	10B
3.2-5	10A	3.4-31	10B
3.2-6	10A	3.4-32	10B
3.2-7	10A	3.4-33	10B
3.2-8	10A	3.4-34	10B
3.2-9	10A	3.4-35	10B
3.2-10	10A	3.4-36	10B
3.3-1	10A	3.4-37	10B
3.3-2	10A	3.4-38	10B
3.3-3	10A	3.4-39	10B
3.3-4	10A	3.4-40	10B
3.3-5	10A	3.4-41	10B
3.3-6	10A	3.4-42	10B
3.3-7	10A	3.4-43	10B
3.3-8	10A	3.4-44	10B
3.3-9	10A	3.4-45	10B
3.3-10	10A	3.4-46	10B
3.3-11	10A	3.4-47	10B
3.3-12	10A	3.4-48	10B
3.3-13	10A	3.4-49	10B
3.3-14	10A	3.4-50	10B
3.3-15	10A	3.4-51	10B
3.4-1	10B	3.4-52	10B
3.4-2	10B	3.4-53	10B
3.4-3	10B	3.4-54	10B
3.4-4	10B	3.4-55	10B
3.4-5	10B	3.4-56	10B
3.4-6	10B	3.4-57	10B
3.4-7	10B	3.4-58	10B
3.4-8	10B	3.4-59	10B
3.4-9	10B	3.4-60	10B
3.4-10	10B	3.4-61	10B
3.4-11	10B	3.4-62	10B
3.4-12	10B	3.4-63	10B
3.4-13	10B	3.4-64	10B
3.4-14	10B	3.4-65	10B
3.4-15	10B	3.4-66	10B
3.4-16	10B	3.4-67	10B
3.4-17	10B	3.4-68	10B
3.4-18	10B	3.4-70	10B
3.4-19	10B	3.4-71	10B
3.4-20	10B		

LIST OF EFFECTIVE PAGES FOR PROPOSED REVISION 10B

<u>Page</u>	<u>Revision</u>	<u>Page</u>	<u>Revision</u>
3.4-72	10B	Fig. 3.5.9	7
3.4-73	10B	3.6-1	10A
3.4-74	10B	3.6-2	10A
Fig. 3.4.1	6	3.6-3	10A
Fig. 3.4.2	7	3.6-4	10A
Fig. 3.4.3	7	3.7-1	10A
Fig. 3.4.4	4	3.7-2	10A
Fig. 3.4.5	7	3.7-3	10A
Fig. 3.4.6	10A	3.A-1	10A
Fig. 3.4.7	6	3.A-2	10A
Fig. 3.4.8	6	3.A-3	10A
Fig. 3.4.9	Deleted in Rev. 7	3.A-4	10A
Fig. 3.4.10	6	3.A-5	10A
Fig. 3.4.11	6	3.A-6	10A
Fig. 3.4.12	7	3.B-1	10A
Fig. 3.4.13	7	3.B-2	10A
Fig. 3.4.14	6	3.B-3	10A
Fig. 3.4.15	7	3.B-4	10A
Fig. 3.4.16	6	Fig 3.B-1	10A
Fig. 3.4.17	6		
Fig. 3.4.18	7		
Fig. 3.4.19	7		
Fig. 3.4.20	7		
Fig. 3.4.21	7		
Fig. 3.4.22	7		
Fig. 3.4.23	7		
Fig. 3.4.24	8		
Fig. 3.4.25	8		
Fig. 3.4.26	8		
Fig. 3.4.27	8		
Fig. 3.4.28	8		
3.5-1	10B		
3.5-2	10B		
3.5-3	10B		
3.5-4	10B		
3.5-5	10B		
3.5-6	10B		
3.5-7	10B		
3.5-8	10B		
3.5-9	10B		
3.5-10	10B		
3.5-11	10B		
Fig. 3.5.1	7		
Fig. 3.5.2	5		
Fig. 3.5.3	6		
Fig. 3.5.4	6		
Fig. 3.5.5	6		
Fig. 3.5.6	7		
Fig. 3.5.7	7		
Fig. 3.5.8	7		

LIST OF EFFECTIVE PAGES FOR PROPOSED REVISION 10B

<u>Page</u>	<u>Revision</u>	<u>Page</u>	<u>Revision</u>
4.0-1	10	4.A-1	8
4.0-2	10	4.A-2	8
4.1-1	10	4.A-3	8
4.1-2	10	4.B-1	8
4.1-3	10	4.B-2	8
4.1-4	10	4.B-3	8
4.1-5	10	4.B-4	8
4.1-6	10	4.B-5	8
4.1-7	10		
Fig. 4.1.1	8		
Fig. 4.1.2	8		
Fig. 4.1.3	8		
Fig. 4.1.4	10		
4.2-1	10		
4.2-2	10		
4.2-3	10		
4.2-4	10		
4.2-5	10		
4.2-6	10		
4.2-7	10		
4.2-8	10		
4.2-9	10		
4.2-10	10		
4.2-11	10		
4.2-12	10		
4.2-13	10		
4.2-14	10		
4.2-15	10		
4.2-16	10		
4.2-17	10		
4.2-18	10		
4.2-19	10		
4.2-20	10		
4.2-21	10		
4.2-22	10		
4.2-23	10		
4.2-24	10		
4.2-25	10		
4.2-26	10		
4.2-27	10		
4.2-28	10		
4.2-29	10		
4.2-30	10		
4.2-31	10		
4.2-32	10		
4.2-33	10		
4.2-34	10		
4.3-1	10		
4.3-2	10		
4.4-1	10		

LIST OF EFFECTIVE PAGES FOR PROPOSED REVISION 10B

<u>Page</u>	<u>Revision</u>	<u>Page</u>	<u>Revision</u>
5.0-1	10A	5.2-26	10A
5.0-2	10A	5.2-27	10A
5.1-1	10A	5.2-28	10A
5.1-2	10A	5.2-29	10A
5.1-3	10A	5.2-30	10A
5.1-4	10A	5.2-31	10A
5.1-5	10A	5.2-32	10A
5.1-6	10A	5.2-33	10A
5.1-7	10A	5.2-34	10A
5.1-8	10A	5.2-35	10A
5.1-9	10A	5.2-36	10A
5.1-10	10A	5.2-37	10A
5.1-11	10A	5.2-38	10A
5.1-12	10A	5.2-39	10A
5.1-13	10A	5.2-40	10A
5.1-14	10A	5.2-41	10A
5.1-15	10A	5.2-42	10A
5.1-16	10A	5.2-43	10A
5.1-17	10A	5.2-44	10A
5.1-18	10A	5.2-45	10A
5.1-19	10A	5.2-46	10A
5.1-20	10A	5.2-47	10A
5.1-21	10A	5.2-48	10A
Fig. 5.1.1	10	5.2-49	10A
Fig. 5.1.2	6	5.2-50	10A
5.2-1	10A	5.2-51	10A
5.2-2	10A	5.2-52	10A
5.2-3	10A	5.2-53	10A
5.2-4	10A	5.2-54	10A
5.2-5	10A	5.2-55	10A
5.2-6	10A	5.2-56	10A
5.2-7	10A	5.2-57	10A
5.2-8	10A	5.2-58	10A
5.2-9	10A	5.2-59	10A
5.2-10	10A	5.3-1	10A
5.2-11	10A	5.3-2	10A
5.2-12	10A	5.3-3	10A
5.2-13	10A	5.3-4	10A
5.2-14	10A	5.3-5	10A
5.2-15	10A	5.3-6	10A
5.2-16	10A	5.3-7	10A
5.2-17	10A	5.3-8	10A
5.2-18	10A	5.3-9	10A
5.2-19	10A	5.3-10	10A
5.2-20	10A	5.3-11	10A
5.2-21	10A	Fig. 5.3.1	10
5.2-22	10A	Fig. 5.3.2	10
5.2-23	10A	Fig. 5.3.3	4
5.2-24	10A	Fig. 5.3.4	10
5.2-25	10A	Fig. 5.3.5	10

LIST OF EFFECTIVE PAGES FOR PROPOSED REVISION 10B

<u>Page</u>	<u>Revision</u>	<u>Page</u>	<u>Revision</u>
Fig. 5.3.6	7	5.4-44	10A
Fig. 5.3.7	6	5.4-45	10A
Fig. 5.3.8	6	Fig. 5.4.1	8
Fig. 5.3.9	10	Fig. 5.4.2	10
Fig. 5.3.10	10	5.5-1	10A
Fig. 5.3.11	8	5.5-2	10A
Fig. 5.3.12	8	5.5-3	10A
5.4-1	10A	5.5-4	10A
5.4-2	10A	5.6-1	10A
5.4-3	10A	5.6-2	10A
5.4-4	10A	5.6-3	10A
5.4-5	10A	5.A-1	7
5.4-6	10A	5.A-2	7
5.4-7	10A	5.A-3	7
5.4-8	10A	5.B-1	7
5.4-9	10A	5.B-2	7
5.4-10	10A	5.B-3	7
5.4-11	10A	5.B-4	7
5.4-12	10A	5.B-5	7
5.4-13	10A	5.B-6	7
5.4-14	10A	5.C-1	7
5.4-15	10A	5.C-2	7
5.4-16	10A	5.C-3	7
5.4-17	10A	5.C-4	7
5.4-18	10A	5.C-5	7
5.4-19	10A	5.C-6	7
5.4-20	10A	5.C-7	7
5.4-21	10A	5.C-8	7
5.4-22	10A	5.C-9	7
5.4-23	10A	5.C-10	7
5.4-24	10A	5.C-11	7
5.4-25	10A	5.C-12	7
5.4-26	10A	5.C-13	7
5.4-27	10A	5.C-14	7
5.4-28	10A	5.C-15	7
5.4-29	10A	5.C-16	7
5.4-30	10A	5.C-17	7
5.4-31	10A	5.C-18	7
5.4-32	10A	5.C-19	7
5.4-33	10A	5.C-20	7
5.4-34	10A	5.C-21	7
5.4-35	10A	5.C-22	7
5.4-36	10A	5.C-23	7
5.4-37	10A	5.C-24	7
5.4-38	10A	5.C-25	7
5.4-39	10A	5.C-26	7
5.4-40	10A	5.C-27	7
5.4-41	10A	5.C-28	7
5.4-42	10A	5.C-29	7
5.4-43	10A	5.C-30	7

LIST OF EFFECTIVE PAGES FOR PROPOSED REVISION 10B

Page	Revision		Page	Revision
5.C-31	7			
5.C-32	7			
5.C-33	7			
5.C-34	7			

LIST OF EFFECTIVE PAGES FOR PROPOSED REVISION 10B

Page	Revision	Page	Revision
6.1-1	10A	6.2-35	10A
6.1-2	10A	6.2-36	10A
6.1-3	10A	6.2-37	10A
6.1-4	10A	6.2-38	10A
6.1-5	10A	6.2-39	10A
6.1-6	10A	6.2-40	10A
6.1-7	10A	6.2-41	10A
6.1-8	10A	6.2-42	10A
6.1-9	10A	6.2-43	10A
6.1-10	10A	6.2-44	10A
6.1-11	10A	6.2-45	10A
6.1-12	10A	6.2-46	10A
6.1-13	10A	6.2-47	10A
6.1-14	10A	6.2-48	10A
6.1-15	10A	6.2-49	10A
6.1-16	10A	6.2-50	10A
6.1-17	10A	6.2-51	10A
6.2-1	10A	6.2-52	10A
6.2-2	10A	6.2-53	10A
6.2-3	10A	6.2-54	10A
6.2-4	10A	6.2-55	10A
6.2-5	10A	6.2-56	10A
6.2-6	10A	6.2-57	10A
6.2-7	10A	6.2-58	10A
6.2-8	10A	6.2-59	10A
6.2-9	10A	6.3-1	10A
6.2-10	10A	6.3-2	10A
6.2-11	10A	6.3-3	10A
6.2-12	10A	6.3-4	10A
6.2-13	10A	6.3-5	10A
6.2-14	10A	6.3-6	10A
6.2-15	10A	6.3-7	10A
6.2-16	10A	6.3-8	10A
6.2-17	10A	6.3-9	10A
6.2-18	10A	6.3-10	10A
6.2-19	10A	6.3-11	10A
6.2-20	10A	6.3-12	10A
6.2-21	10A	6.3-13	10A
6.2-22	10A	6.3-14	10A
6.2-23	10A	6.3-15	10A
6.2-24	10A	6.3-16	10A
6.2-25	10A	6.3-17	10A
6.2-26	10A	6.3-18	10A
6.2-27	10A	Fig. 6.3.1	10
6.2-28	10A	Fig. 6.3.2	10
6.2-29	10A	Fig. 6.3.3	10
6.2-30	10A	Fig. 6.3.4	10
6.2-31	10A	Fig. 6.3.5	10
6.2-32	10A	Fig. 6.3.6	4
6.2-33	10A	Fig. 6.3.7	10
6.2-34	10A		

LIST OF EFFECTIVE PAGES FOR PROPOSED REVISION 10B

<u>Page</u>	<u>Revision</u>	<u>Page</u>	<u>Revision</u>
6.4-1	10A	6.7-1	10
6.4-2	10A	6.7-2	10
6.4-3	10A	6.7-3	10
6.4-4	10A	6.7-4	10
6.4-5	10A	6.A-1	10
6.4-6	10A	6.A-2	10
6.4-7	10A	6.A-3	10
6.4-8	10A	6.A-4	10
6.4-9	10A	6.A-5	10
6.4-10	10A	6.A-6	10
6.4-11	10A	6.A-7	10
6.4-12	10A	6.A-8	10
6.4-13	10A	6.A-9	10
6.4-14	10A	6.A-10	10
6.4-15	10A	6.A-11	10
6.4-16	10A	6.A-12	10
6.4-17	10A	6.A-13	10
6.4-18	10A	6.A-14	10
6.4-19	10A	6.A-15	10
6.4-20	10A	6.A-16	10
6.4-21	10A	6.A-17	10
6.4-22	10A	6.A-18	10
6.4-23	10A	6.A-19	10
6.4-24	10A	6.A-20	10
6.4-25	10A	Fig. 6.A.1	7
6.4-26	10A	Fig. 6.A.2	7
6.4-27	10A	Fig. 6.A.3	7
6.4-28	10A	Fig. 6.A.4	7
6.4-29	10A	Fig. 6.A.5	7
6.4-30	10A	Fig. 6.A.6	7
6.4-31	10A	6.B-1	7
6.4-32	10A	6.B-2	7
6.4-33	10A	6.C-1	Deleted in Rev. 10A
6.4-34	10A	6.C-2	Deleted in Rev. 10A
6.4-35	10A	6.C-3	Deleted in Rev. 10A
6.4-36	10A	6.C-4	Deleted in Rev. 10A
Fig. 6.4.1	9	6.C-5	Deleted in Rev. 10A
Fig. 6.4.2	9	6.C-6	Deleted in Rev. 10A
Fig. 6.4.3	9	6.C-7	Deleted in Rev. 10A
Fig. 6.4.4	9	6.C-8	Deleted in Rev. 10A
Fig. 6.4.5	9	6.D-1	10
Fig. 6.4.6	9	6.D-2	10
Fig. 6.4.7	9	6.D-3	10
Fig. 6.4.8	7	6.D-4	10
Fig. 6.4.9	10	6.D-5	10
Fig. 6.4.10	9	6.D-6	10
Fig. 6.4.11	10	6.D-7	10
Fig. 6.4.12	10	6.D-8	10
6.5-1	10	6.D-9	10
6.6-1	10	6.D-10	10

LIST OF EFFECTIVE PAGES FOR PROPOSED REVISION 10B

<u>Page</u>	<u>Revision</u>	<u>Page</u>	<u>Revision</u>
7.0-1	10A	Fig. 7.1.2c	7
7.0-2	10A	Fig. 7.1.3	7
7.0-3	10A	Fig. 7.1.4	10
7.1-1	10A	Fig. 7.1.5	10
7.1-2	10A	Fig. 7.1.6	10
7.1-3	10A	Fig. 7.1.7	10
7.1-4	10A	Fig. 7.1.8	7
7.1-5	10A	Fig. 7.1.9	10
7.1-6	10A	Fig. 7.1.10	10
7.1-7	10A	Fig. 7.1.11	10
7.1-8	10A	Fig. 7.1.12	10
7.1-9	10A	Fig. 7.1.13	10
7.1-10	10A	Fig. 7.1.14	7
7.1-11	10A	Fig. 7.1.15	7
7.1-12	10A	Fig. 7.1.16	7
7.1-13	10A	Fig. 7.1.17	10
7.1-14	10A	Fig. 7.1.18	7
7.1-15	10A	Fig. 7.1.19	7
7.1-16	10A	Fig. 7.1.20	10
7.1-17	10A	Fig. 7.1.21	7
7.1-18	10A	Fig. 7.1.22	10A
7.1-19	10A	Fig. 7.1.23	10A
7.1-20	10A	Fig. 7.1.24	10A
7.1-21	10A	Fig. 7.1.25	10A
7.1-22	10A	Fig. 7.1.26	10A
7.1-23	10A	Fig. 7.1.27	7
7.1-24	10A	Fig. 7.1.28	7
7.1-25	10A	Fig. 7.1.29	7
7.1-26	10A	Fig. 7.1.30	7
7.1-27	10A	7.2-1	10A
7.1-28	10A	7.2-2	10A
7.1-29	10A	7.2-3	10A
7.1-30	10A	7.2-4	10A
7.1-31	10A	7.2-5	10A
7.1-32	10A	7.2-6	10A
7.1-33	10A	7.2-7	10A
7.1-34	10A	7.2-8	10A
7.1-35	10A	7.2-9	10A
7.1-36	10A	7.2-10	10A
7.1-37	10A	Fig. 7.2.1	10A
7.1-38	10A	Fig. 7.2.2a	7
7.1-39	10A	Fig. 7.2.2b	7
7.1-40	10A	Fig. 7.2.2c	7
7.1-41	10A	Fig. 7.2.3	10A
7.1-42	10A	Fig. 7.2.4	10A
7.1-43	10A	Fig. 7.2.5	10A
7.1-44	10A	7.3-1	10A
Fig. 7.1.1	10A	7.3-2	10A
Fig. 7.1.2a	7	7.3-3	10A
Fig. 7.1.2b	7		

LIST OF EFFECTIVE PAGES FOR PROPOSED REVISION 10B

<u>Page</u>	<u>Revision</u>		<u>Page</u>	<u>Revision</u>
7.4-1	10A			
7.4-2	10A			
7.4-3	10A			
7.4-4	10A			
7.5-1	8			
7.6-1	10A			

LIST OF EFFECTIVE PAGES FOR PROPOSED REVISION 10B

<u>Page</u>	<u>Revision</u>	<u>Page</u>	<u>Revision</u>
8.1-1	10A		
8.1-2	10A		
8.1-3	10A		
8.1-4	10A		
8.1-5	10A		
8.1-6	10A		
8.1-7	10A		
8.1-8	10A		
8.1-9	10A		
8.1-10	10A		
8.1-11	10A		
8.1-12	10A		
8.1-13	10A		
8.1-14	10A		
8.1-15	10A		
8.1-16	10A		
8.1-17	10A		
8.1-18	10A		
8.1-19	10A		
8.1-20	10A		
8.1-21	10A		
8.1-22	10A		
8.1-23	10A		
8.1-24	10A		
8.1-25	10A		
8.1-26	10A		
8.1-27	10A		
8.1-28	10A		
8.1-29	10A		
8.1-30	10A		
Fig. 8.1.1	Deleted in Rev. 7		
Fig. 8.1.2	7		
Fig. 8.1.3	7		
Fig. 8.1.4	7		
8.2-1	10A		
8.2-2	10A		
8.2-3	10A		
8.2-4	10A		
8.2-5	10A		
Fig. 8.2.1	7		
8.3-1	10A		
8.3-2	10A		
8.4-1	10		

3.4 THERMAL EVALUATION FOR NORMAL CONDITIONS OF TRANSPORT

3.4.1 Thermal Model

The HI-STAR MPC basket designs consist of ~~two~~ *four* distinct geometries engineered to hold 24 and 32 PWR (*MPC-24, MPC-24E and MPC-32*) or 68 BWR (*MPC-68*) fuel assemblies. The fuel basket forms a honeycomb matrix of square-shaped fuel compartments to retain the fuel assemblies during transport (refer to Figures 1.2.3 and 1.2.5 for an illustration of PWR and BWR baskets). The basket is formed by an interlocking honeycomb structure of steel plates and full-length edge welding of the cell corners to form an integral basket configuration. Individual cell walls (except outer periphery MPC-68 and MPC-32 cell walls) are provided with Boral neutron absorber panels, which consists of a Boral plate sandwiched between the cell wall and a stainless steel sheathing plate, for the full length of the active fuel region.

The design basis decay heat generation per PWR or BWR assembly for normal transport for each MPC type is specified in Table 1.2.13. The decay heat is considered to be nonuniformly distributed over the active fuel length based on the design basis axial burnup distribution specified in Chapter 1 (see Table 1.2.15 and Figures 1.2.13 and 1.2.14).

Transport of heat from the MPC basket interior to the basket periphery is accomplished by conduction through the MPC basket metal grid structure and the narrow helium gaps between the fuel assemblies and fuel cell walls. Heat dissipation in the MPC basket periphery-to-MPC shell gap is by a combination of helium conduction, natural convection (by means of the "Rayleigh" effect), and radiation across the gap. ~~and conduction through the aluminum alloy 1100 heat conduction elements.~~ Between the MPC shell and the overpack inner shell is a small clearance region which is evacuated and backfilled with helium. Helium, besides being inert, is a better conductor of heat than air. Thus, heat conduction through the helium gap between the MPC and the overpack will minimize temperature differentials across this region.

The overpack, under normal transport conditions, passively rejects heat to the environment. Cooling of the exterior system surfaces is by natural convection and radiation. During transport, the HI-STAR System is placed in a horizontal position with stainless steel encased aluminum honeycomb impact limiters installed at both ends of the overpack. To conservatively maximize the calculated internal temperatures, the thermal conductivity of the impact limiters is set essentially equal to zero. Under normal transport conditions, the MPC shell rests on the overpack internal cavity surface forming an eccentric gap. Direct contact between the MPC and overpack surfaces is expected to minimize heat transfer resistance in this region of intimate contact. Significantly improved conductive heat transport due to reduction in the helium gap near the contact region is accounted for in the thermal analysis of the HI-STAR System. The HI-STAR System is conservatively analyzed assuming a minimum 0.02-inch gap at the line of metal-to-metal contact. Analytical modeling details of the various thermal transport mechanisms are provided in the following.

3.4.1.1 Analytical Model - General Remarks

Transport of heat from the heat generation region (fuel assemblies) to the outside environment is analyzed broadly in terms of three interdependent thermal models.

- i. The first model considers transport of heat from the fuel assembly to the basket cell walls. This model recognizes the combined effects of conduction (through helium) and radiation, and is essentially a finite element technology-based update of the classical Wootton & Epstein [3.4.1] formulation (which considers radiative heat exchange between fuel rod surfaces).
- ii. The second model considers heat transport within an MPC cross section by conduction and radiation. The effective cross sectional thermal conductivity of the basket region obtained from the combined fuel assembly/basket heat conduction radiation model is applied to an axisymmetric thermal model of the HI-STAR System on the FLUENT [3.1.2] code.
- iii. The third model deals with the transmission of heat from the MPC exterior surface to the external environment (heat sink). From the MPC shell to the cask exterior surface, heat is conducted through an array of concentric shells representing the MPC-to-overpack helium gap, the overpack inner shell, the intermediate shells, the Holtite-A neutron shielding and finally the overpack outer shell. Heat rejection from the outside cask surfaces to ambient air is considered by accounting for natural convection and thermal radiation heat transfer mechanisms from the exposed cask surfaces. Insulation on exposed cask surfaces is based on 12-hour levels prescribed in 10CFR71, averaged over a 24-hour period.

The following subsections contain a systematic description of the mathematical models devised to articulate the temperature field in the HI-STAR System. Table 3.4.2 shows the relationship between the mathematical models and the corresponding regions (i.e., fuel, MPC, overpack, etc.) of the HI-STAR System. The description begins with the method to characterize the heat transfer behavior of the prismatic (square) opening referred to as the "fuel space" containing a heat emitting fuel assembly. The methodology utilizes a finite-volume procedure to replace the heterogeneous SNF/fuel space region with an equivalent solid body having a well-defined temperature-dependent conductivity. In the following subsection, the method to replace the composite walls of the fuel basket cells with equivalent "solid" walls is presented. Having created the mathematical equivalents for the SNF/fuel spaces and the fuel basket walls, the method to represent the MPC cylinder containing the fuel basket by an equivalent cylinder whose thermal conductivity is a function of the spatial location and coincident temperature is presented.

Following the approach of presenting descriptions starting from the inside and moving to the outer region of a cask, the next subsections present the mathematical model to simulate the overpack. Subsection 3.4.1.1.12 concludes the presentation with a description of how the different models for the specific regions within the HI-STAR System are assembled into the final finite element model.

3.4.1.1.1 Overview of the Thermal Model

Thermal analysis of the HI-STAR System is performed by assuming that the system is subject to its maximum heat duty with each storage location occupied and with the heat generation rate in each stored fuel assembly equal to the design basis maximum value. While the assumption of equal heat generation imputes a certain symmetry to the cask thermal problem, the thermal model must incorporate three attributes of the physical problem to perform a rigorous analysis:

- i. While the rate of heat conduction through metals is a relatively weak function of temperature, radiation heat exchange is a nonlinear function of surface temperatures.
- ii. Heat generation in the MPC is axially non-uniform due to a non-uniform axial burnup profile in the fuel assemblies.
- iii. Inasmuch as the transfer of heat occurs from the inside of the basket region to the outside, the temperature field in the MPC is spatially distributed with the maximum values reached in the central region.

It is clearly impractical to explicitly model every fuel rod in every stored fuel assembly explicitly. Instead, the cross section bounded by the inside of the storage cell, which surrounds the assemblage of fuel rods and the interstitial helium gas, is replaced with an "equivalent" square (solid) section characterized by an effective thermal conductivity. Figure 3.4.1 pictorially illustrates the homogenization concept. Further details on this process for determining the effective conductivity is presented in Subsection 3.4.1.1.2. It suffices to state here that the effective conductivity of the cell space will be a function of temperature, because radiation heat transfer (a major component of the heat transport mechanism between the fuel rods to the basket metal square) is a strong function of the absolute temperatures of the participating bodies. Therefore, in effect, every storage cell location will have a different value of effective conductivity in the homogenized model. The process of determining the temperature-dependent effective conductivity is carried out using a finite volume procedure.

In the next step of homogenization, a planar section of MPC is considered. With each storage cell inside space replaced with an equivalent solid square, the MPC cross section consists of a metallic gridwork (basket cell walls with each cell space containing a solid fuel square with an effective thermal conductivity) circumscribed by a circular ring (MPC shell). There are ~~five~~ *four principal distinct* materials in this section *that are included in all MPCs*, namely the homogenized fuel cell squares, the Alloy X MPC structural materials in the MPC (including Boral sheathing material), Boral, ~~aluminum heat conduction elements,~~ and helium gas. *Aluminum heat conduction elements (AHCEs), included optionally in the MPC design, are appropriately ignored in the heat dissipation calculations.* Each of the ~~five~~ *four* constituent materials in this section has a different conductivity. As discussed earlier, the conductivity of the homogenized fuel cell is a strong function of temperature.

In order to replace this thermally heterogeneous MPC section with an equivalent conduction-only lamina, resort to the finite-element procedure is necessary. Because the rate of transport of heat within the MPC is influenced by radiation, which is a temperature-dependent effect, the equivalent conductivity of the MPC lamina must be computed as a function of temperature. Finally, it is recognized that the MPC section consists of two discrete regions, namely, the basket region and the periphery region. The periphery region is the space between the peripheral storage cells and the MPC enclosure shell. This space is essentially full of helium gas surrounded by Alloy X plates and *optionally* aluminum heat conduction elements. Accordingly, as illustrated in Figure 3.4.2 for MPC-68, the MPC cross section is replaced with two homogenized regions with temperature-dependent conductivities. In particular, the effective conductivity of the fuel cells is subsumed into the equivalent conductivity of the basket cross section using a finite element procedure. The ANSYS finite-element code is the vehicle for all modeling efforts described in the foregoing.

In summary, appropriate finite element models are used to replace the MPC cross section with an equivalent two-region homogeneous conduction lamina whose local conductivity is a known function of coincident absolute temperature. Thus, the MPC cylinder containing discrete fuel assemblies, helium, Boral, ~~aluminum,~~ and Alloy X and *optionally AHCEs** is replaced with a right circular cylinder whose material conductivity will vary with radial and axial position as a function of the coincident temperature.

The MPC-to-overpack gap is simply an annular space that is readily modeled with an equivalent conductivity that reflects the conduction and radiation modes of heat transfer. The overpack is a radially symmetric structure except for the neutron absorber region which is built from radial connectors and Holtite. Using the classical equivalence procedure as described in Section 3.4.1.1.9, this region is replaced with an equivalent radially symmetric annular cylinder.

The thermal analysis procedure described above makes frequent use of equivalent thermal properties to ease the geometric modeling of the cask components. These equivalent properties are rigorously calculated values based on detailed evaluations of actual cask system geometries. All these calculations are performed conservatively to ensure a bounding representation of the cask system. This process, commonly referred to as submodeling, yields accurate (not approximate) results. Given the detailed nature of the submodeling process, experimental validation of the individual submodels is not necessary.

In this manner, a HI-STAR System overpack containing a loaded MPC is replaced with a right circular cylinder with spatially varying temperature-dependent conductivity. Heat is generated within the basket space in this cylinder in the manner of the prescribed axial distribution. In addition, heat is deposited from insolation on its external surface. Natural convection and thermal radiation to ambient air dissipate heat. Details of the elements of mathematical modeling are provided in the following sections.

* In the thermal modeling, AHCEs are appropriately ignored.

3.4.1.1.2 Fuel Region Effective Thermal Conductivity Calculation

Thermal properties of a large number of PWR and BWR fuel assembly configurations manufactured by the major fuel suppliers (i.e., Westinghouse, CE, B&W, and GE) have been evaluated for inclusion in the HI-STAR System thermal analysis. Bounding PWR and BWR fuel assembly configurations are determined using the simplified procedure described below. This is followed by the determination of temperature-dependent properties of the bounding PWR and BWR fuel assembly configurations to be used for cask thermal analysis using a finite-volume (FLUENT) approach.

To determine which of the numerous PWR assembly types listed in Table 3.4.4 should be used in the thermal model for the MPC-24 PWR fuel baskets, we must establish which assembly has the maximum thermal resistance. The same determination must be made for the MPC-68, out of the menu of SNF types listed in Table 3.4.5. For this purpose, we utilize a simplified procedure that we describe below.

Each fuel assembly consists of a large array of fuel rods typically arranged on a square layout. Every fuel rod in this array is generating heat due to radioactive decay in the enclosed fuel pellets. There is a finite temperature difference required to transport heat from the innermost fuel rods to the storage cell walls. Heat transport within the fuel assembly is based on principles of conduction heat transfer combined with the highly conservative analytical model proposed by Wooton and Epstein [3.4.1]. The Wooton-Epstein model considers radiative heat exchange between individual fuel rod surfaces as a means to bound the hottest fuel rod cladding temperature.

Transport of heat energy within any cross section of a fuel assembly is due to a combination of radiative energy exchange and conduction through the helium gas that fills the interstices between the fuel rods in the array. With the assumption of uniform heat generation within any given horizontal cross section of a fuel assembly, the combined radiation and conduction heat transport effects result in the following heat flow equation:

$$Q = \sigma C_o F_\epsilon A [T_C^4 - T_B^4] + 13.5740 L K_{cs} [T_C - T_B]$$

where,

$$F_\epsilon = \text{Emissivity Factor} = \frac{1}{\left(\frac{1}{\epsilon_C} + \frac{1}{\epsilon_B} - 1\right)}$$

ϵ_C, ϵ_B = emissivities of fuel cladding, fuel basket (see Table 3.2.4)

C_o = Assembly Geometry Factor

$$= \frac{4N}{(N+1)^2} \text{ (when } N \text{ is odd)}$$

$$= \frac{4}{N+2} \text{ (when } N \text{ is even)}$$

- N = Number of rows or columns of rods arranged in a square array
- A = fuel assembly "box" heat transfer area
= $4 \times \text{width} \times \text{length}$ (ft²)
- L = fuel assembly length (ft)
- K_{cs} = fuel assembly constituent materials volume fraction weighted mixture conductivity (Btu/ft-hr-°F)
- T_C = hottest fuel cladding temperature (°R)
- T_B = box temperature (°R)
- Q = net radial heat transport from the assembly interior (Btu/hr)
- σ = Stefan-Boltzman Constant (0.1714×10^{-8} Btu/ft²-hr-°R⁴)

In the above heat flow equation, the first term is the Wooten-Epstein radiative heat flow contribution while the second term is the conduction heat transport contribution based on the classical solution to the temperature distribution problem inside a square shaped block with uniform heat generation [3.4.3]. The 13.574 factor in the conduction term of the equation is the shape factor for two-dimensional heat transfer in a square section. Planar fuel assembly heat transport by conduction occurs through a series of resistances formed by the interstitial helium fill gas, fuel cladding and enclosed fuel. An effective planar mixture conductivity is determined by a volume fraction weighted sum of the individual constituent materials resistances. For BWR assemblies, this formulation is applied to the region inside the fuel channel. A second conduction and radiation model is applied between the channel and the fuel basket gap. These two models are combined, in series, to yield a total effective conductivity.

The effective thermal conductivities of several representative intact PWR and BWR assemblies are presented in Tables 3.4.4 and 3.4.5. At higher temperatures (greater than 450°F), the zircaloy clad fuel assemblies with the lowest effective thermal conductivities are the Westinghouse 17×17 OFA (PWR) and the General Electric GE-11 9×9 (BWR). A discussion of fuel assembly conductivities for some of the newer 10×10 array *and plant specific* BWR fuel designs is presented near the end of this

subsection. Based on this *simplified* analysis, the Westinghouse 17x17 OFA PWR and GE-11 9x9 BWR fuel assemblies are determined to be the bounding configurations for analysis at design basis maximum heat loads. As discussed in Section 3.3.2, stainless clad fuel assemblies with significantly lower decay heat emission characteristics are not deemed to be bounding.

Several of the assemblies listed in Tables 3.4.5 were excluded from consideration when determining the bounding assembly because of their extremely low decay heat loads. The excluded assemblies, which were each used at a single reactor only, are physically small and have extremely low burnups and long cooling times. These factors combine to result in decay heat loads that are much lower than the design basis maximum. The excluded assemblies are:

- Dresden Unit 1 8x8
- Dresden Unit 1 6x6
- Allis-Chalmers 10x10 Stainless
- Exxon Nuclear 10x10 Stainless
- Humboldt Bay 7x7
- Quad⁺ 8x8

The Allis-Chalmers and Exxon assemblies are used only in the LaCrosse reactor of the Dairyland Power Cooperative. The design basis assembly decay heat loads for Dresden Unit 1 and LaCrosse SNF (Tables 1.2.14 and 1.2.19) are approximately 58% lower and 69% lower, respectively, than the MPC-68 design basis assembly maximum heat load (Table 1.2.13). Examining Table 3.4.5, the effective thermal conductivity of damaged Dresden Unit 1 fuel assemblies inside DFCs (the lowest of any Dresden Unit 1 assembly) and LaCrosse fuel assemblies are approximately 40% lower and 30% lower, respectively, than that of the bounding (GE-11 9x9) fuel assembly. Consequently, the fuel cladding temperatures in the HI-STAR System with Dresden Unit 1 and LaCrosse fuel assemblies (intact or damaged) will be bounded by design basis fuel cladding temperatures.

To accommodate Trojan Nuclear Plant (TNP) SNF in a HI-STAR System's MPC-24E canister, the discharged fuel characteristics at this permanently shutdown site are evaluated herein. To permit TNP fuel in the HI-STAR System, it is necessary to confirm that certain key fuel parameters, viz. burnup (B) and cask decay heat (D) are bounded by the thermal design limits (42,500 MWD/MTU and 20 kW for PWR MPCs). The TNP SNF is a member of the 17x17 class of fuel types. The bulk of the fuel inventory is from Westinghouse and balance from B&W. The B&W SNF configuration and cladding dimensions are same as that of the Westinghouse 17x17 SNF. The fuel is more than nine years old and the burnups are in the range of 5073 MWD/MTU to 41889 MWD/MTU. The TNP SNF burnups are bounded by the design maximum for PWR class of fuel (i.e. B < 42500 MWD/MTU). Because the fuel decay heat is exponentially attenuating with time, it is conservative to evaluate decay heat on a date that precedes fuel loading. For this purpose, a reference date (RD) of 11/9/2001 is employed herein. The decay heat from the most emissive Trojan fuel is bounded by 725 W on RD. Postulating every cell location in an MPC-24E is occupied by this most heat emissive fuel*

* The height of MPC-24E for Trojan SNF is shorter than the height of generic HI-STAR MPCs.

assembly, a conservatively bounding $D = 17.4 \text{ kW}^*$ is computed. The Trojan MPC-24E heat loads are below the HI-STAR System design heat load (i.e. $D < 20 \text{ kW}$) by a significant margin.

A limited number of Trojan assemblies have poison inserts (RCCAs and BPRAs) and other non-fuel hardware (Thimble Plugs). The inclusion of PWR non-fuel hardware influences the MPC thermal response in two ways: (i) The presence of non-fuel hardware increases the effective basket conductivity, thus enhancing heat dissipation and lowering fuel temperatures and (ii) Volume displaced by the mass of non-fuel hardware lowers the available cavity free volume for accommodating gas released in hypothetical rod rupture scenarios. For a conservatively bounding evaluation, the thermal modeling ignores the presence of non-fuel hardware and the MPC cavity volume is computed based on volume displacement by the heaviest fuel (bounding weight) with non-fuel hardware included.

Having established the governing (most resistive) PWR and BWR SNF types, a finite-volume code is used to determine the effective conductivities in a conservative manner. Detailed conduction-radiation finite-volume models of the bounding PWR and BWR fuel assemblies are developed in the FLUENT code as shown in Figures 3.4.7 and 3.4.8, respectively. The PWR model was originally developed on the ANSYS code which enables individual rod-to-rod and rod-to-basket wall view factor calculations to be performed using that code's AUX12 processor. Limitations of radiation modeling techniques implemented in ANSYS make it difficult to take advantage of the symmetry of the fuel assembly geometry. Unacceptably long CPU time and large workspace requirements necessary for performing gray body radiation calculations for a complete fuel assembly geometry on ANSYS prompted the development of an alternate simplified model on the FLUENT code. The FLUENT model was benchmarked with the ANSYS model results for a Westinghouse 17x17 OFA fuel assembly geometry for the case of black body radiation (emissivities = 1). The FLUENT model was found to yield conservative results in comparison to the ANSYS model for the "black" surface case. The FLUENT model benchmarked in this manner is used to solve the gray body radiation problem to provide the necessary results for determining the effective thermal conductivity of the governing PWR fuel assembly. The same modeling approach using FLUENT is then applied to the governing BWR fuel assembly and the effective conductivity of GE-11 9x9 fuel is determined.

An equivalent homogeneous material that fills the basket opening replaces the combined fuel rods-helium matrix by the following two-step procedure. In the first step, the FLUENT-based fuel assembly model is solved by applying equal heat generation per unit length to the individual fuel rods and a uniform boundary temperature along the basket cell opening inside periphery. The temperature difference between the peak cladding and boundary temperatures is used to determine an effective conductivity as described in the next step. For this purpose, we consider a two-dimensional cross section of a square shaped block of size equal to $2L$ and a uniform volumetric heat source (q_g) cooled at the periphery with a uniform boundary temperature. Under the assumption of constant material thermal conductivity (K), the temperature difference (ΔT) from the center of the cross section to the periphery is analytically given by [3.4.3]:

* Projected MPC heat loads are much lower (in the range of 6 kw to 14.5 kW in circa 2003).

$$\Delta T = 0.29468 \frac{q_g L^2}{K}$$

This analytical formula is applied to determine the effective material conductivity from a known quantity of heat generation applied in the FLUENT model (smeared as a uniform heat source, q_g), basket opening size and ΔT calculated in the first step.

As discussed earlier, the effective fuel space conductivity is a function of the temperature coordinate. The above two step analysis is carried out for a number of reference temperatures. In this manner, the effective conductivity as a function of temperature is established.

In Table 3.4.25, 10×10 array type BWR fuel assembly effective thermal conductivity results from a simplified analysis are presented to determine the most resistive fuel assembly in this class. Using the simplified analysis procedure discussed earlier, the Atrium-10 fuel type is determined to be the most resistive in this class of fuel assemblies. A detailed finite-element model of this assembly type was developed to rigorously quantify the heat dissipation characteristics. The results of this study are presented in Table 3.4.26 and compared to the bounding BWR fuel assembly effective thermal conductivity depicted in Figure 3.4.13. The results of this study demonstrate that the bounding BWR fuel assembly effective thermal conductivity is conservative with respect to the 10×10 class of BWR assemblies. Table 3.4.34 summarizes plant specific fuel types' effective conductivities. From these analytical results, the SPC-5 is determined to be the most resistive fuel assembly in this group of fuel types. A rigorous finite element model of SPC-5 fuel assembly was developed to confirm that its in-plane heat dissipation characteristics are bounded from below by the design basis BWR fuel conductivities used in the HI-STAR thermal analysis.

Temperature-dependent effective conductivities of PWR and BWR design basis fuel assemblies (most resistive SNF types) are shown in Figure 3.4.13. The finite-volume results are also compared to results reported from independent technical sources. From this comparison, it is readily apparent that FLUENT-based fuel assembly conductivities are conservative. The FLUENT computed values (not the published literature data) are used in the MPC thermal analysis presented in this document.

3.4.1.1.3 Effective Thermal Conductivity of Sheathing/Boral/Cell Wall Sandwich

Each MPC basket cell wall (except outer periphery MPC-68 & *mpc-32* cell walls) is manufactured with a Boral neutron absorbing plate for criticality control. Each Boral plate is sandwiched in a sheathing-to-basket wall pocket. A schematic of the "Box Wall-Boral-Sheathing" sandwich geometry of an MPC basket is illustrated in Figure 3.4.5. During fabrication, a uniformly applied normal pressure on each sheathing-Boral-cell wall sandwich prior to stitch welding of the sheathing periphery to the box wall ensures adequate surface-to-surface contact for elimination of any macroscopic air-gaps. The mean coefficient of linear expansion of Boral is higher than the basket materials thermal expansion coefficients. Consequently, basket heat-up from the contained SNF will

further ensure a tight fit of the Boral plate in the sheathing-to-cell wall pocket. The presence of small microscopic gaps due to less than perfect surface finish characteristics requires consideration of an interfacial contact resistance between the Boral and the box and sheathing surfaces. A conservative contact resistance resulting from a 2 mils Boral-to-pocket air-gap is applied to the analysis. Note that this gap would actually be filled with helium, so this is very conservative. In other words, no credit is taken for the interfacial pressure between Boral and stainless plate/sheet stock produced by the fixturing and welding process. Furthermore, no credit is taken for the presence of helium and radiative heat exchange across the Boral to sheathing or Boral to box wall gaps.

Heat conduction properties of a composite "Box Wall-Boral-Sheathing" sandwich in the two principal basket cross sectional directions as illustrated in Figure 3.4.5 (i.e., lateral "out-of-plane" and longitudinal "in-plane") are unequal. In the lateral direction, heat is transported across layers of sheathing, air helium-gap, Boral (B₄C and cladding layers) air helium-gap, and cell wall resistances that are in series (except for the small helium filled end regions shown in Figure 3.4.6). Heat conduction in the longitudinal direction, in contrast, is through an array of essentially parallel resistances comprised of these same layers. Resistance network models applicable to the two directions are illustrated in Figure 3.4.6. It is noted that in addition to the essentially series and parallel resistances of the composite wall layers for the "out-of-plane" and "in-plane" directions, respectively, the effect of small helium filled end regions is also included in the resistance network analogy. For the ANSYS based MPC basket thermal model, corresponding non-isotropic effective thermal conductivities in the two orthogonal directions are determined and applied in the analysis.

The non-isotropic conductivities are determined by constructing ANSYS models of the composite "Box Wall-Boral-Sheathing" sandwich for the "in-plane" and "out-of-plane" directions. For determining the effective conductivity (K_{eff}), a heat flux is applied to the to one end of the sandwich and an ANSYS numerical solution to the sandwich temperature differential obtained. From Fourier equation for one-dimensional conduction heat transfer, the following equation for K_{eff} is obtained:

$$K_{eff} = \frac{qL}{\Delta T}$$

where:

q = Sandwich heat flux

L = Sandwich length in the direction of heat transfer

ΔT = Sandwich temperature differential (obtained from ANSYS solution)

In the equation above, L is the width or thickness of the sandwich, respectively, for in-plane or out-of-plane heat transfer directions.

3.4.1.1.4 Modeling of Basket Conductive Heat Transport ~~ANSYS Modeling of Basket In-Plane Conductive Heat Transport~~

Conduction of heat in a fuel basket is a combination of planar and axial contributions. These component contributions are individually calculated for each MPC basket design and combined (as described later in this subsection) to obtain an equivalent isotropic thermal conductivity. The heat rejection capability of each MPC design (i.e., MPC-24, MPC-24E, MPC-32 and MPC-68) is evaluated by developing a thermal model of the combined fuel assemblies and composite basket walls geometry on the ANSYS finite element code. The ANSYS model includes a geometric layout of the basket structure in which the "Box Wall-Boral-Sheathing" sandwich is replaced by a "homogeneous wall" with an equivalent thermal conductivity. Since the thermal conductivity of the Alloy X material is a weakly varying function of temperature, the equivalent "homogeneous wall" must have a temperature-dependent effective conductivity. Similarly, as illustrated in Figure 3.4.6, the conductivities in the in-plane and through-thickness direction of the equivalent "homogeneous wall" are different. Finally, as discussed earlier, the fuel assemblies occupying the basket cell openings are modeled as homogeneous heat generating regions with effective temperature dependent in-plane conductivities. The methodology used to reduce the heterogeneous MPC basket - fuel assemblage to an equivalent homogeneous region with effective thermal properties is discussed in the following.

Consider a cylinder of height L and radius r_o with a uniform volumetric heat source term q_g , with insulated top and bottom faces and its cylindrical boundary maintained at a uniform temperature T_c . The maximum centerline temperature (T_h) to boundary temperature difference is readily obtained from classical one-dimensional conduction relationships (for the case of a conducting region with constant thermal conductivity K_s):

$$(T_h - T_c) = q_g r_o^2 / (4 K_s)$$

Noting that the total heat generated in the cylinder (Q_t) is $\pi r_o^2 L q_g$, the above temperature rise formula can be reduced to the following simplified form in terms of the total heat generation per unit length (Q_t/L):

$$(T_h - T_c) = (Q_t / L) / (4 \pi K_s)$$

This simple analytical approach is employed to determine an effective basket cross-sectional conductivity by applying an equivalence between the ANSYS finite element model of the basket and the analytical case. The equivalence principle employed in the HI-STAR System thermal analysis is depicted in Figure 3.4.2. The 2-dimensional ANSYS finite element model of the MPC basket is solved by applying a uniform heat generation per unit length in each basket cell region and a constant basket periphery boundary temperature, T_c' . Noting that the basket region with uniformly distributed heat sources and a constant boundary temperature is equivalent to the analytical case of a cylinder with uniform volumetric heat source discussed earlier, an effective MPC basket conductivity (K_{eff}) is readily derived from the analytical formula and the ANSYS solution leading to the following relationship:

$$K_{eff} = N (Q_f' / L) / (4 \pi [T_h' - T_c'])$$

where:

N = number of fuel assemblies

(Q_f'/L) = each fuel assembly heat generation per unit length applied in ANSYS model

T_h' = peak basket cross-section temperature from ANSYS model

Cross sectional views of the MPC basket ANSYS models are depicted-illustrated in Figures 3.4.10 and 3.4.11 for a PWR and BWR MPC. Notice that many of the basket supports and all shims have been conservatively neglected in the models. This conservative geometry simplification, coupled with the conservative neglect of thermal expansion which would minimize the gaps, yields conservative gap thermal resistances. Temperature dependent equivalent thermal conductivities of the fuel region and composite basket walls, as determined from analysis procedures described earlier, are applied to the ANSYS model. The planar ANSYS conduction model is solved by applying a constant basket periphery temperature with uniform heat generation in the fuel region. Table 3.4.6 summarizes effective thermal conductivity results of each basket design obtained from the ANSYS models. The effective calculated basket cross-sectional conductivity and the effective axial direction effective conductivity are conservatively assumed to be equal in the comprehensive HI-STAR System thermal model (see Section 3.4.1.1.2). It is recalled that the equivalent thermal conductivity values presented in Table 3.4.6 are lower bound values because, among other elements of conservatism, the effective conductivity of the most resistive SNF type (Tables 3.4.4 and 3.4.5) is used in the MPC finite-element simulations.

The axial conductivity of a fuel basket is determined by calculating a cross-sectional area-weighted sum of the component conductivities (Helium, Alloy-X, Boral and fuel cladding). In accordance with NUREG-1536 guidelines, credit for fuel rod axial heat conduction is conservatively limited to cladding.

Having obtained planar and axial thermal conductivities as described above, an equivalent isotropic conductivity (defined as the Square Root of the Mean Sum of Squares (SRMSS)) is obtained as shown below:*

$$k_{iso} = \sqrt{\frac{k_{rad}^2 + k_{ax}^2}{2}}$$

where:

k_{iso} = equivalent isotropic thermal conductivity

k_{rad} = equivalent planar thermal conductivity

** This formulation has been benchmarked for specific application to the MPC basket designs and confirmed to yield conservative results.*

k_{ax} = equivalent axial thermal conductivity

The equivalent isotropic conductivities are employed in the HI-STAR thermal modeling as discussed in Subsection 3.4.2.

3.4.1.1.5 Heat Transfer in MPC Basket Peripheral Regions

Each of the MPC designs for storing PWR or BWR fuel are provided with relatively large helium filled regions formed between the relatively cooler MPC shell and hot basket peripheral panels. For a horizontally oriented cask under normal transport conditions, heat transfer in these helium-filled regions is similar to heat transfer in closed cavities under three cases listed below:

- i. differentially heated short vertical cavity
- ii. horizontal channel heated from below
- iii. horizontal channel heated from above

In a closed cavity (case i scenario), an exchange of hot and cold fluids occurs near the top and bottom ends of the cavity, resulting in a net transport of heat across the gap.

The case (ii) scenario is similar to the classical Rayleigh-Benard instability of a layer of fluid heated from below [3.4.6]. If the condition for onset of fluid motion is satisfied, then a multi-cellular natural convection pattern is formed. The flow pattern results in upward motion of heated fluid and downward motion of relatively cooler fluid from the top plate, resulting in a net transport of heat across the heated fluid channel.

The case (iii) is a special form of case (ii) with an inverted (stably stratified) temperature profile. No fluid motion is possible in this circumstance and heat transfer is thus limited to fluid (helium) conduction only.

The three possible cases of closed cavity natural convection are illustrated in Figure 3.4.3 for an MPC-68 basket geometry. Peripheral spaces labeled B and B' illustrate the case (i) scenario, the space labeled D illustrates the case (ii) scenario, and the space labeled D' illustrates the case (iii) scenario. The basket is oriented to conservatively maximize the number of peripheral spaces having *no* fluid motion. A small alteration in the basket orientation will result in a non-zero gravity component in the x-direction which will induce case (i) type fluid motion in the D' space. The rate of natural convection heat transfer is characterized by a Rayleigh number for the cavity defined as follows:

$$Ra_L = \frac{C_p \rho^2 g \beta \Delta T L^3}{\mu K}$$

where:

- C_p = fluid heat capacity
- ρ = average fluid density
- g = acceleration due to gravity
- β = coefficient of thermal expansion (equal to reciprocal of absolute temperature for gases)
- ΔT = temperature difference between hot and cold surfaces
- L = spacing between hot and cold surfaces
- μ = fluid viscosity
- K = fluid conductivity

Hewitt et al. [3.4.5] report Nusselt number correlations for the closed cavity natural convection cases discussed earlier. A Nusselt number equal to unity implies heat transfer by fluid conduction only. A higher than unity Nusselt number is due to the so-called "Rayleigh" effect, which monotonically rises with increasing Rayleigh number. Nusselt numbers applicable to helium filled PWR and BWR HI-STAR MPCs in the peripheral voids are provided in Table 3.4.1. ~~These numbers are used to enhance helium conductivity only in the basket peripheral spaces. For conservatism, the heat dissipation enhancement due to Rayleigh effect is ignored.~~

3.4.1.1.6 Effective Conductivity of Multi-Layered Intermediate Shell Region

Fabrication of the layered overpack intermediate shells is discussed in Section 1.2 of this SAR. In the thermal analysis, each intermediate shell metal-to-metal interface presents an additional resistance to heat transport. The contact resistance arises from microscopic pockets of air trapped between surface irregularities of the contacting surfaces. Since air is a relatively poor conductor of heat, this results in a reduction in the ability to transport heat across the interface compared to that of the base metal. Interfacial contact conductance depends upon three principal factors, namely: (i) base material conductivity, (ii) interfacial contact pressure, and (iii) surface finish.

Rohsenow and Hartnett [3.2.2] have reported results from experimental studies of contact conductance across air entrapped stainless steel surfaces with a typical 100 μ -inch surface finish. A minimum contact conductance of 350 Btu/ft-hr- $^{\circ}$ F is determined from extrapolation of results to zero

contact pressure.

The thermal conductivity of carbon steel is about three times that of stainless steel. Thus the choice of carbon steel as the base material in a multi-layered construction significantly improves heat transport across interfaces. The fabrication process guarantees interfacial contact. Contact conductance values extrapolated to zero contact pressures are therefore conservative. The surface finish of hot-rolled carbon steel plate stock is generally in the range of 250-1000 μ -inch [3.2.1]. The process of forming hot-rolled flat plate stock to cylindrical shapes to form the intermediate shells by rolling will result in a smoother surface finish. This results from the large surface pressures exerted by the hardened roller faces that flatten out any surface irregularities.

In the HI-STAR thermal analysis, a conservatively bounding interfacial contact conductance value is determined based on the following assumptions:

1. No credit is taken for high base metal conductivity.
2. No credit is taken for interfacial contact pressure.
3. No credit is taken for a smooth surface finish resulting from rolling of hot-rolled plate stock to cylindrical shapes.
4. Contact conductance is based on a uniform 2000 μ -inch (1000 μ -inch for each surface condition) interfacial air gap at all interfaces.
5. No credit for radiation heat exchange across this hypothetical inter-surface air gap.
6. Bounding low thermal conductivity at 200°F.

These assumptions guarantee a conservative assessment of heat dissipation characteristics of the multi-layered intermediate shell region. The resistances of the five carbon steel layers along with the associated interfacial resistances are combined as resistances in series to determine an effective conductivity of this region leading to the following relationship:

$$K_{gs} = r_o \ell n \left[\frac{r_5}{r_o} \right] \left[\sum_{i=1}^5 \frac{\delta}{K_{air} r_i} + \frac{r_o \ell n \left[\frac{r_5}{r_o} \right]}{K_{cst}} \right]^{-1}$$

where (in conventional U.S. units):

K_{gs}	=	effective intermediate shell region thermal conductivity
r_o	=	inside radius of inner gamma shield layer
r_i	=	outer radius of i^{th} intermediate shell layer
δ	=	interfacial air gap (2000 μ -inch)
K_{air}	=	air thermal conductivity
K_{cst}	=	carbon steel thermal conductivity

3.4.1.1.7 Heat Rejection from Overpack and Impact Limiter Outside Surfaces

Jakob and Hawkins [3.2.9] recommend the following correlations for natural convection heat transfer to air from heated vertical surfaces (flat impact limiter ends) and from single horizontal cylinders (overpack and impact limiter curved surfaces):

Turbulent range:

$$h = 0.19 (\Delta T)^{1/3} \text{ (Vertical, GrPr} > 10^9 \text{)}$$

$$h = 0.18 (\Delta T)^{1/3} \text{ (Horizontal Cylinder, GrPr} > 10^9 \text{)}$$

(in conventional U.S. units)

Laminar range:

$$h = 0.29 \left(\frac{\Delta T}{L}\right)^{1/4} \text{ (Vertical, GrPr} < 10^9 \text{)}$$

$$h = 0.27 \left(\frac{\Delta T}{D}\right)^{1/4} \text{ (Horizontal Cylinder, GrPr} < 10^9 \text{)}$$

(in conventional U.S. units)

where ΔT is the temperature differential between the system exterior surface and ambient air. During normal transport conditions, the surfaces to be cooled are the impact limiter and overpack cylindrical surfaces, and the flat vertical faces of the impact limiters. The corresponding length scales for these surfaces are the impact limiter diameter, overpack diameter, and impact limiter diameter, respectively. Noting that $\text{Gr} \times \text{Pr}$ is expressed as $L^3 \Delta T Z$, where Z (from Table 3.2.7) is at least 2.6×10^5 at a conservatively high upper bound system exterior surface temperature of 340°F , it is apparent that the turbulent condition is always satisfied for ΔT in excess of a few degrees Fahrenheit. Under turbulent conditions, the more conservative heat transfer correlation for horizontal cylinders (i.e., $h = 0.18 \Delta T^{1/3}$) is utilized for thermal analyses on all exposed system surfaces.

Including both convective and radiative heat loss from the system exterior surfaces, the following relationship for surface heat flux is developed:

$$q_s = 0.18 (T_s - T_A)^{1/3} + \sigma \times \epsilon \times [(T_s + 460)^4 - (T_A + 460)^4]$$

where:

- $T_s, T_A =$ surface, ambient temperatures ($^\circ\text{F}$)
- $q_s =$ surface heat flux ($\text{Btu}/\text{ft}^2\text{-hr}$)
- $\epsilon =$ surface emissivity (see Table 3.2.4)
- $\sigma =$ Stefan-Boltzman Constant ($0.1714 \times 10^{-8} \text{ Btu}/\text{ft}^2\text{-hr-}^\circ\text{R}^4$)

3.4.1.1.8 Determination of Solar Heat Input

The intensity of solar radiation incident on an exposed surface depends on a number of time varying

parameters. The solar heat flux strongly depends upon the time of the day as well as on latitude and day of the year. Also, the presence of clouds and other atmospheric conditions (dust, haze, etc.) can significantly attenuate solar intensity levels. Rapp [3.4.2] has discussed the influence of such factors in considerable detail.

The HI-STAR System thermal analysis is based upon insolation levels specified in 10CFR71, Subpart F, which are for a 12-hour daytime period. During normal transport conditions, the HI-STAR System is cyclically subjected to solar heating during the 12-hour daytime period followed by cooling during the 12-hour nighttime. However, due to the large mass of metal and the size of the system, the inherent dynamic time lag in the temperature response is substantially larger than the 24-hour heating-cooling time period. Accordingly, the HI-STAR System cask model includes insolation at exposed surfaces averaged over a 24-hour time period. A bounding solar absorption coefficient of 1.0 is applied to cask exterior surfaces. The 10CFR71 mandated 12-hour average incident solar radiation levels are summarized in Table 3.4.7. The combined incident insolation heat flux absorbed by exposed cask surfaces and decay heat load from the MPC is rejected by natural convection and radiation to ambient air.

3.4.1.1.9 Effective Thermal Conductivity of Radial Channels - Holtite Region

In order to minimize heat transfer resistance limitations due to the poor thermal conductivity of the Holtite-A neutron shield material, a large number of thick radial channels formed from high strength and conductivity carbon steel material are embedded in the neutron shield region. These radial channels form highly conductive heat transfer paths for efficient heat removal. Each channel is welded to the outside surface of the outermost intermediate shell and at the overpack enclosure shell, thereby providing a continuous path for heat removal to the ambient environment.

The effective thermal conductivity of the composite neutron shielding and radial channels region is determined by combining the heat transfer resistance of individual components in a parallel network. In determining the heat transfer capability of this region to the outside ambient environment for normal transport conditions, *no credit is taken for conduction through the neutron shielding material*. Thus, heat transport from the outer intermediate shell surface to the overpack outer shell is conservatively based on heat transfer through the carbon steel radial channel legs alone. Thermal conductivity of the parallel neutron shield and radial channel leg region is given by the following formula:

$$K_{ne} = \frac{K_R N_R t_R \ln \left[\frac{r_B}{r_A} \right]}{2 \pi L_R} + \frac{K_{ns} N_R t_{ns} \ln \left[\frac{r_B}{r_A} \right]}{2 \pi L_R}$$

where (in consistent U.S. units):

K_{ne} = effective thermal conductivity of neutron shield region
 r_A = inner radius of neutron shielding

r_B	=	outer radius of neutron shielding
K_R	=	effective thermal conductivity of carbon steel radial channel leg
N_R	=	total number of radial channel legs (also equal number of neutron shield sections)
t_R	=	minimum (nominal) thickness of each radial channel leg
L_R	=	effective radial heat transport length through radial channel leg
K_{ns}	=	neutron shield thermal conductivity
t_{ns}	=	neutron shield circumferential thickness (between two radial channel legs)

The radial channel leg to outer intermediate shell surface weld thickness is equal to half the plate thickness. The additional weld resistance is accounted for by reducing the plate thickness in the weld region for a short radial span equal to the weld size. Conductivity of the radial carbon steel channel legs based on the full thickness for the entire radial span is correspondingly reduced. Figure 3.4.4 depicts a resistance network developed to combine the neutron shield and radial channel legs resistances to determine an effective conductivity of the neutron shield region. Note that in the resistance network analogy only the annulus region between overpack outer enclosure inner surface and intermediate shells outer surface is considered in this analysis. The effective thermal conductivity of neutron shield region is provided in Table 3.4.8.

3.4.1.1.10 Effective Thermal Conductivity of the Eccentric MPC to Overpack Gap

During horizontal shipment of the HI-STAR System under normal transport conditions, the MPC will rest on the inside surface of the overpack. In the region of line contact, the resistance to heat transfer across the gap will be negligibly small due to a vanishingly small gap thickness. The resistance to heat transfer at other regions along the periphery of the MPC will, however, increase in direct proportion to the thickness of the local gap. This variation in gap thickness can be accounted for in the thermal model by developing a relation for the total heat transferred across the gap as given below:

$$Q_E = 2 \int_0^\pi \frac{K_{He}}{g(\theta)} L R_o \Delta T d\theta$$

where:

Q_E	=	total heat transfer across the gap (Btu/hr)
K_{He}	=	helium conductivity Btu/ft-hr-°F
L	=	length of MPC (ft.)
R_o	=	MPC radius (ft.)
θ	=	angle from point of line contact
$g(\theta)$	=	variation of gap thickness with angle (ft.)
ΔT	=	temperature difference across the gap (°F)

A corresponding relationship for heat transferred across a uniform gap is given by:

$$Q_c = \frac{K_{eff}}{(R_1 - R_0)} 2\pi R_0 L \Delta T$$

where R_1 is the inside radius of the overpack and K_{eff} is the effective thermal conductivity of an equivalent concentric MPC/overpack gap configuration. From these two relationships, the ratio of effective gap conductivity to helium thermal conductivity in the MPC/overpack region is shown below:

$$\frac{K_{eff}}{K_{He}} = \frac{R_1 - R_0}{\pi} \int_0^\pi \frac{1}{g(\theta)} d\theta$$

Based on an analysis of the geometry of a thin gap between two eccentrically positioned cylinders, the following relationship is developed for variation of the gap thickness with position:

$$g(\theta) = (R_1 - R_0)(1 - \cos \theta) + \epsilon \cos \theta$$

The above equation conservatively accounts for imperfect contact by postulating a minimum gap ϵ at the point where the two surfaces would ideally form a line of perfect contact. The relatively thin MPC shell is far more flexible than the much thicker overpack inner shell, and will ovalize to yield greater than line contact. The substantial weight of the fuel basket and contained fuel assemblies will also cause the MPC shell to conform to the overpack inner shell. An evaluation based on contact along a line would therefore be reasonable and conservative. However, a minimum gap is assumed to further increase conservatism in this calculation.

Based on an applied gap of 0.02-inch, which is conservative compared to contact along a line, the effective gap thermal conductivity determined from analytical integration [3.4.7] is in excess of 200% of the conductivity of helium gas. In the HI-STAR analysis, a conservative effective gap conductivity equal to twice the helium gas conductivity is applied to the performance evaluation.

3.4.1.1.11 Effective Thermal Conductivity of MPC Basket-to-Shell Aluminum Heat Conduction Elements

As shown in MPC Drawings 1395 and 1401, The HI-STAR MPCs feature an option to install full-length heat conduction elements fabricated from aluminum alloy 1100 ~~are placed in the large MPC basket-to-shell gaps. to provide uninterrupted metal pathways to transport heat from the basket periphery to the MPC shell.~~ Due to the high aluminum alloy 1100 thermal conductivity (about 15 times that of Alloy X), a significant rate of net heat transfer is possible along the thin plates. For conservatism, heat dissipation by the Aluminum Heat Conduction Elements (AHCEs) is ignored in normal transport analyses. This overstates the initial fuel temperature for hypothetical fire accident evaluation. To conservatively compute heating of MPC contents in a hypothetical fire condition, the presence of heat conduction elements in AHCE equipped MPCs is duly recognized.

Figure 3.4.12 shows a mathematical idealization of a heat conduction element inserted between basket periphery panels and the MPC shell. The aluminum insert is shown to cover the MPC basket Alloy X peripheral panel and MPC shell surfaces (Regions I and III depicted in Figure 3.4.12) along the full-length of the basket. Heat transport to and from the aluminum insert is conservatively postulated to occur across a thin helium gap as shown in the figure (i.e., no credit is considered for aluminum insert to Alloy X metal-to-metal contact). Aluminum surfaces inside the hollow region are sandblasted prior to fabrication to result in a rough surface finish which has a significantly higher emissivity compared to smooth surfaces of rolled aluminum. The untreated aluminum surfaces directly facing Alloy X panels have a smooth finish to minimize contact resistance.

Net heat transfer resistance from the hot basket periphery panel to the relatively cooler MPC shell along the aluminum heat conduction element pathway is a sum of three individual resistances in regions labeled I, II, and III. In Region I, heat is transported from the basket to the aluminum insert surface directly facing the basket panel across a thin helium resistance gap. Longitudinal transport of heat (in the z direction) in the aluminum plate (in Region I) will result in an axially non-uniform temperature distribution. Longitudinal one-dimensional heat transfer in the Region I aluminum plate is analytically formulated to result in the following ordinary differential equation for the non-uniform temperature distribution:

$$t K_{Al} \frac{\partial^2 T}{\partial z^2} = - \frac{K_{He}}{h} (T_h - T) \quad \text{(Equation a)}$$

Boundary Conditions

$$\begin{aligned} \frac{\partial T}{\partial z} &= 0 \text{ at } z = 0 \\ T &= T_h' \text{ at } z = P \end{aligned} \quad \text{(Equation b)}$$

where (see Figure 3.4.12):

T(z)	=	non-uniform aluminum metal temperature distribution
t	=	conduction element thickness
K _{Al}	=	conduction element conductivity
K _{He}	=	helium conductivity
h	=	helium gap thickness
T _h	=	hot basket temperature
T _h '	=	conduction element Region I boundary temperature at z = P
P	=	conduction element Region I length

Solution of this ordinary differential equation subject to the imposed boundary condition is:

$$(T_h - T) = (T_h - T_h') \left[\frac{e^{\frac{z}{\sqrt{\alpha}}} + e^{-\frac{z}{\sqrt{\alpha}}}}{e^{\frac{P}{\sqrt{\alpha}}} + e^{-\frac{P}{\sqrt{\alpha}}}} \right] \quad (\text{Equation c})$$

where α is a dimensional parameter equal to htK_{Al}/K_{He} . The net heat transfer (Q_I) across the Region I helium gap can be determined by the following integrated heat flux to a conduction element of length L as:

$$Q_I = \int_0^P \frac{K_{He}}{h} (T_h - T) (L) dz \quad (\text{Equation d})$$

Substituting the analytical temperature distribution result obtained in Equation c into Equation d and then integrating, the following expression for net heat transfer is obtained:

$$Q_I = \frac{K_{He} L \sqrt{\alpha}}{h} \left(1 - \frac{1}{e^{\frac{P}{\sqrt{\alpha}}} + e^{-\frac{P}{\sqrt{\alpha}}}} \right) (T_h - T_h') \quad (\text{Equation e})$$

Based on this result, an expression for Region I resistance is obtained as shown below:

$$R_I = \frac{T_h - T_h'}{Q_I} = \frac{h}{K_{He} L \sqrt{\alpha}} \left(1 - \frac{1}{e^{\frac{P}{\sqrt{\alpha}}} + e^{-\frac{P}{\sqrt{\alpha}}}} \right)^{-1} \quad (\text{Equation f})$$

Similarly, a Region III resistance expression can be analytically determined as shown below:

$$R_{III} = \frac{(T_c' - T_c)}{Q_{III}} = \frac{h}{K_{He} L \sqrt{\alpha}} \left(1 - \frac{1}{e^{\frac{P}{\sqrt{\alpha}}} + e^{-\frac{P}{\sqrt{\alpha}}}} \right)^{-1} \quad (\text{Equation g})$$

A Region II resistance expression can be developed from the following net heat transfer equation in

the vertical leg of the conduction element as shown below:

$$Q_{II} = \frac{K_{AI} L t}{W} (T_h' - T_c') \quad (\text{Equation h})$$

Hence,

$$R_{II} = \frac{T_h' - T_c'}{Q_{II}} = \frac{W}{K_{AI} L t} \quad (\text{Equation i})$$

This completes the analysis for the total thermal resistance attributable to the heat conduction elements equal to sum of the three individual resistances. The total resistance is smeared across the basket-to-MPC shell region as an effective uniform annular gap conductivity (see Figure 3.4.2). Note that heat transport along the conduction elements is an independent conduction path in parallel with conduction and radiation mechanisms in the large helium gaps. Helium conduction and radiation between the MPC basket and the MPC shell is accounted for separately in the ANSYS MPC models described earlier in this section. Therefore, the total MPC basket-to-MPC shell peripheral gaps conductivity will be the sum of the conduction elements effective conductivity and the helium conduction-radiation gap effective conductivity.

3.4.1.1.12 FLUENT Model for HI-STAR Temperature Field Computation

In the preceding subsections, the series of analytical and numerical models to define the thermal characteristics of the various elements of the HI-STAR System are presented. The thermal modeling begins with the replacement of the SNF cross section and surrounding fuel cell space by a solid lamina with an equivalent conductivity. Since radiation is an important constituent of the heat transfer process in the SNF/storage cell space and the rate of radiation heat transfer is a strong function of the surface temperatures, it is necessary to treat the equivalent lamina conductivity as a function of temperature. In fact, because of the relatively large range of temperatures which will exist in a loaded HI-STAR System under the design basis heat loads, it is necessary to include the effect of variation in the thermal conductivity of materials with temperature throughout the system finite volume model. The presence of significant radiation effect in the storage cell spaces adds to the imperative to treat the equivalent lamina conductivity as temperature-dependent.

FLUENT finite volume simulations have been performed to establish the equivalent thermal conductivity as a function of temperature for the limiting (thermally most resistive) BWR and PWR spent fuel types. By utilizing the most limiting SNF (established through a simplified analytical process for comparing conductivities) the numerical idealization for the fuel space conductivity is ensured to be conservative for all non-limiting fuel types.

Having replaced the interior of the cell spaces by solid prismatic (square) columns possessing a temperature-dependent conductivity essentially renders the basket into a non-homogeneous three-dimensional solid where the non-homogeneity is introduced by the honeycomb basket structure. The basket panels themselves are a composite of Alloy X cell wall, Boral neutron absorber, and Alloy X sheathing metal. A conservative approach to replace this composite section with an equivalent "solid wall" is described in a preceding subsection.

In the next step, a planar section of the MPC is considered. The MPC, externally radially symmetric, contains a non-symmetric basket lamina wherein the equivalent fuel space solid squares are separated by the "equivalent" solid metal walls. The space between the basket and the MPC, called the peripheral gap, is filled with helium gas and *optionally* aluminum heat conduction elements (shown in MPC Drawings 1395 and 1401). The equivalent thermal conductivity of this MPC section is computed using a finite element procedure on ANSYS, as described previously. *For hypothetical fire conditions* the "helium-conduction-radiation" based peripheral gap conductivity, ~~the~~ and the effective conductivity of aluminum conduction elements *is are* added to obtain a combined effective conductivity. At this stage in the thermal analysis, the SNF/basket/MPC assemblage has been replaced with a two-zone (Figure 3.4.2) cylindrical solid whose thermal conductivity is a strong function of temperature.

The idealization for the overpack is considerably more straightforward. The overpack is radially symmetric except for the Holtite region (discussed in Subsection 3.4.1.1.9). The procedure to replace the multiple shell layers, Holtite-A and radial connectors with an equivalent solid utilizes classical heat conduction analogies, as described in the preceding subsections.

In the final step of the analysis, the equivalent two-zone MPC cylinder, the equivalent overpack shell, the top and bottom plates, and the impact limiters are assembled into a comprehensive finite volume model. A cross section of this axisymmetric model implemented on FLUENT is shown in Figure 3.4.14. A summary of the essential features of this model is presented in the following:

- The overpack shell is represented by 840×9 elements. The effective thermal conductivity of the overpack shell elements is set down as a function of temperature based on the analyses described earlier.
- The overpack bottom plate and bolted closure plate are modeled by 312×9 axisymmetric elements.
- The two-zone MPC "solid" is represented by 1,144×9 axisymmetric elements.
- The space between the MPC "solid" and the overpack interior space is assumed to contain helium.
- Heat input due to insolation is applied to the impact limiter surfaces and the cylindrical

surface of the overpack.

- The heat generation in the MPC solid basket region is assumed to be uniform in each horizontal plane, but to vary in the axial direction to correspond to the axial burnup distribution in the active fuel region postulated in Chapter 1.

The finite volume model constructed in this manner will produce an axisymmetric temperature distribution. The peak temperature will occur near the centerline and is expected to correspond to the axial location of peak heat generation. As is shown later, the results from the finite element solution bear out these observations.

3.4.1.1.13 Effect of Fuel Cladding Crud Resistance

In this subsection, a conservatively bounding estimate of the temperature drop across a crud film adhering to a fuel rod during dry storage conditions is determined. The evaluation is performed for a BWR fuel assembly based on an upper bound crud thickness obtained from PNL-4835 report ([3.3.5], Table 3). The crud present on fuel assemblies is predominantly iron oxide mixed, with small quantities of other metals such as cobalt, nickel, chromium, etc. Consequently, the effective conductivity of the crud mixture is expected to be in the range of typical metal alloys. Metals have thermal conductivities several orders of magnitude larger than that of helium. In the interest of extreme conservatism, however, a film of helium with the same thickness replaces the crud layer. The calculation is performed in two steps. In the first step, a crud film resistance is determined based on bounding maximum crud layer thickness replaced as a helium film on the fuel rod surfaces. This is followed by a peak local cladding heat flux calculation for the smaller GE 7x7 fuel assembly postulated to emit a conservatively bounding decay heat equal to 0.5kW. The temperature drop across the crud film obtained as a product of the heat flux and crud resistance terms is determined to be less than 0.1°F. The calculations are presented below:

Bounding Crud Thickness (δ) = 130 μ m (4.26×10^{-4} ft)
(PNL-4835)

Crud Conductivity (K) = 0.1 Btu/ft-hr-°F (conservatively assumed as helium)

GE 7x7 Fuel Assembly:

Rod O.D.	=	0.563"
Active Fuel Length	=	150"
Heat Transfer Area	=	(7x7) ($\pi \times 0.563$) \times 150/144
	=	90.3 ft ²
Axial Peaking Factor	=	1.195 (Burnup distribution Table 1.2.15)
Decay Heat	=	500W (conservative assumption)

$$\text{Crud Resistance} = \frac{\delta}{K} = \frac{4.26 \times 10^{-4}}{0.1} = 4.26 \times 10^{-3} \frac{\text{ft}^2 \cdot \text{hr} \cdot ^\circ\text{F}}{\text{Btu}}$$

$$\begin{aligned} \text{Peak Heat Flux} &= \frac{(500 \times 3.417) \text{ Btu/hr}}{90.3 \text{ ft}^2} \times 1.195 \\ &= 18.92 \times 1.195 = 22.6 \frac{\text{Btu}}{\text{ft}^2 \cdot \text{hr}} \end{aligned}$$

Temperature drop (ΔT_c) across crud film:

$$\begin{aligned} &= 4.26 \times 10^{-3} \frac{\text{ft}^2 \cdot \text{hr} \cdot ^\circ\text{F}}{\text{Btu}} \times 22.6 \frac{\text{Btu}}{\text{ft}^2 \cdot \text{hr}} \\ &= 0.096^\circ\text{F} \\ &\text{(i.e., less than } 0.1^\circ\text{F)} \end{aligned}$$

Therefore, it is concluded that deposition of crud does not materially change the SNF cladding temperature.

3.4.1.1.14 Maximum Time Limit During Wet Transfer

While loading an empty HI-STAR System for transport directly from a spent fuel pool, water inside the MPC cavity is not permitted to boil. Consequently, uncontrolled pressures in the de-watering, purging, and recharging system that may result from two-phase condition, are completely avoided. This requirement is accomplished by imposing a limit on the maximum allowable time duration for fuel to be submerged in water after a loaded HI-STAR cask is removed from the pool and prior to the start of vacuum drying operations.

When the HI-STAR overpack and the loaded MPC under water-flooded conditions are removed from the pool, the combined mass of the water, the fuel, the MPC, and the overpack will absorb the decay heat emitted by the fuel assemblies. This results in a slow temperature rise of the entire system with time, starting from an initial temperature of the contents. The rate of temperature rise is limited by the thermal inertia of the HI-STAR system. To enable a bounding heat-up rate determination for the HI-STAR system, the following conservative assumptions are imposed:

- i. Heat loss by natural convection and radiation from the exposed HI-STAR surfaces to the pool building ambient air is neglected (i.e., an adiabatic temperature rise calculation is performed).
- ii. Design Basis maximum decay heat input from the loaded fuel assemblies is imposed on the HI-STAR system.
- iii. The smallest of the *minimum* MPC cavity-free volumes between the two

MPC types is considered for flooded water mass determination.

- iv. Fifty percent of the water mass in the MPC cavity is credited towards water thermal inertia evaluation.

Table 3.4.19 summarizes the weights and thermal inertias of several components in the loaded HI-STAR system. The rate of temperature rise of the HI-STAR and its contents during an adiabatic heat-up is governed by the following equation:

$$\frac{dT}{d\tau} = \frac{Q}{C_h}$$

where:

Q = decay heat load (Btu/hr) [equal to Design Basis maximum (between the two MPC types) 20.0 kW (i.e., 68,260 Btu/hr)]

C_h = combined thermal inertia of the loaded HI-STAR system (Btu/°F)

T = temperature of the contents (°F)

τ = time after HI-STAR system is removed from the pool (hr)

A bounding heat-up rate for the HI-STAR system contents is determined to be equal to 2.19°F/hr. From this adiabatic rate of temperature rise estimate, the maximum allowable time duration (t_{max}) for fuel to be submerged in water is determined as follows:

$$t_{\max} = \frac{T_{\text{boil}} - T_{\text{initial}}}{dT/d\tau}$$

where:

T_{boil} = boiling temperature of water (equal to 212°F at the water surface in the MPC cavity)

T_{initial} = initial temperature of the HI-STAR contents when removed from the pool

Table 3.4.20 provides a summary of t_{max} at several initial HI-STAR contents temperatures.

As set forth in Section 7.4, in the unlikely event where the maximum allowable time provided in Table 3.4.20 is found to be insufficient to complete all wet transfer operations, a forced water circulation shall be initiated and maintained to remove the decay heat from the MPC cavity. In this case, relatively cooler water will enter via the MPC lid drain port connection and heated water will exit from the vent port. The minimum water flow rate required to maintain the MPC cavity water temperature below boiling with an adequate subcooling margin is determined as follows:

$$M_w = \frac{Q}{C_{pw}(T_{max} - T_{in})}$$

where:

M_w = minimum water flow rate (lb/hr)

C_{pw} = water heat capacity (Btu/lb-°F)

T_{max} = maximum MPC cavity water mass temperature

T_{in} = temperature of water supply to MPC

With the MPC cavity water temperature limited to 150°F, MPC inlet water maximum temperature equal to 125°F and at the design basis maximum heat load, the water flow rate is determined to be 2,731 lb/hr (5.5 gpm).

3.4.1.1.15 Cask Cooldown and Reflood Analysis During Fuel Unloading Operation

Before a loaded HI-STAR System can be unloaded (i.e., fuel removed from the MPC) the cask must be cooled from the operating temperatures and reflooded with water*. Past industry experience generally supports cooldown of cask internals and fuel from hot storage conditions by direct water quenching. However, the extremely rapid cooldown rates that are typical during water injection, to which the hot cask internals and fuel cladding are subjected to, may result in uncontrolled thermal stresses and failure in the structural members. Moreover, water injection results in large amounts of steam generation and unpredictable transient two-phase flow conditions inside the MPC cavity, which may result in over-pressurization of the MPC helium retention boundary and a potentially unacceptable reduction in the safety margins to prevent criticality. To avoid potential safety concerns related to rapid cask cooldown by direct water quenching, the HI-STAR MPCs are designed to be cooled in a gradual manner, thereby eliminating thermal shock loads on the cask internals and fuel cladding.

In the unlikely event that a HI-STAR system is required to be unloaded, it will be transported back to the fuel handling building. Prior to reflooding the MPC cavity with water, a forced flow helium recirculation system with adequate flow capacity shall be operated to remove the decay heat and initiate a slow cask cooldown lasting for several days. The operating procedures in Section 7.2 provide a detailed description of the steps involved in the cask unloading. In this section, an analytical evaluation is presented to provide the basis for helium flow rates and time of forced cooling to meet the objective of eliminating thermal shock when the MPC cavity is eventually

* Certain fuel configurations in PWR MPCs require Borated water for criticality control (Chapter 6). Such MPCs are reflooded with Borated water.

flooded with water.

Under a closed loop forced helium circulation condition, the helium gas is cooled via an external chiller, down to 100°F, and then introduced inside the MPC cavity from the drain line near the bottom baseplate. The helium gas enters the MPC basket from the bottom oversized flow holes and moves upward through the hot fuel assemblies, removing heat and cooling the MPC internals. The heated helium gas exits from the basket top and collects in the top plenum, from where it is expelled through the MPC lid vent connection to the helium recirculation and cooling system. The bulk average temperature reduction of the MPC contents as a function of time is principally dependent upon the rate of helium circulation. The temperature transient is governed by the following heat balance equation:

$$C_h \frac{dT}{d\tau} = Q_D - m C_p (T - T_i) - Q_c$$

Initial Condition: $T = T_o$ at $\tau = 0$

where:

T = MPC bulk average temperature (°F)

T_o = initial MPC bulk average temperature in the HI-STAR system
(equal to 483°F* {3.4.16})

τ = time after start of forced circulation (hr)

Q_D = decay heat load (Btu/hr)
(equal to Design Basis maximum 20.0 kW (i.e., 68,260 Btu/hr))

m = helium circulation rate (lb/hr)

C_p = helium heat capacity (Btu/lb-°F)
(equal to 1.24 Btu/lb-°F)

Q_c = heat rejection from cask exposed surfaces to ambient (Btu/hr)
(conservatively neglected)

C_h = thermal capacity of the loaded MPC (Btu/°F)
(For a bounding upper bound 100,000 lb loaded MPC weight, and heat capacity of Alloy X equal to 0.12 Btu/lb-°F, the heat capacity is equal to 12,000 Btu/°F)

* Bounding for HI-STAR normal transport.

$T_i =$ MPC helium inlet temperature ($^{\circ}\text{F}$)

The differential equation is analytically solved, yielding the following expression for time-dependent MPC bulk temperature:

$$T(t) = \left(T_i + \frac{Q_D}{m C_p}\right) \left(1 - e^{-\frac{m C_p t}{c_h}}\right) + T_o e^{-\frac{m C_p t}{c_h}}$$

This equation is used to determine the minimum helium mass flow rate that would cool the MPC cavity down from initially hot conditions to less than 200°F . For example, to cool the MPC to less than 200°F in 72 hours would require a helium mass flow rate of 574 lb/hr (i.e., 859 SCFM).

Once the helium gas circulation has cooled the MPC internals to less than 200°F , water can be injected to the MPC without risk of boiling and the associated thermal stress concerns. Because of the relatively long cooldown period, the thermal stress contribution to the total cladding stress would be negligible, and the total stress would therefore be bounded by the normal (dry) condition. The elimination of boiling eliminates any concern of over-pressurization due to steam production.

3.4.1.1.16 MPC Temperature Distribution Evaluation Under Vacuum-Drying Conditions

The initial loading of SNF in the MPC requires that the water within the MPC be drained, *residual moisture removed* and MPC filled ~~replaced~~ with helium. This operation on the HI-STAR MPCs will be carried out using a ~~conventional vacuum drying approach. In this method, Forced Helium Dehydrator (FHD) for a "load-and-go" operation. A "load-and-go" operation is defined as an activity wherein an MPC is loaded for direct off-site shipment in a HI-STAR transport cask. MPCs prepared via other competent methods for MPC drying as approved by the NRC on other dockets (1008 and 1014) are duly recognized for transport under this docket. removal of the last traces of residual moisture from the MPC cavity is accomplished by evacuating the MPC for a short time after draining the MPC.~~

~~Prior to the start of the MPC draining operation, both the overpack annulus and the MPC are full of water. The presence of water in the MPC ensures that the fuel cladding temperatures are lower than design basis limits by large margins. As the heat generating active fuel length is uncovered during the draining operation, the fuel and basket mass will undergo a gradual heat up from the initially cold conditions when the heated surfaces were submerged under water.~~

~~A vacuum condition steady state analysis has been performed, for Holtec MPCs, at conservatively higher than transport design basis heat loads (22.25 kW for MPC 24 and 21.4 kW for MPC 68) to demonstrate that fuel cladding temperature limits are not exceeded. The results of this analysis, therefore, bound HI-STAR vacuum condition temperatures. The bounding analysis demonstrates that the steady state maximum temperatures in the vacuum condition will remain below short term~~

temperature limits:

To reduce moisture to trace levels in the MPC using a Forced Helium Dehydration (FHD) system, a closed loop system consisting of a condenser, a demohurizer, a compressor, and a pre-heater is utilized to extract moisture from the MPC cavity through repeated displacement of its contained helium, accompanied by vigorous flow turbulence. Appendix 3.B contains detailed discussion of the design and operation criteria for the FHD system.

The FHD system provides concurrent fuel cooling during the moisture removal process through forced convective heat transfer. The attendant forced convection-aided heat transfer occurring during operation of the FHD system ensures that the fuel cladding temperature will remain below the applicable peak cladding temperature limit for normal conditions of transport (752°F) for all combinations of SNF type, burnup, decay heat, and cooling time. Because the FHD operation induces a state of forced convection heat transfer in the MPC, (in contrast to the quiescent mode of natural convection in transport), it is readily concluded that the peak fuel cladding temperature under the latter condition will be greater than that during the FHD operation phase. In the event that the FHD system malfunctions, the forced convection state will degenerate to natural convection, which corresponds to the conditions of normal transport. As a result, the peak fuel cladding temperatures will approximate the values reached during normal transport as described elsewhere in this chapter.

3.4.1.1.17 Effects of Helium Dilution from Fuel Rod Gases

In this subsection, the generic cask transportation accident issue raised in a USNRC Spent Fuel Project Office (SFPO) staff guidance letter[†] is addressed. This issue directs cask designers to evaluate the impact of fission gas release into the canister, from a 100% fuel rods rupture accident, on the cask component temperatures and pressures when the MNOP* is within 10% of the design pressure.- To determine whether the HI-STAR System falls within the stipulated criteria, the MNOP results from Table 3.4.15 are provided below:

Canister	MNOP (psig)	Threshold Criteria [†] for Accident Evaluation (psig)
MPC-24	88.8	90
MPC-68	86.9	90
MPC-24E	88.9	90
MPC-32	89.3	90

[†] SFPO Director's Interim Staff Guidance Letter(s), W.F. Kane, (Interim Staff-Guidance-7), October 8, 1998.

* MNOP is a regulatory term defined in NUREG-1617 as the maximum gauge pressure that would develop in the containment in a period of 1 year under the heat condition specified in 10 CFR 71.71(c)(1) in the absence of venting, external ancillary cooling or operational controls.

[†] Accident evaluation required when MNOP is within 10% of the design pressure. This translates to a pressure that is between 100 psig (HI-STAR Design Pressure (Table 2.1.1) and 90 psig.

As shown above the MNOPs are below the threshold and an accident evaluation is not required. The Nevertheless, for illustrative purposes, a 100% rods rupture accident for a HI-STAR package with an MPC-24 canister is evaluated. ~~impact is illustrated from the limiting MPC-24 design, in which the MNOP is within 10% of the design pressure.~~

Under a severe hypothetical accident scenario 100% of the fuel rods may rupture, releasing the rod fill gas (helium) and a portion of the gaseous fission products (^3H , ^{85}Kr , ^{129}I and ^{131}Xe). The gaseous fission products release fractions are stipulated in NUREG-1536. The released gases will mix with the MPC backfill gas and reduce its thermal conductivity. This reduction in conductivity will result in a small increase in MPC temperatures and pressures.

Appendix C of NUREG/CR-0497 [3.4.13] describes a method for calculating the effective thermal conductivity of a mixture of gases. The same method is also described by Rohsenow and Hartnett [3.2.2]. The following expression is provided by both references:

$$k_{\text{mix}} = \sum_{i=1}^n \left(\frac{k_i x_i}{x_i + \sum_{\substack{j=1 \\ j \neq i}}^n \varphi_{ij} x_j} \right)$$

where:

- k_{mix} = thermal conductivity of the gas mixture (Btu/hr-ft-°F)
- n = number of gases
- k_i = thermal conductivity of gas component i (Btu/hr-ft-°F)
- x_i = mole fraction of gas component i

In the preceding equation, the term φ_{ij} is given by the following:

$$\varphi_{ij} = \phi_{ij} \left[1 + 2.41 \frac{(M_i - M_j)(M_i - 0.142 \cdot M_j)}{(M_i + M_j)^2} \right]$$

where M_i and M_j are the molecular weights of gas components i and j , and ϕ_{ij} is:

$$\phi_{ij} = \frac{\left[1 + \left(\frac{k_i}{k_j} \right)^{\frac{1}{2}} \left(\frac{M_i}{M_j} \right)^{\frac{1}{4}} \right]^2}{2^{\frac{3}{2}} \left(1 + \frac{M_i}{M_j} \right)^{\frac{1}{2}}}$$

Table 3.4.30 presents a summary of the gas mixture thermal conductivity calculations for an MPC-24 containing design basis PWR fuel assemblies.

Having calculated the gas mixture thermal conductivity, the effective thermal conductivity of the design basis PWR fuel assembly is calculated using the finite-volume model described in Subsection 3.4.1.1.2. Only the helium gas conductivity is changed, all other modeling assumptions are the same. The fuel assembly effective thermal conductivity with diluted helium is compared to that with undiluted helium in Table 3.4.31.

Next, the effective thermal conductivities of the MPC fuel basket and basket periphery regions are determined as described in Subsections 3.4.1.1.3 and 3.4.1.1.4. This calculation incorporates both the diluted helium thermal conductivity and the effective thermal conductivity of the fuel assembly with diluted helium. The Rayleigh effect thermal conductivity multipliers are unchanged in this analysis. This is conservative because the released rod gases will increase the average fluid density and decrease the gas thermal conductivity, consequently increasing the Rayleigh number. The effective thermal conductivities with diluted helium are compared to those with undiluted helium in Table 3.4.31.

The MPC fuel basket and basket periphery effective thermal conductivities are input to a finite-volume model of the HI-STAR System arranged for transport. The cask system temperature distribution with diluted MPC helium is determined using the finite-volume model, as described in Subsection 3.4.1.1.12. Design basis normal environmental conditions are applied to the model and a temperature field solution obtained. Cask system temperatures with diluted MPC helium are summarized in Table 3.4.32.

The slightly higher MPC cavity temperature with MPC helium dilution will result in a small perturbation in MPC internal pressure. Based on the temperature field obtained with helium dilution, the MPC internal pressure is determined using the Ideal Gas Law. The calculated MPC internal pressure with helium dilution is presented in Table 3.4.33.

The *results of analyses* presented in this subsection are performed to ~~determine~~ *illustrate* the effect of a hypothetical *100% rods rupture of all fuel rods in on* a HI-STAR package with an MPC-24 System. ~~during a severe transportation accident~~ *Even Under* under the extreme postulated conditions, the MPC component temperatures and pressures ~~are~~ *remain substantially below the design limits.* ~~within design limits.~~ Based on the results of these conservative calculations, it is determined that the effects of this severe hypothetical condition do not exceed the abilities of the HI-STAR System.

3.4.1.1.18 HI-STAR Temperature Field With Low Heat Emitting Fuel

The HI-STAR 100 thermal evaluations for BWR fuel are divided in two groups of fuel assemblies proposed for storage in MPC-68. These groups are classified as Low Heat Emitting

(LHE) fuel assemblies and Design Basis (DB) fuel assemblies. The LHE group of fuel assemblies are characterized by low burnup, long cooling time, and short active fuel lengths. Consequently, their heat loads are dwarfed by the DB group of fuel assemblies. The Dresden-1 (6x6 and 8x8), *Quad*⁺, and Humboldt Bay (7x7 and 6x6) fuel characteristics warrant their classification as LHE fuel. These characteristics, including burnup and cooling time limits imposed on this class of fuel, are presented in Table 2.1.6. This fuel (*except Quad*⁺ is permitted to be loaded when encased in Damaged Fuel Containers (DFCs). As a result of interruption of radiation heat exchange between the fuel assembly and the fuel basket by the DFC boundary, this loading configuration is bounding for thermal evaluation. In Subsection 4.3.4.1.1.2, two canister designs for encasing LHE fuel are evaluated – a previously approved Holtec Design (Holtec Drawing-1783) and an existing canister in which some of the Dresden-1 fuel is currently stored (Transnuclear D-1 Canister). The most resistive fuel assembly determined by analytical evaluation is considered for thermal evaluation (see Table 4.4.6). The MPC-68 basket effective conductivity, loaded with the most resistive fuel assembly from the LHE group of fuel (*encased in a canister*) is provided in Table 4.4.7. To this basket, LHE fuel decay heat load, is applied and a HI-STAR 100 System temperature field obtained. The low heat load burden limits the initial peak cladding temperature to less than 579°F which is substantially below the *cladding* temperature limit (*Table 3.3.1*) ~~for long-cooled fuel (~643°F)~~.

A thorium rod canister designed to hold a maximum of 20 fuel rods arrayed in a 5x4 configuration is currently stored at the Dresden-1 spent fuel pool. The fuel rods contain a mixture of enriched UO₂ and Thorium Oxide in the fuel pellets. The fuel rods were originally constituted as part of an 8x8 fuel assembly and used in the second and third cycle of Dresden-1 operation. The maximum fuel burnup of these rods is quite low (~13,100 MWD/MTU). The thorium rod canister internal design is a honeycomb structure formed from 12 gage stainless steel plates. The rods are loaded in individual square cells and are isolated from each other by the cell walls. The few number of rods (18 per assembly) and very low burnup of fuel stored in these Dresden-1 canisters render them as miniscule sources of decay heat. The canister all-metal internal honeycomb construction serves as an additional means of heat dissipation in the fuel cell space. In accordance with preferential fuel loading requirements, low burnup fuel shall be loaded toward the basket periphery (i.e., away from the hot central core of the fuel basket). All these considerations provide ample assurance that these fuel rods will be stored in a benign thermal environment and therefore remain protected during transport.

3.4.1.2 Test Model

A detailed analytical model for evaluating the thermal design of the HI-STAR System was developed using the FLUENT CFD code and the industry standard ANSYS modeling system as discussed in Subsection 3.4.1.1. Furthermore, the analysis incorporates many conservative assumptions in order to demonstrate compliance with specified temperature limits for operation with adequate margins. In view of these considerations, the HI-STAR thermal design complies with the thermal criteria set forth in the design basis for normal transport conditions. Additional experimental verification of the

thermal design is therefore not required. Acceptance and periodic thermal testing for the HI-STAR System is discussed in Sections 8.1 and 8.2.

3.4.2 Maximum Temperatures Under Normal Transport Conditions

Both MPC-basket designs developed for the HI-STAR System have been analyzed to determine temperature distributions under normal transport conditions. In the HI-STAR System thermal analysis models developed on FLUENT, the overpack impact limiters are included in the finite volume geometry. However, no credit is considered for the presence of heat conducting aluminum honeycomb material. In other words, heat transmission through the ends is conservatively neglected in the analysis. The thermal results are therefore bounding with respect to impact limiter design. The MPC baskets are considered to be loaded at design-basis maximum heat load with PWR or BWR fuel assemblies, as appropriate.

As discussed in Subsection 3.4.1.1.1, the thermal analysis is performed using a submodeling process where the results of an analysis on an individual component are incorporated into the analysis of a larger set of components. Specifically, the submodeling process yields directly computed fuel temperatures from which fuel basket temperatures are indirectly calculated. This modeling process differs from previous analytical approaches wherein the basket temperatures were evaluated first and then a basket-to-cladding temperature difference calculation by Wooten-Epstein or other means provided a basis for cladding temperatures. Subsection 3.4.1.1.2 describes the calculation of an effective fuel assembly thermal conductivity for an equivalent homogenous region. It is important to note that the result of this analysis is a function for thermal conductivity versus temperature. This function for fuel thermal conductivity is then input to the fuel basket effective thermal conductivity calculation described in Subsection 3.4.1.1.4. This calculation uses a finite-element methodology, wherein each fuel cell region containing multiple finite-elements has temperature varying thermal conductivity properties. The resultant temperature varying fuel basket thermal conductivity computed by this basket-fuel composite model is then input to the fuel basket region of the FLUENT cask model.

Because the FLUENT cask model incorporates the results of the fuel basket submodel, which in turn incorporates the fuel assembly submodel, the peak temperature reported from the FLUENT model is the peak temperature in any component. In a dry storage cask, the hottest components are the fuel assemblies. It should be noted that, because the fuel assembly models described in Subsection 3.4.1.1.2 include the fuel pellets, the FLUENT calculated peak temperatures reported in Tables 3.4.10 and 3.4.11 are actually peak pellet centerline temperatures which bound the peak cladding temperatures. We conservatively assume that the peak clad temperature is equal to the peak pellet centerline temperature.

From a thermal/hydraulic standpoint, the HI-STAR transport cask must cover two scenarios:

- i. *MPCs equipped with AHCEs*

ii. MPCs without AHCEs

In the thermal analysis submitted in support of HI-STAR's original transport certification, which we now refer to as the Baseline Thermal Model (BTM), the AHCEs are included in the thermal models and the basket thermal model is constructed in an exceedingly conservative manner. In particular, the axial conductance of the basket fuel assemblage is assumed to be equal to the in-plane conductance (in reality, the in-plane conductance is much smaller than the axial conductance due to the presence of physical gaps between the fuel and the cell and within the fuel assemblies). For the Scenario (ii) analysis, such an overarching conservatism is removed while certain other less sweeping conservatisms are retained. The revised model, which we refer to as the Refined Thermal Model (RTM), forms the licensing basis for thermal evaluation. The conservatisms germane to the RTM are summarized in Appendix 3.A. To summarize, the principal difference between the BTM and RTM are as follows:

<i>Item</i>	<i>Description</i>	<i>BTM Assumption</i>	<i>RTM Assumption</i>
<i>1</i>	<i>AHCE heat dissipation</i>	<i>Included</i>	<i>Excluded</i>
<i>2</i>	<i>Rayleigh effect</i>	<i>Included</i>	<i>Excluded</i>
<i>3</i>	<i>Basket Axial Conductivity</i>	<i>Grossly Understated</i>	<i>Realistic modeling of axial conductivity (See discussion in Subsection 3.4.1.1.4)</i>

For both the representative PWR (MPC-24) 24-PWR and BWR (MPC-68) 68-BWR assembly MPC-basket configurations with AHCEs installed, the temperature contours obtained with the Baseline Thermal Model (BTM) converged temperature contours corresponding to steady-state hot conditions (100°F ambient, maximum design basis maximum decay heat and full insolation) are shown in Figures 3.4.16 and 3.4.17. Figures 3.4.19 and 3.4.20 show the axial temperature variation of the hottest fuel rod in the MPC-24 and MPC-68 basket designs, respectively. Figures 3.4.22 and 3.4.23 show the radial temperature profile in the MPC-24 and MPC-68 basket designs, respectively, in the horizontal plane where maximum fuel cladding temperature is indicated. Tables 3.4.10 and 3.4.11 summarize maximum calculated temperatures in different parts of the HI-STAR System at design-basis maximum decay heat loads. Tables 3.4.28 and 3.4.29 summarize the peak fuel cladding temperatures with heat loads lower than the design basis maximum. In Tables 3.4.22 and 3.4.23, maximum calculated temperatures in different parts of the HI-STAR System under steady-state cold conditions (-40°F ambient, maximum design basis maximum decay heat and no insolation) are summarized. To confirm the BTM fuel temperatures provided herein are bounding for all MPCs without the AHCEs option (MPC-24, MPC-24E, MPC-32 and MPC-68) a Refined Thermal Model (RTM) is articulated as discussed in the preceding paragraph. As shown next, the results of the refined calculations confirm the BTM results are bounding.

<i>Maximum Cladding Temperatures</i>		
<i>MPC Type</i>	<i>BTM [°F]</i>	<i>RTM [°F]</i>
<i>PWR</i>	<i>701</i>	<i>671 (MPC-24) 668 (MPC-24E) 699 (MPC-32)</i>
<i>BWR</i>	<i>713</i>	<i>642 (MPC-68)</i>

The following additional observations can be derived by inspecting the temperature field obtained from the finite element analysis:

- The maximum fuel cladding temperature is well within the PNL recommended temperature limit.
- The maximum temperature of basket structural material is well within the stipulated design temperatures.
- The maximum temperature of the Boral neutron absorber is below the material supplier's recommended limit.
- The maximum temperatures of the MPC helium retention boundary materials are well below their respective ASME Code limits.
- The maximum temperatures of the aluminum heat conduction elements are well below the stipulated design temperature limits.
- The maximum temperature of the HI-STAR containment boundary materials is well below their respective ASME Code limits.
- The neutron shielding material (Holtite-A) will not experience temperatures in excess of its qualified limit.

The above observations lead us to conclude that the temperature field in the HI-STAR System with a fully loaded MPC containing design-basis heat emitting SNF complies with all regulatory and industry thermal requirements for normal conditions of transport. In other words, the thermal environment in the HI-STAR System will be conducive to safe transport of spent nuclear fuel.

3.4.2.1 Maximum Accessible Surface Temperatures

Access to the HI-STAR overpack cylindrical surface is restricted by the use of a personnel barrier (See Holtec Drawing 1809 in Chapter 1). Therefore, the HI-STAR System surfaces accessible during normal transport are the exposed impact limiter surfaces outside the personnel barrier. In this

subsection, the exposed impact limiter surface temperatures are computed by including heat transmission from the hot overpack ends through the impact limiters. A conservatively bounding analysis is performed by applying the thermal conductivity of aluminum to the encased aluminum-honeycomb material in the impact limiter shells to the normal condition thermal model discussed earlier in this chapter. In this manner heat transport to the exposed surfaces from the hot overpack is maximized and accessible surface temperatures over estimated. The maximum exposed *cask* surface temperatures of *for a PWR MPC (MPC-24) and a BWR MPC (MPC-68) basket designs at design maximum heat loads* are 142°F and 139°F respectively. In Figure 3.4.28, a color contour map of the regions of HI-STAR System less than 185°F (358°K) is depicted for the hotter MPC-24 basket design. From this map, it is apparent that the accessible (impact limiter) surface temperatures are below the 10CFR71.43(g) mandated limit by a significant margin.

3.4.3 Minimum Temperatures

As specified in 10CFR71, the minimum ambient temperature conditions for the HI-STAR System are -20°F and a cold environment at -40°F. The HI-STAR System design does not have any minimum decay heat load restrictions for transport. Therefore, under zero decay heat load in combination with no solar input conditions, the temperature distribution will be uniformly equal to the imposed minimum ambient conditions. All HI-STAR System materials of construction would satisfactorily perform their intended function in the transport mode at this minimum postulated temperature condition. Evaluations in Chapter 2 demonstrate the acceptable structural performance of the overpack and MPC steel materials at low temperature. Shielding and criticality functions of the HI-STAR System materials (Chapters 5 and 6) are unaffected by exposure to this minimum temperature.

3.4.3.1 Post Rapid Ambient Temperature Drop Overpack Cooldown Event

In this section, the thermal response of the HI-STAR overpack to a rapid ambient temperature drop is analyzed and evaluated. The ambient temperature is postulated to drop from the maximum to minimum temperature under normal condition of transport in a very short time (100°F to -40°F during a 1 hour period) and is assumed to hold steady at -40°F thereafter. The initial overpack condition prior to this rapid temperature drop corresponds to normal steady state transport with maximum design basis heat load. During this postulated cooldown event, the outer surface of the overpack will initially cool more rapidly than the bulk of metal away from the exposed surfaces. Consequently, it is expected that the through-thickness temperature gradients will increase for a period of time, reach a maximum and follow an asymptotic return to the initial steady condition through thickness temperature gradients as the overpack temperature field approaches the -40°F ambient steady condition. The results of the transient analysis reported in this sub-section verify these observations.

Noting that the state of thermal stress is influenced by changes in the overpack temperature field during the cooldown transient, a number of critical locations in the containment boundary depicted in Figure 3.4.24 are identified as pertinent to a structural integrity evaluation discussed in Subsection

2.6.2.3 of this SAR. Locations (1) and (2) are chosen to track the through-thickness temperature gradients in the overpack top forging which is directly exposed to the ambient. Locations (3) and (4) are chosen to track the overpack inner containment shell through-thickness temperature gradient in a plane of maximum heat generation (i.e. active fuel mid-height) where the heat fluxes and corresponding temperature gradients are highest. Locations (A) and (B) are similarly chosen to track the temperature differential in the multi-layered shells (outer-to-inner shells).

The normal transport condition thermal model discussed previously in this chapter is employed in the overpack cooldown transient analysis. This analysis is carried out by applying time-dependent thermal boundary conditions to the model and starting the transient solution in the FLUENT program. In the cooldown event, the ambient temperature is decreased from 100°F to -40°F in 10°F steps every 4 minutes (i.e. a total of 14 steps lasting 56 minutes). The ambient temperature is held constant thereafter. The maximum design basis heat load cask (i.e. the MPC-24 design) was selected to maximize the thermal gradients (by Fourier's Law, thermal gradient is proportional to heat flow). The overpack cooldown event is tracked by the thermal model for a period of 24 hours and results are reported in Figures 3.4.25 through 3.4.27 as discussed below.

In Figure 3.2.25, the overpack containment through-thickness temperature gradient responses are plotted. From this figure, it is evident that the exposed surface of the overpack forging (location (2)) initially cools at a faster rate than the recessed location (1). A similar but less pronounced result is observed in the multi-layered shells temperature changes depicted in Figure 3.4.26. This out-of-phase rate of cooling results in an increasing temperature gradient through the overpack metal layers. The thermal response of deeply recessed locations (3) and (4) show gradual temperature changes that follow each other closely. In other words, while through-thickness temperature gradients in the forging are somewhat altered the overpack inner shell gradients are essentially unchanged during the cooldown period. A closer examination of the forging temperature gradient is therefore warranted.

In Figure 3.4.27, the time dependent forging through thickness temperature differential is depicted. The gradient increases to a maximum in a short time period followed by a slow return towards the starting state. In absolute terms, both the steady state and transient temperature gradients in the forging are quite modest. In the steady state the forging through thickness temperature gradient is approximately 3°F. This value reaches a maximum plateau of 7°F during the transient event (Figure 3.4.27). The incremental thermal stress arising from this short-term gradient elevation is computed and discussed in Subsection 2.6.2.3 of this SAR.

3.4.4 Maximum Internal Pressures

The MPC is initially filled with dry helium after fuel loading and prior to sealing the MPC lid port cover plates and closure ring. During normal transport conditions, the gas temperature within the MPC rises to its maximum operating temperature as determined by the thermal analysis methodology described earlier (see Subsection 3.4.1). The gas pressure inside the MPC will increase with rising temperature. The pressure rise is determined using the Ideal Gas Law which states that the absolute pressure of a fixed volume of entombed gas is proportional to its absolute temperature.

The HI-STAR Maximum Normal Operating Pressure (MNOP) is calculated for *10 CFR 71.71(c)(1) heat condition (100°F ambient & insolation) and the HI-STAR Overpack passively cooled at design maximum heat load. For other lower than design maximum heat load scenarios, (e.g. transport with Trojan fuel) the MNOP results are confirmed to be bounding.* ~~a postulated 100% fuel rod failure and the release of fill and fission gases from the rods.~~ In Tables 3.4.13 and 3.4.14, summary calculations for determining net free volume in the ~~MPC 24 and MPC 68 PWR and BWR canisters~~ are presented. Based on a 30% release of the significant radioactive gases, a 100% release of the rod fill gas *from postulated cladding breaches*, the net free volume and the initial fill gas pressure (see Table 3.3.2), ~~the MNOP results are maximum MPC gas pressure for the 100% rod rupture condition~~ is given in Table 3.4.15. The overpack containment boundary MNOP for a hypothetical MPC breach condition is bounded by the MPC pressure results reported in this table.

3.4.5 Maximum Thermal Stresses

Thermal expansion induced mechanical stresses due to imposed non-uniform temperature distributions have been determined and reported in Chapter 2. Tables 3.4.17 and 3.4.18 summarize the HI-STAR System components temperatures, under steady-state hot conditions, for structural evaluation.

Additionally, Table 3.4.24 provides a summary of MPC helium retention boundary temperatures during normal transport conditions (steady state hot). Structural evaluations in Section 2.6 reference these temperature results to demonstrate the MPC helium retention boundary integrity.

3.4.6 Evaluation of System Performance for Normal Conditions of Transport

The HI-STAR System thermal analysis is based on detailed and complete heat transfer models that properly account for radiation, conduction and natural convection modes of heat transfer. The thermal models incorporate many conservative assumptions that are listed below. *A quantitative evaluation of HI-STAR conservatisms is provided in Appendix 3.A.*

1. No credit for gap reduction between the MPC and overpack due to differential thermal expansion under hot condition is considered.
2. No credit is considered for MPC basket internal thermosiphon heat transfer. Under a perfectly horizontal transport condition, axial temperature gradients with peaking at active fuel mid-height induces buoyancy flows from both ends of the basket in each MPC cell. Buoyancy flow in shallow horizontal channels has been widely researched and reported in the technical literature [3.4.10 to 3.4.12]. An additional mode of heat transport due to thermosiphon flow within the basket cells is initiated for any cask orientation other than a perfectly horizontal condition. In practice this is a highly likely scenario. However, in the interest of conservatism, no credit is considered for this mode of heat transfer.

3. An upper bound solar absorbtivity of unity is applied to all exposed surfaces.
4. No credit considered for radiative heat transfer between the Boral neutron absorber panels and the Boral pocket walls, or for the presence of helium in the pocket gaps.
5. No credit is considered for conduction through the neutron shielding materials.
6. No credit is considered for contact between fuel assemblies and the MPC basket wall or between the MPC basket and the MPC basket supports. The fuel assemblies and MPC basket are conservatively considered to be in concentric alignment.
7. No credit considered for presence of highly conducting aluminum honeycomb material inside impact limiters.
8. *The fuel assembly contribution to MPC basket axial conductivity is conservatively assumed to be equal to the lower basket cross-sectional effective conductivity limited to the fuel cladding only (i.e. axial heat transfer through fuel pellets is neglected).*
9. The MPC is assumed to be loaded with the SNF type which has the maximum equivalent thermal resistance of all fuel types in its category (BWR or PWR), as applicable.
10. The design basis maximum decay heat loads are used for all thermal-hydraulic analyses. For casks loaded with fuel assemblies having decay heat generation rates less than design basis, additional thermal margins of safety will exist.
11. Interfacial contact conductance of multi-layered intermediate shell contacting layers was conservatively determined to bound surface finish, contact pressure, and base metal conductivity conditions.
12. *Flow turbulation in the MPC space neglected.*

Temperature distribution results obtained from a conservatively developed thermal model show that maximum fuel cladding temperature limits are met with adequate margins. Margins during actual normal transport conditions are expected to be greater due to the many conservative assumptions incorporated in the analysis. The maximum local temperatures in the neutron shield and overpack seals are lower than design limits. The maximum local MPC basket temperature level is below the recommended limits for structural materials in terms of susceptibility to stress, corrosion and creep induced degradation. Furthermore, structural evaluation (Chapter 2) has demonstrated that stresses (including those induced due to imposed temperature gradients) are within ASME B&PV Code limits. Section 3.6 provides a discussion of compliance with the regulatory requirements and acceptance criteria listed in Section 3.0. As a result of the above-mentioned considerations, it is concluded that the HI-STAR thermal design is in compliance with 10CFR71 requirements for normal conditions of transport.

Table 3.4.1

CLOSED CAVITY NUSSELT NUMBER*
RESULTS FOR HELIUM FILLED MPC PERIPHERAL VOIDS

Temperature (°F)	Case (i) Nusselt Number		Case (ii) Nusselt Number	
	MPC-24, MPC-24E, MPC-32	MPC-68	MPC-24, MPC-24E, MPC-32	MPC-68
200	6.93	4.72	5.45	3.46
450	5.44	3.71	4.09	2.58
700	4.60	3.13	3.36	2.12

* For conservatism, the heat dissipation enhancement due to Rayleigh effect discussed in Sub-section 3.4.1.1.5 is ignored.

Table 3.4.2

RELATIONSHIP BETWEEN HI-STAR SYSTEM REGIONS
AND MATHEMATICAL MODEL DESCRIPTIONS

<u>HI-STAR System Region</u>	<u>Mathematical Model</u>	<u>Subsections</u>
Fuel Assembly	Fuel Region Effective Thermal Conductivity	3.4.1.1.2
MPC	Effective Thermal Conductivity of Boral/Sheathing/Box Wall Sandwich	3.4.1.1.3
	Basket In-Plane Conductive Heat Transport	3.4.1.1.4
	Heat Transfer in MPC Basket Peripheral Region	3.4.1.1.5
	Effective Thermal Conductivity of MPC Basket-to-Shell Aluminum Heat Conduction Elements	3.4.1.1.11
Overpack	Effective Conductivity of Multi-Layered Intermediate Shell Region	3.4.1.1.6
	Effective Thermal Conductivity of Holtite Neutron Shielding Region	3.4.1.1.9
Ambient Environment	Heat Rejection from Overpack Exterior Surfaces	3.4.1.1.7
	Solar Heat Input	3.4.1.1.8
Assembled Cask Model	Overview of the Thermal Model	3.4.1.1.1
	Effective Conductivity of MPC to Overpack Gap	3.4.1.1.10
	FLUENT Model for HI-STAR	3.4.1.1.12

Table 3.4.3

THIS TABLE IS INTENTIONALLY DELETED.

Table 3.4.4

SUMMARY OF PWR FUEL ASSEMBLIES
EFFECTIVE THERMAL CONDUCTIVITIES

No.	Fuel	@ 200°F (Btu/ft-hr-°F)	@ 450°F (Btu/ft-hr-°F)	@ 700°F (Btu/ft-hr-°F)
1	<u>W</u> 17×17 OFA	0.182	0.277	0.402
2	<u>W</u> 17×17 Std	0.189	0.286	0.413
3	<u>W</u> 17×17 Vantage-5H	0.182	0.277	0.402
4	<u>W</u> 15×15 Std	0.191	0.294	0.430
5	<u>W</u> 14×14 Std	0.182	0.284	0.424
6	<u>W</u> 14×14 OFA	0.175	0.275	0.413
7	B&W 17×17	0.191	0.289	0.416
8	B&W 15×15	0.195	0.298	0.436
9	CE 16×16	0.183	0.281	0.411
10	CE 14×14	0.189	0.293	0.435
11	HN [†] 15×15 SS	0.180	0.265	0.370
12	<u>W</u> 14×14 SS	0.170	0.254	0.361
13	B&W 15x15 Mark B-11	0.187	0.289	0.424
14	CE 14x14 (MP2)	0.188	0.293	0.434

Note: Boldface values denote the lowest thermal conductivity in each column (excluding stainless steel clad fuel assemblies).

[†] Haddam Neck B&W or Westinghouse stainless steel clad fuel assemblies.

Table 3.4.5

SUMMARY OF BWR FUEL ASSEMBLIES EFFECTIVE THERMAL CONDUCTIVITIES

No.	Fuel	@ 200°F (Btu/ft-hr-°F)	@ 450°F (Btu/ft-hr-°F)	@ 700°F (Btu/ft-hr-°F)
1	Dresden 1 8x8*	0.119	0.201	0.319
2	Dresden 1 6x6	0.126	0.215	0.345
3	GE 7x7	0.171	0.286	0.449
4	GE 7x7R	0.171	0.286	0.449
5	GE 8x8	0.168	0.278	0.433
6	GE 8x8R	0.166	0.275	0.430
7	GE-10 8x8	0.168	0.280	0.437
8	GE-11 9x9	0.167	0.273	0.422
9	AC† 10x10 SS	0.152	0.222	0.309
10	Exxon 10x10 SS	0.151	0.221	0.308
11	Damaged Dresden 1 8x8 in a DFC§	0.107	0.169	0.254
12	Dresden-1 Thin Clad 6x6§	0.124	0.212	0.343
13	Humboldt Bay-7x7§	0.127	0.215	0.343
14	Damaged Dresden-1 8x8 (in TND-1 canister) §	0.107	0.168	0.252
15	8x8 Quad ⁺ Westinghouse§	0.164	0.278	0.435

Note: Boldface values denote the lowest thermal conductivity in each column (excluding Dresden and LaCrosse clad fuel assemblies).

† Allis-Chalmers stainless steel clad fuel assemblies.

§ Low heat emitting fuel assemblies excluded from list of fuel assemblies (zircaloy clad) evaluated to determine the most resistive SNF type.

Table 3.4.6

**MPC BASKET EFFECTIVE THERMAL CONDUCTIVITY RESULTS
FROM ANSYS MODELS**

Basket	@200°F (Btu/ft-hr-°F)	@450°F (Btu/ft-hr-°F)	@700°F (Btu/ft-hr-°F)
MPC-24 (Zircaloy Clad Fuel)	1.108 1.127	1.495 1.535	1.954 2.026
MPC-68 (Zircaloy Clad Fuel)	0.959 1.025	1.188 1.257	1.432 1.500
MPC-24 (Stainless Steel Clad Fuel) (Note 1)	0.995 0.901	1.321 1.230	1.700 1.615 ^(a)
MPC-68 (Stainless Steel Clad Fuel) (Note 1)	0.931 0.987	1.125 1.180	1.311 1.360 ^(b)
MPC-68 (Dresden-1 8x8 in canisters)	0.861 0.921	1.055 1.118	1.242 1.306
MPC-32 (Zircaloy Clad Fuel)	0.964	1.214	1.486
MPC-32 (Stainless Steel Clad Fuel) (Note 1)	0.762	0.936	1.104
MPC-24E (Zircaloy Clad Fuel)	1.211	1.635	2.137
MPC-24E (Stainless Steel Clad Fuel) (Note 1)	0.988	1.348	1.766

(a) — 13% lower effective thermal conductivity than corresponding zircaloy fueled basket

(b) — 9% lower effective thermal conductivity than corresponding zircaloy fueled basket

Note-1: Evaluated for a conservatively bounding configuration (fuel in a damaged fuel canister)

Table 3.4.7

INSOLATION DATA SPECIFIED BY 10CFR71, SUBPART F

Surface Type	12-Hour Total Insolation Basis	
	(g-cal/cm ²)	(Watts/m ²)
Horizontally Transported Flat Surfaces		
- Base	None	None
- Other Surfaces	800	774.0
Non-Horizontal Flat Surfaces	200	193.5
Curved Surfaces	400	387.0

Table 3.4.8

EFFECTIVE THERMAL CONDUCTIVITY OF THE NEUTRON SHIELD/RADIAL CHANNELS REGION

Condition/Temperature (°F)	Thermal Conductivity (Btu/ft-hr-°F)
Normal Condition: 200 450 700	 1.953 1.812 1.645
Fire Condition: 200 450 700	 3.012 2.865 2.689

Table 3.4.9

THIS TABLE IS INTENTIONALLY DELETED.

Table 3.4.10

HI-STAR SYSTEM NORMAL TRANSPORT[†] MAXIMUM TEMPERATURES
(MPC-24) (PWR MPCs)

	<i>Bounding Calculated Maximum Temperature [°F]</i>	<i>Normal Condition Temperature Limit [°F]</i>
Fuel Cladding	701	720 752
MPC Basket Centerline	667	725
MPC Basket Periphery	430	725
MPC Outer Shell Surface	315	450
MPC/Overpack Helium Gap Outer Surface	291	400
Radial Neutron Shield Inner Surface	271	300
Overpack Enclosure Shell Surface	222	350
Axial Neutron Shield	292	300
Impact Limiter Exposed Surface	121	176
Overpack Closure Plate ^{††}	163	400
Overpack Bottom Plate ^{††}	295	350

[†] Steady-state hot (100°F ambient) with maximum decay heat and insolation.

^{††} Overpack closure plate and vent/drain port plug seals normal condition design temperature is 400°F. The maximum seals temperatures are bounded by the reported closure plate and bottom plate maximum temperatures. Consequently, a large margin of safety exists to permit safe operation of seals in the overpack helium retention boundary.

Table 3.4.11

**HI-STAR SYSTEM NORMAL TRANSPORT[†] MAXIMUM TEMPERATURES
(MPC-68)**

	Calculated Maximum Temperature Bounding Temperature [°F]	Normal Condition Temperature Limit [°F]
Fuel Cladding	713	749 752
MPC Basket Centerline	697	725
MPC Basket Periphery	365	725
MPC Outer Shell Surface	306	450
MPC/Overpack Gap Outer Surface	282	400
Radial Neutron Shield Inner Surface	264	300
Overpack Enclosure Shell Surface	217	350
Axial Neutron Shield	255	300
Impact Limiter Exposed Surface	121	176
Overpack Closure Plate ^{††}	162	400
Overpack Bottom Plate ^{††}	256	350

[†] Steady-state hot (100°F ambient) with maximum decay heat and insolation.

^{††} Overpack closure plate and vent/drain port plug seals normal condition design temperature is 400°F. The maximum seals temperatures are bounded by the reported closure plate and bottom plate maximum temperatures. Consequently, a large margin of safety exists to permit safe operation of seals in the overpack helium retention boundary.

Table 3.4.12

THIS TABLE IS INTENTIONALLY DELETED.

Table 3.4.13

SUMMARY OF BOUNDING MINIMUM
MPC-24-FREE VOLUME CALCULATIONS (PWR MPCs)

Item	MPC-24 Volume (ft ³)	MPC-24E Volume (ft ³)	MPC-32 Volume (ft ³)
Cavity Volume	368.3 367	367	367
Basket Metal Volume	47.0 45	52	25
Bounding Fuel Assemblies Volume	78.8 79	79	106
Basket Supports and Fuel Spacers Volume	6.1 7	7	9
Aluminum Conduction Elements [†]	5.9 6	6	6
Net Free Volume	230.5 230 (6529 6512 liters)	223 (6314 liters)	221 (6258 liters)

[†] Bounding 1,000 lbs aluminum weight.

Table 3.4.14

SUMMARY OF BOUNDING MINIMUM
MPC-68 FREE VOLUME CALCULATIONS

Item	Volume (ft ³)
Cavity Volume	367.2 367
Basket Metal Volume	45.5 35
Bounding Fuel Assemblies Volume	93.0 93
Basket Supports and Fuel Spacers Volume	11.3 12
Aluminum Conduction Elements [†]	5.9 6
Net Free Volume	211.5 221 (5989 6258 liters)

[†] Bounding 1,000 lbs aluminum weight.

Table 3.4.15

SUMMARY OF MAXIMUM NORMAL OPERATING PRESSURE (MNOP)[†]
FOR HORIZONTAL TRANSPORT CONDITIONS

Condition	Pressure (psig)	Bounding MPC Cavity Bulk Temperature (°F)
MPC-24: Initial Backfill (at 70°F) Normal Condition With 100% 3% Rods Rupture ^(Note 1)	28.3 42.8 61.8 87.7 98.9 88.8	483
MPC-68: Initial Backfill (at 70°F) Normal Condition With 100% 3% Rods Rupture ^(Note 1)	28.5 42.8 61.0 86.0 89.3 86.9	468
MPC-24E: Initial Backfill (at 70 °F) Normal Condition With 3% Rods Rupture ^(Note 1)	42.8 87.7 88.9	483
MPC-32: Initial Backfill (at 70 °F) Normal Condition With 3% Rods Rupture ^(Note 1)	42.8 87.7 89.3	483

Note 1: NUREG-1617 requires an assumption for normal transport that 3% of the rods are breached with release of 100% fill gas and 30% fission gas to containment.

[†] Pressure analysis in accordance with heat condition specified in 10 CFR 71.71(c)(1) in the absence of venting, external ancillary cooling or operational controls is based on release of 100% of the rods fill gas and 30% of the significant radioactive gases from a ruptured rod.

Table 3.4.16

THIS TABLE IS INTENTIONALLY DELETED.

Table 3.4.17

**MPC-24PWR MPCs NORMAL HORIZONTAL TRANSPORT CONDITION
HI-STAR SYSTEM COMPONENTS *BOUNDING* TEMPERATURE [°F] SUMMARY**

	MPC Basket Axial Mid-Length	MPC Basket Axial Ends
Overpack enclosure shell	222	147
Overpack inner shell	291	163
MPC shell	315	164
Basket periphery	430	166
Basket center	667	177

Table 3.4.18

MPC-68 NORMAL HORIZONTAL TRANSPORT CONDITION
HI-STAR SYSTEM COMPONENTS TEMPERATURE [°F] SUMMARY

	MPC Basket Axial Mid-Length	MPC Basket Axial Ends
Overpack enclosure shell	217	146
Overpack inner shell	282	161
MPC shell	306	163
Basket periphery	365	164
Basket center	697	175

Table 3.4.19

**SUMMARY OF LOADED HI-STAR SYSTEM
BOUNDING COMPONENT WEIGHTS AND THERMAL INERTIAS**

Component	Weight (lbs)	Heat Capacity (Btu/lb-°F)	Thermal Inertia (Btu/°F)
Holtite-A	11,000	0.39	4,290
Carbon Steel	140,000	0.1	14,000
Alloy-X MPC (empty)	35,000	0.12	4,200
Fuel	40,000	0.056	2,240
MPC Cavity Water [†]	6,500	1.0	6,500
			31,230 (Total)

[†] Based on smallest MPC-68 cavity net free volume with 50% credit for flooded water mass.

Table 3.4.20

MAXIMUM ALLOWABLE TIME DURATION
FOR WET TRANSFER OPERATIONS

Initial Temperature (°F)	Time Duration (hr)
115	44.3
120	42.0
125	39.7
130	37.4
135	35.2
140	32.9
145	30.6
150	28.3

Table 3.4.21

THIS TABLE IS INTENTIONALLY DELETED.

Table 3.4.22

HI-STAR SYSTEM MAXIMUM BOUNDING TEMPERATURES [°F]
 UNDER STEADY-STATE COLD[†] CONDITIONS (MPC-24 PWR MPCs)

Fuel Cladding	620
MPC Basket Centerline	586
MPC Basket Periphery	329
MPC Outer Shell Surface	190
MPC/Overpack Gap Outer Surface	165
Radial Neutron Shield Inner Surface	141
Overpack Enclosure Shell Surface	96
Axial Neutron Shield	165
Impact Limiter Exposed Surface	-40

[†] -40°F ambient temperature with maximum decay heat and no insolation.

Table 3.4.23

HI-STAR SYSTEM MAXIMUM TEMPERATURES [°F]
 UNDER STEADY-STATE COLD[†] CONDITIONS (MPC-68)

Fuel Cladding	621
MPC Basket Centerline	605
MPC Basket Periphery	254
MPC Outer Shell Surface	178
MPC/Overpack Gap Outer Surface	153
Radial Neutron Shield Inner Surface	130
Overpack Enclosure Shell Surface	88
Axial Neutron Shield	123
Impact Limiter Exposed Surface	-40

[†] -40°F ambient temperature with maximum decay heat and no insolation.

Table 3.4.24

SUMMARY OF MPC HELIUM RETENTION BOUNDARY *BOUNDING* TEMPERATURE DISTRIBUTION DURING NORMAL STORAGE CONDITIONS

Location	Figure 2.6.20 Designation	MPC-24 PWR MPCs [°F]	MPC-68 [°F]
MPC Lid Inside Surface at Centerline	A	176	173
MPC Lid Outside Surface at Centerline	B	171	169
MPC Lid Inside Surface at Periphery	C	164	163
MPC Lid Outside Surface at Periphery	D	162	161
MPC Baseplate Inside Surface at Centerline	E	301	260
MPC Baseplate Outside Surface at Centerline	F	295	256
MPC Baseplate Inside Surface at Periphery	G	267	239
MPC Baseplate Outside Surface at Periphery	H	267	239
MPC Shell Maximum	I	315	306

Table 3.4.25

SUMMARY OF 10×10 ARRAY BWR FUEL ASSEMBLY TYPES
EFFECTIVE THERMAL CONDUCTIVITIES[†]

Fuel	k_{eff} at 200°F [Btu/(ft-hr-°F)]	k_{eff} at 450°F [Btu/(ft-hr-°F)]	k_{eff} at 700°F [Btu/(ft-hr-°F)]
GE-12/14	0.166	0.269	0.412
Atrium-10	0.164	0.266	0.409
SVEA-96	0.164	0.269	0.416

[†] The conductivities reported in this table are obtained by the simplified method described in the beginning of Subsection 3.4.1.1.2.

Table 3.4.26

COMPARISON OF ATRIUM-10[†] AND BOUNDING^{††} BWR FUEL ASSEMBLY
EFFECTIVE THERMAL CONDUCTIVITIES

Temperature °F	Atrium-10 Assembly		Bounding BWR Assembly	
	Btu/(ft-hr-°F)	W/m-K	Btu/(ft-hr-°F)	W/m-K
200	0.225	0.389	0.171	0.296
450	0.345	0.597	0.271	0.469
700	0.504	0.872	0.410	0.710

[†] The reported effective thermal conductivity has been obtained from a rigorous finite-element modeling of the Atrium-10 assembly.

^{††} The bounding BWR fuel assembly effective thermal conductivity applied in the MPC-68 basket thermal analysis.

Table 3.4.27

THIS TABLE IS INTENTIONALLY DELETED.

Table 3.4.28

**MPC-24 PWR MPCs BOUNDING PEAK FUEL CLADDING TEMPERATURE
AS A FUNCTION OF TOTAL HEAT LOAD**

Total MPC Decay Heat Load (kW)	Peak Fuel Cladding Temperature (°F)
20.0 [†]	700.6
19.0	678.9
17.0	633.9
15.5	598.8

[†] Design Basis Maximum.

Table 3.4.29

MPC-68 PEAK FUEL CLADDING TEMPERATURE
AS A FUNCTION OF TOTAL HEAT LOAD

Total MPC Decay Heat Load (kW)	Peak Fuel Cladding Temperature (°F)
18.5 [†]	712.7
17.0	674.0
15.5	634.1

[†] Design Basis Maximum.

Table 3.4.30

**SUMMARY OF THERMAL CONDUCTIVITY CALCULATIONS
FOR MPC HELIUM DILUTED BY RELEASED ROD GASES**

Component Gas	Molecular Weight (g/mole)	Mole Fraction	Thermal Conductivity* (Btu/hr-ft-°F)
MPC and Fuel Rod Backfill Helium	4	0.817	0.098 @ 200°F 0.129 @ 450 °F 0.158 @ 700°F
Rod Tritium	3	8.007×10^{-5}	0.119 @ 200 0.148 @ 450°F 0.177 @ 700°F
Rod Krypton	85	0.016	6.76×10^{-3} @ 200°F 8.782×10^{-3} @ 450°F 0.011 @ 700°F
Rod Xenon	131	0.160	3.987×10^{-3} @ 200°F 5.258×10^{-3} @ 450°F 6.471×10^{-3} @ 700°F
Rod Iodine	129	6.846×10^{-3}	2.496×10^{-3} @ 200°F 3.351×10^{-3} @ 450°F 4.201×10^{-3} @ 700°F
Mixture of Gases (diluted helium)	N/A	1.000	0.053 @ 200°F 0.069 @ 450°F 0.085 @ 700°F

* References [3.2.2], [3.4.18] & [3.4.19] consulted for fission gases (Tritium, Krypton, Xenon and Iodine) conductivities.

Table 3.4.31

COMPARISON OF COMPONENT EFFECTIVE THERMAL CONDUCTIVITIES
WITH AND WITHOUT MPC HELIUM DILUTION

	Effective Thermal Conductivity (Btu/hr-ft-°F)		
	Value at 200°F	Value at 450°F	Value at 700°F
Fuel Assembly with Undiluted Helium	0.257	0.406	0.604
Fuel Assembly with Diluted Helium	0.160	0.278	0.458
MPC Fuel Basket with Undiluted Helium	1.108 1.127	1.495 1.535	1.954 2.026
MPC Fuel Basket with Diluted Helium	0.933 0.948	1.303 1.338	1.758 1.829
Basket Periphery with Undiluted Helium [†]	0.3136	0.4456	0.6459
Basket Periphery with Diluted Helium [†]	0.2286	0.3550	0.5538

[†] — These thermal conductivity values do not include the contribution of the aluminum heat conduction elements.

Table 3.4.32

MPC-24 HYPOTHETICAL 100% RODS RUPTURE ACCIDENT
 MAXIMUM TEMPERATURES*

	Calculated Maximum Temperature (°F)	Accident Condition Temperature Limit (°F)
Fuel Cladding	743	1058
MPC Basket Centerline	709	950
MPC Basket Periphery	444	950
MPC Outer Shell Surface	314	775
MPC/Overpack Helium Gap Outer Surface	291	500
Radial Neutron Shield Inner Surface	271	N/A
Overpack Enclosure Shell Surface	222	1350
Overpack Closure Plate	176	700
Overpack Bottom Plate	296	700

* The results reported herein are obtained from thermal models employing grossly understated fuel basket conductivities.

Table 3.4.33

MPC-24 HYPOTHETICAL 100% RODS RUPTURE ACCIDENT PRESSURES

Calculated Accident Pressure (psig)	Accident Condition Design Pressure (psig)
102.1 134	125 200

Table 3.4.34

PLANT SPECIFIC BWR FUEL TYPES EFFECTIVE THERMAL CONDUCTIVITY*

Fuel	@200°F [Btu/ft-hr-°F]	@450°F [Btu/ft-hr-°F]	@700°F° [Btu/ft-hr-°F]
Oyster Creek (7x7)	0.165	0.273	0.427
Oyster Creek (8x8)	0.162	0.266	0.413
TVA Browns Ferry (8x8)	0.160	0.264	0.411
SPC-5 (9x9)	0.149	0.245	0.380

* The conductivities reported in this table are obtained by a simplified analytical method described in Subsection 3.4.1.1.2.

3.5 HYPOTHETICAL ACCIDENT THERMAL EVALUATION

As mandated by 10CFR71 requirements, the HI-STAR System is subjected to a sequence of hypothetical accident conditions. The objective is to determine and assess the cumulative damage sustained by the system. The accident scenarios specified in order are: (1) a 30 foot free drop onto an unyielding surface; (2) a 40-inch drop onto a mild steel bar; and (3) exposure to a 30-minute fire at 1475°F. The initial conditions for the fire accident specify steady state at an ambient temperature between -20°F and 100°F [3.5.1]. In the HI-STAR System hypothetical fire accident evaluation, full effects of insolation before, during, and after the fire are considered. The effects of the first two drop accidents are evaluated in Chapter 2. In this section, the transient thermal response of the HI-STAR System to a 30-minute fire followed by a post-fire cooldown is determined. The fire accident evaluation is performed by consideration of a worst case combination of factors which conservatively overestimate heat input to the HI-STAR System during the fire followed by an underestimation of the ability of the cask to reject heat to the environment after the fire.

The impact limiters are designed to crush and absorb energy during the hypothetical drops. In the hypothetical fire accident evaluation, the impact limiter is assumed to be crushed to the bounding maximum condition of a solid block of highly conducting aluminum, resulting in increased heat input to the overpack ends through the reduced impact limiter thickness during the fire. The fire condition thermal analysis results are therefore bounding with respect to impact limiter design and amount of crush experienced during a hypothetical drop accident.

A puncture event may locally buckle some of the radial connector plates through the neutron shielding, thereby reducing the ability of the system to reject heat after the fire. As described in Section 2.7, the puncture bar is 6 inches in diameter and correspondingly has a face area of approximately 28.3 in². The enclosure shell area is greater than 52,200 in². Therefore, while the puncture bar would directly impact less than 0.06% of the exposed area, a conservative 10% reduction in the neutron shield region effective thermal conductivity is considered during the post-fire cooldown phase.

During the initial 30-minute fire event, some of the neutron shield will be exposed to high temperatures. Therefore, in determining heat input to the system, a conservative value maximizing the heat input is utilized for the neutron shield thermal conductivity. During the post-fire cooldown phase, no credit is considered for conduction through the neutron shield material. During the fire, a 10CFR71 mandated cask surface emissivity is considered to maximize radiant heat input to the cask. Destruction of the painted surfaces due to exposure to intense heat during the fire event is a credible possibility. Therefore, the lower emissivity of exposed carbon steel is conservatively considered for post-fire cooldown analysis.

The initial condition prior to the start of the fire accident is based on the bounding normal transport condition MPC basket temperature distribution. The smallest of the ~~two~~ four baskets (*MPC-24, MPC-24E, MPC-32 and MPC-68*) average density and heat capacity are applied to the fire transient analysis. Thus, maximum basket heat load coincident with minimum thermal inertia provides a

conservatively bounding response of the HI-STAR System to a fire accident condition.

In the fire event, analyzed in this Section of the SAR, the aim of the analysis is to bound two HI-STAR cask scenarios namely (a) MPCs installed with AHCEs and (b) MPCs without AHCEs. To achieve this objective, the analysis to characterize the response of the HI-STAR package in enveloping a Part 71 fire event assumes that the AHCE heat transfer bridge is present while the fire is raging so that the computed heat flow to the fuel is maximized. Further, the absorptivity of the overpack is increased from its normal operating condition value of 0.85 to the Part 71 value of 0.9. To account for the "no-AHCE" scenario, the emissivity of the overpack is reduced below its normal operating condition value (Table 3.5.2), as soon as the fire event ends, thus retarding the rejection of heat to the environment.

The temperature history of a number of critical control points in the HI-STAR System are monitored during the 30-minute fire and the subsequent relaxation of temperature profiles during the post-fire cooldown phase. The impact of transient temperature excursions on HI-STAR System materials is assessed in this section.

3.5.1 Thermal Model

3.5.1.1 Analytical Model

A thermal transient simulation model to determine the fire condition temperature response is developed on the FLUENT CFD code [3.1.2]. The basic underlying finite volume model is based on the steady-state FLUENT model developed and described in Section 3.4. This basic model is modified by incorporating time dependent thermal loads on the exposed surfaces of the HI-STAR System for determining transient responses at every computational cell defined in the FLUENT model.

The HI-STAR System configuration during a hypothetical fire accident is schematically depicted in Figure 3.5.1. The initial thermal condition of the HI-STAR System prior to the accident condition is the normal transport steady-state temperature distribution. The HI-STAR System is then subjected to a 1475°F fire environment for 30 minutes. During this fire event, the impact limiters installed on both ends are assumed to be in a fully crushed state. This is a conservative assumption which results in an increased heat input to the overpack due to the higher thermal conductivity and reduced thickness of the crushed impact limiter. After 30 minutes, the ambient temperature is restored to 100°F and the HI-STAR System is allowed to proceed through a post-fire cooldown phase. During this entire transient event (fire and post-fire cooldown), the temperature history of several control points in the HI-STAR System is monitored. These points are schematically depicted in Figure 3.5.1.

Heat input to the HI-STAR System while it is engulfed in a fire is from a combination of radiation and forced convection heat transfer to all overpack/impact limiter exposed surfaces. This can be expressed by the following equation:

$$q_F = h_{fc} (T_F - T_s) + \sigma \epsilon [(T_F + 460)^4 - (T_s + 460)^4]$$

where:

- q_F = surface heat input flux (Btu/ft²-hr)
- T_F = fire condition temperature (1475°F)
- T_s = transient surface temperature (°F)
- h_{fc} = forced convection heat transfer coefficient [Btu/ft-hr-°F]
- ϵ = surface emissivity = 0.9 (per 10CFR71)
- σ = Stefan-Boltzmann Constant (0.1714×10⁻⁸ Btu/ft²-hr-°R⁴)

The forced convection heat transfer coefficient is calculated to bound the convective heat flux contribution to the exposed cask surfaces due to a fire induced air flow velocity of 15 m/s. For the case of air flow past a heated cylinder, Jakob [3.5.2] recommends the following correlation for convective heat transfer, obtained from experimental data:

$$Nu_{fc} = 0.028 Re^{0.8} \left[1 + 0.4 \left(\frac{L_{st}}{L_{tot}} \right)^{2.75} \right]$$

where:

- L_{tot} = length traversed by flow
- L_{st} = length of unheated section
- K_f = thermal conductivity of air evaluated at the average film temperature
- Re = flow Reynolds Number based on L_{tot}
- Nu_{fc} = Nusselt Number ($h_{fc} L_{tot}/K_f$)

Consideration of the wide range of temperatures to which the exposed surfaces are subjected to during the fire and the temperature dependent trend of air properties requires a careful selection of parameters to determine a conservatively large bounding value of the convective heat transfer coefficient. In Table 3.5.1, a summary of the parameter selections with justifications provides an appropriate basis for application of this correlation to determine forced convection heating of the HI-STAR System during the short-term fire event.

After the 30-minute fire event, the ambient temperature is restored to 100°F. The HI-STAR System cools down during this post-fire cooldown phase. Heat loss from outside exposed surfaces of the overpack is determined by the following equations:

$$q_s = 0.18 (T_s - T_A)^{4/3} + \sigma \epsilon [(T_s + 460)^4 - (T_A + 460)^4]$$

where:

- q_s = surface heat loss flux (Btu/ft²-hr)
- T_s = transient surface temperature (°F)
- T_A = ambient temperature (100°F)
- ϵ = surface emissivity
- σ = Stefan-Boltzmann Constant (0.1714×10⁻⁸ Btu/ft²-hr-°R⁴)

During the fire event, some region of Holtite will be overheated and thus lose its ability to conduct heat. In the fire transient analysis, full credit is given to conduction through Holtite to conservatively increase heat input to the overpack. In the post-fire cooldown phase, all of the Holtite is conservatively assumed to be lost (no conduction through Holtite material).

During the 30-foot drop and puncture accident events, the mechanical integrity of the HI-STAR System is maintained. From a thermal analysis standpoint, the impact limiters are crushed and there is at most localized damage to radial channels. While the resulting localized damage would not significantly degrade the heat transfer ability of the Holtite region, a 10% effective conductivity reduction is conservatively (as described earlier in Section 3.5) applied during the post-fire cooldown phase. In Table 3.5.2, a summary of inputs used in the determination of the effect of a hypothetical fire accident is provided.

3.5.1.2 Test Model

For determining the transient response of the HI-STAR System under a hypothetical fire accident condition, a detailed finite volume model has been developed on the validated and benchmarked FLUENT code. The dynamic model features several conservative assumptions to bound temperature excursions during the heat up and cooldown phases of the accident. Accordingly, development of a separate test model to verify the results is not considered necessary. Evaluation of the HI-STAR System thermal design in the event of a hypothetical fire event is shown to be in compliance with 10CFR71 requirements.

3.5.2 System Conditions and Environment

The HI-STAR System is shown to maintain its mechanical integrity following a 30 foot drop and puncture accident with stresses within applicable ASME Code requirements. The impact limiters absorb the impact forces and are crushed in the drop event. Completely crushed impact limiters provide a conservatively limiting situation for increased heat absorption during the 30-minute fire. The effect of a puncture accident results in localized damage to the radial connectors embedded in Holtite neutron shielding. This will *not* reduce the heat transfer capability of the region containing Holtite by a significant factor. The fire is specified to be at a temperature of 1475°F and last for 30 minutes. Emissivity of all exposed surfaces is set to 0.9. Some of the Holtite will decompose and lose its ability to conduct heat during the fire event due to exposure to severe temperature conditions. Thermal analysis of the HI-STAR System is performed by postulating worst case conditions whereby increased heat absorption takes place during the 30-minute fire and a reduced ability of the HI-STAR System to reject heat takes place during the post-fire cooldown phase.

3.5.3 System Temperatures

The hypothetical fire accident condition is evaluated by imposing a 1475°F fire temperature for 30 minutes followed by a post-fire equilibrium phase that is followed for more than 30 hours. The temperature-time history of several control points is monitored. These points are selected because of

their importance relating to safety evaluation. In Figures 3.5.2 to 3.5.4, the transient temperature profiles of the monitored points shown in Figure 3.5.1 are plotted. From these plots, the temperature of exposed surfaces is seen to increase rapidly and peak at about 1348°F at the end of the fire (i.e., 30 minutes). Figure 3.5.5 shows the peak axial fuel cladding temperature profile during post-fire cooldown. In the post-fire equilibrium phase, there is an initial rapid cooldown of the peak surface temperature followed by an asymptotic approach to the final steady-state condition. The closure bolts and mechanical seals peak temperatures are below short-term limits. The MPC basket center temperature rises sluggishly to a broad peak and then slowly decays to a final steady-state condition. Portions of Holtite neutron shielding material near the overpack enclosure shell experience a short duration high temperature excursion. The crushed aluminum alloy inside the impact limiter begins to melt at 1105°F. The latent heat of melting of aluminum alloy during the melting phase would absorb the incident heat flux from the fire. This ablation mechanism will protect the cask by limiting the surface temperature excursion and restricting the amount of heat input to the overpack lid. In the HI-STAR System fire transient evaluation, credit for this protective feature is not considered.

The HI-STAR fire event model is depicted in Figure 3.5.6. Fire condition containment boundary through thickness temperature profiles are presented in Figures 3.5.7, 3.5.8, and 3.5.9 across Sections A-A, B-B, and C-C, as shown in Figure 3.5.6. The figures present through-thickness temperature profiles at the end of the 30-minute fire and 60 minutes after the start of the fire (30 minutes into the post-fire cooldown period).

In the fire event, the dominant heat input source is located on the outside of the cask. The temperature gradient, as seen in Figures 3.5.7, 3.5.8, and 3.5.9, is reversed from the normal condition, with the maximum temperature occurring at the outermost layer. From Figure 3.5.7, it is apparent that the overpack inner shell remains below the 500°F short-term design basis temperature limit. At the end of the 30-minute fire, the outermost layer of the multi-layered shells is heated to approximately 540°F. During the post-fire cooldown phase the temperature of this outer layer rapidly drops below 500°F, as shown on the 60-minute profile.

An examination of the overpack forging temperature profile (Section B-B, Figure 3.5.8) shows that the outer layers of the forging, directly adjacent to the surface exposed to the fire, are heated to in excess of 700°F during the fire. The bulk of the forging metal mass (in excess of 6 inches out of the total 8.5 inches) remains below the 700°F short-term design basis temperature limit. The portion of the overpack forging which is covered by the impact limiters remains below 700°F both during and after the fire. This is illustrated by the temperature profiles presented in Figure 3.5.9.

The following observations can be drawn from an examination of Figures 3.5.6 through 3.5.9:

- The containment boundary regions that are within the confines of the multi-layered shells remain below 500°F.
- The containment boundary regions that are within the confines of the impact limiters remain

below 700°F.

- The bulk of the containment boundary in the regions that are directly exposed to the fire remain below 700°F.

The outer region of the HI-STAR 100 overpack consists of forty sector shaped annular spaces enclosed in half inch thick carbon steel plates. These annular spaces contain Holtite-A neutron absorber material. Holtite-A is a stable material under the environmental and thermal conditions corresponding to normal operation. Under a fire condition, the temperature in the enclosure shell cavity rises resulting in loosening of the water intermolecular bonds to the neutron shield material leading to liberation of water vapor. *For conservatism, a 6% weight loss factor for the neutron shield when exposed to a direct fire is assumed.* Information on stability of neutron shield materials when exposed to a direct fire (temperatures between 800°C to 900°C for thirty minutes) is provided in Appendix 1.B. From reported test data, weight loss under extreme conditions is relatively small (less than 6%). Under a conservatively postulated scenario wherein all of the radial neutron shield material (approximately 12,850 lbs required to completely fill the forty spaces) is exposed to a direct fire, 771 lbs of water vapor (i.e 6% of neutron shield) generation in 30 minutes is required to be expelled from the neutron shield cavities. To protect the enclosure shell from overpressure, two rupture discs (each having the required vapor expulsion capacity) are incorporated in the HI-STAR overpack design. The rupture discs have a relatively low set pressure (30 psig) to relieve water vapor if the generation is rapid during a fire condition. Appendix 2.AM demonstrates structural integrity of the enclosure shell at the 30 psig internal pressure.

3.5.4 Maximum Internal Pressure

Based on bounding transient temperature excursions calculated for the HI-STAR System during a hypothetical fire accident condition, maximum calculated cask internal pressures are reported in Table 3.5.3. Maximum pressure calculations assume 100% of the fuel rods rupture, releasing conservatively determined rod fill gas and fission gases volumes into the MPC cavity.

3.5.5 Maximum Thermal Stresses

Maximum thermal stresses generated during transient temperature excursions within the HI-STAR System are reported in Chapter 2.

3.5.6 Evaluation of System Performance for the Hypothetical Accident Thermal Conditions

The HI-STAR System was subjected to a hypothetical fire accident condition with the impact limiters crushed and enclosure shell punctured as a result of previously imposed drop and puncture accidents. However, mechanical integrity of the overpack intermediate and inner shells, mechanical seals, and MPC shell is retained. During the fire accident event, portions of neutron shielding material in the overpack enclosure shell experience high transient temperature excursions and thus

partially lose the ability to conduct heat and shield neutrons. Portions of aluminum alloy inside the crushed impact limiters near the exposed surfaces melt, but do not ignite.

For assessing the impact of transient temperature excursions on the integrity of the HI-STAR System, the significant components and quantities of interest are the closure plate bolts temperatures, the mechanical seals temperatures, the neutron shield temperature, the peak pressure and the peak fuel cladding temperature. The closure plate bolts maintain their ability to hold the seals (see ~~structural evaluation Appendix 2.V~~). The neutron shield material in the post-accident shielding analysis is conservatively assumed to be completely lost. The peak system pressure remains below the design basis accident pressure. The fuel cladding temperature peak does not exceed short-term accident limits. Consequently, the HI-STAR System integrity during the most severe fire event followed by a post-fire cooldown phase is not compromised. In Table 3.5.4, a summary of peak HI-STAR System component temperatures during fire and post-fire accident conditions is provided. The calculated results demonstrate that the HI-STAR System is in compliance with 10CFR71 thermal requirements for hypothetical accident conditions of transport.

Table 3.5.1

SUMMARY OF TEMPERATURE-DEPENDENT FORCED CONVECTION
HEAT TRANSFER CORRELATION PARAMETERS FOR AIR

Parameter	Trend with Increasing Temperatures	Criteria to Maximize h_{fc}	Conservative Parameter Value	Evaluated At
Temperature Range	100°F-1475°F	NA	NA	NA
Density	Decreases	Reynolds Number	High	100°F
Viscosity	Increases	Reynolds Number	Low	100°F
Conductivity (K_f)	Increases	h_{fc} Proportional to K_f	High	1475°F

Table 3.5.2

SUMMARY OF HYPOTHETICAL FIRE ACCIDENT INPUTS

	Steady-State Initial [†] Condition	30-minute Fire	Post-Fire Equilibrium
1. Conduction through Holtite	No	Yes	No
2. Holtite Region Conductivity Reduction (Loss of Radial Connectors)	No	No	Yes
3. Insolation	Yes	Yes	Yes
4. Radiation Heat Transfer	Yes	Yes	Yes
5. Surface Convection	Natural	Forced	Natural
6. Impact Limiters Installed ^{††}	Yes	Yes (crushed)	Yes (crushed)
7. Surface Emissivity	0.85	0.9	0.66

[†] A bounding initial temperature condition is imposed for fire transient analysis.

^{††} Based on minimum 15,000 lbs impact limiter weight modeled as a solid aluminum cap to maximize heat input to cask.

Table 3.5.3

MAXIMUM HI-STAR SYSTEM HYPOTHETICAL FIRE
CONDITION EVENT PRESSURES[†]

Condition	Pressure (psig)			
	MPC-24	MPC-68	MPC-24E	MPC-32
Without fuel rods rupture	70.7 99.6	70.0 98.0	99.6	99.6
With 100% fuel rods rupture	114.7 143.8	101.7 128.5	145.2	160.9

[†] Pressure analysis is based on release of 100% of the rods fill gas and 30% of the significant radioactive gases from a ruptured rod.

Table 3.5.4

MAXIMUM HI-STAR SYSTEM COMPONENTS AND MATERIALS
TEMPERATURES DURING AND AFTER HYPOTHETICAL FIRE CONDITION

Material/Component	Initial Condition (°F)	During Fire (°F)	Post Fire Cooldown (°F)	Accident Limit (°F)
Fuel cladding	708	708	751	1058
Overpack closure bolts	159	415	514	600
Overpack closure plate seals	160	392	490	1200
Drain port plug seal	259	645	662	932
Vent port plug seal	160	283	443	932
Holtite outer surface	223	1232	1232	N/A [†]
Holtite inner surface	259	604	604	N/A
MPC shell	309	313	419	775
Impact limiter surface	127	983	983	1105
Overpack outer enclosure	226	1348	1348	1350

[†] Holtite is conservatively assumed to be completely lost during the fire accident.